This is to certify that the

dissertation entitled

DEVELOPMENT AND ANALYSIS OF A FIRE RING WEAR MODEL FOR A PISTON ENGINE

presented by

Yooseok Chung

has been accepted towards fulfillment of the requirements for

Ph.D. degree in Mechanical Engineering

Harold J. Schock
Major professor

Date 8/3/92

DEVELOPMENT AND ANALYSIS OF A FIRE RING WEAR MODEL FOR A PISTON ENGINE

By

Yooseok Chung

A DISSERTATION

Submitted to
Michigan State University
in partial fulfillment of the requirements
for the degree of

DOCTOR OF PHILOSOPHY

Department of Mechanical Engineering

1992

ABSTRACT

DEVELOPMENT AND ANALYSIS OF A FIRE RING WEAR MODEL FOR A PISTON ENGINE

By

Yooseok Chung

Ring wear may not be a problem in most current automotive engines, however a small alteration in the ring face geometry can significantly affect the hydrodynamic lubrication characteristics of the ring. This in turn can cause excessive frictional losses and blowby in an engine. As engines become more compact and highly loaded, ring wear is likely to be more severe than in current engines. To be able to assess the effect of ring loading, a piston ring wear model has been developed through the use of ring dynamics analysis with the assumption of a linear relationship between ring wear and the friction work applied on the surface of the ring. It is also assumed that ring wear occurs only in the mixed or boundary lubrication regime, where the hydrodynamic film breaks down. The lubrication regimes are separated by the nominal minimum film thickness, which is defined by the ratio of the minimum oil film thickness to the effective surface roughness of the joint.

Input dynamics to the piston ring wear model were provided by a commercially available ring dynamics analysis program which has been under development for the past five years. Analysis shows that the minimum oil film thickness at a given engine speed tends to be lower just after TDC and BDC, which implies that mixed lubrication occurs between the piston ring and the cylinder wall at these points. This effect appears more prominent at the lower engine speeds than at the higher engine speeds

under the same power output. The equation developed for the piston ring wear model is based on the several results of experimental wear efforts. This ring wear analysis clearly shows that the higher the engine speed, the lower the wear rates at the same power output, as is obtained through the experiment. The specific wear rate at steady state drawn from this analysis corresponds to the maximum value of the wear coefficient observed in other experimental studies

The present analysis was developed and the predictions were compared to data available for a Diesel engine. The model developed in this study can be applied to any piston engine, as long as the specifications of the engine such as the oil viscosity, temperature distributions in the cylinder bore, the ring geometry, the ratio of cylinder bore hardness to ring hardness, and the ring face profile are given as the same. This is the first model of piston ring wear which includes ring dynamics, and is intended to provide a framework for a general model which can include the factors mentioned above. This ring wear model can be used to estimate *apriori* wear rates for RII or SLA studies.

To My Parents

ACKNOWLEDGMENTS

I would like to express my appreciation to my adviser, Dr. Harold Schock, for his inspiring guidance and encouragement during this dissertation work. His priceless suggestions and insights have greatly enriched this research.

Dr. Craig Somerton is due special thanks for putting forth a special effort in listening to a number of my presentations and providing helpful comments.

I am also grateful to my other committee members, Dr. David Grummon and Dr. William McHarris, for their helpful suggestions.

Other who have provided valuable comments throughout this dissertation work include Dr. L. Brombolich, Dr. K. Lee, Dr. R. Ronningen, Mr. S. Yoo, and Mr. R. Schafer.

Finally, I thank my parents and my lovely wife for their love and continuous support throughout my graduate studies.

TABLE OF CONTENTS

LIST OF TABLES

LIST OF FIGURES

CHAPTER 1

INTRODUCTION

1. 1 Problem Statement

Piston rings in a piston engine play important roles in the performance and endurance of the engine, viz., sealing the combustion gas between the piston and cylinder wall to prevent excessive blowby, controlling the amount of lubricating oil deposited on the cylinder wall as well as working as the passage of heat flow from the piston into the cylinder. Yet it must perform this task with minimum frictional resistance to avoid excessive energy loss and with minimum wear to ensure an acceptable life of the piston and cylinder liner. These requirements must be satisfied under severe conditions of high temperature and pressures and cyclic variations of loads, speeds, and lubricant viscosity.

Wear within design limits (normal wear) is acceptable from the viewpoint of both safety and economics, since the frictional compatibility of the ring is often improved during an initial stage of the engine operation. However, after a substantial period of running-in, the mean wear rate experienced by a piston ring should be sufficiently low to provide a satisfactory life for the engine. This long term wear rate would be governed by piston ring design, ring and liner materials, and lubrication. During engine development, or during the running-in process, occasionally engines experience a catastrophic form of wear known as scuffing. Generally, this is initiated by inadequate lubrication of the ring and cylinder wall interface, particularly during the critical period immediately after TDC of the power stroke, where the gas pressures and temperatures are high and the ability to develop protective hydrodynamic films is severely

handicapped by low piston speed. This condition causes asperities contact between the rings and the cylinder wall.

Although there are various methods available for ring wear reduction, the fundamental mechanism causing the ring wear is still not completely known because of the large number of interacting factors. Ring wear is one of the most complicated wear phenomena since it often involves processes associated with other modes of wear such as fatigue, abrasion, corrosion as well as adhesion. Generally, the formation of a ring wear pattern can be accounted for qualitatively by examining the variations of speed, viscosity, temperature, gas pressure behind the ring, and contact geometry between the ring and cylinder wall. However, so far there has been no reliable quantitative analysis of a ring wear pattern for an engine under various operating conditions.

Therefore, the first purpose of this research is to understand how friction is developed for a piston ring, and attempt to evaluate the wear rate that occurs between the ring and cylinder wall through the use of this ring friction analysis. The second is to study the wear mechanisms under such low wear rates and investigate the effect of the power output and engine speed on ring wear to provide a reasonable estimate for the life of the piston ring. The third is to provide a useful research tool for developing new materials and lubrication strategies for the piston ring.

1. 2 Dissertation Arrangement

This dissertation is arranged as follows:

Chapter 2 reviews and discusses the piston ring tribology. Experimental studies on ring wear measurement follow to provide background on the theoretical analysis of ring friction and wear.

The inter-ring gas pressures determined from the mass flow rate passing through the ring gaps are discussed in Chapter 3. A complete flow chart is presented

to provide a detailed description of the gas flow analysis. The ring position is also studied to find the pressure behind the ring. Simulation results under different engine operating conditions are presented.

In Chapter 4, assuming axial symmetry throughout the circumference of the ring, ring friction analysis is performed using the Reynolds equation, the load equation, and the Stribeck diagram. Depending on system conditions, the ring may demonstrate different lubricated conditions. Ring friction has been calculated with the lubricated regimes determined from the nominal minimum film thickness, which is defined as the ratio of the minimum oil film thickness over the surface roughness. The minimum oil film thickness and ring friction force are illustrated at each engine speed.

In Chapter 5, the mathematical model of fire ring wear is presented with the aid of ring dynamics analysis. Simulation results are presented to support the analytical findings.

In Chapter 6, some concluding remarks drawn from this research are presented.

In Chapter 7, some limitations of this model, and recommendations for future research work are discussed.

In the Appendices, the TRIM Simulations [1] which have been conducted for the Radioactive Ion Implantation (RII) studies are presented along with some preliminary results. Analysis of measurement sensitivity is discussed for the purpose of providing estimates of the quantity of the experimental data required to perform in-situ piston ring wear measurement using the RII or SLA technique.

CHAPTER 2

BACKGROUND

Reduction of friction between the piston ring assembly and cylinder bore, either through improved design, or through the use of more suitable contacting materials, or again through the application of better lubricating substances, is an extremely important problem for improving fuel economy and energy efficiency in engines. Since piston ring tribology has been a subject of interest for many automotive researchers and designers for a long time, numerous papers containing significant and useful concepts, and reviews for research and technologies are available. These topics with previously published information are reviewed and discussed, and experimental studies on ring wear measurement are described to provide background on the theoretical analysis.

2. 1 Piston Ring Design

The construction of a typical piston and ring assembly is shown in Figure 2.1 [2]. There are two types of rings: compression and oil rings. Compression rings are designed to seal the clearance between the piston and cylinder to retain gas pressure and minimize blowby, and oil rings are designed to limit the passage of oil from the crankcase to the combustion space. Automobile engines normally use two compression rings and one oil ring, though two-ring designs exist. Most piston rings are made of gray cast iron because of its excellent wearing properties in all kinds of cylinder

bores. The axial profiles are chosen to facilitate hydrodynamic lubrication [2]. In today's gasoline and diesel engines, upper compression rings are normally the barrel face design, having a smooth face surface for lower initial engine friction, and lower compression rings are the taper face design. Wear resistant coating is usually applied on the outer ring surface. In compression rings, the force between the piston ring and the cylinder wall is due partly to the ring tension and partly to the gas pressure that leaks into the groove between the ring and the piston [3]. Because of their spring action, piston rings press against the cylinder wall at all times, and the gas pressures behind the rings are given as a function of piston speed and load. To maintain satisfactory levels of oil control and blowby, minimum surface pressure must be maintained on both compression and oil rings.

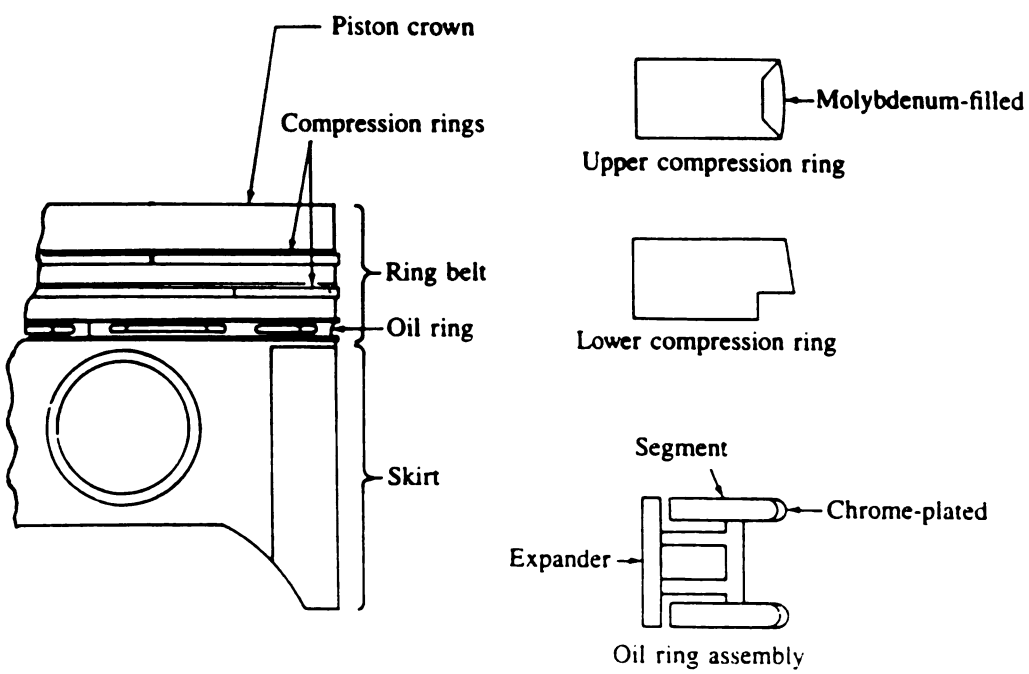

Figure 2.1 Schematic of piston and ring assembly in a piston engine [2]

Because of the importance of rings in normal engine operation and the potential energy savings through improved design, several studies have been conducted over the years. McCormick *et al.* [4, 5] presented new developments in piston ring designs and their relationship to blowby and oil control. Sunden and Schaub [6] discussed practically orientated principles for the successful manufacture of gray cast iron piston rings and suggested that, when considered with the sciences of strength of materials and diesel engineering, the subject of piston rings is almost an embodiment of the wider subject of tribology. Taylor and Eyre [7] have presented a more detailed review of piston ring design and piston ring materials as well as cylinder liner materials. Hill and Newman [8] have discussed theoretical considerations affecting piston ring friction and their implication in ring design. Holt and Murray [9] have observed that the compression ring of the two ring piston system can be used with advantage as the top compression ring of an orthodox three ring piston. Young *et al.* [10] have attempted to develop a new ring face coating to extend the life of the internal combustion engine. In recent studies on friction and scuff resistance of ceramic coatings for rings, Yoshida *et al.* [11] revealed that ceramic coatings show lower friction than conventional chromium plate and molybdenum spray coating. Heywood [2] suggested that the major design parameters which influence ring assembly friction are ring width, ring face profile, ring tension, ring gap which governs inter-ring gas pressure, and ring land width. Jeng [12] has also attempted to investigate the effects of engine design parameters on tribological performance, and suggested that the piston speed, surface roughness, and ring tension are the most important design variables.

2. 2 Piston and Ring Assembly Friction

Energy losses due to friction between the ring assembly and cylinder wall are purely mechanical energy losses. Most of the heat generated by this friction is dissipated and wasted. In addition to this direct energy loss, excessive wear or scuffing can result from a high friction force due to poor lubrication. It is well known that even a small reduction of piston friction results in both better mechanical efficiency and improved fuel economy. Piston friction refers to the friction forces on cylinder surfaces caused by the reciprocating piston assembly. Measurement of piston frictional forces during engine operation is valuable for improved fuel economy and good engine design.

Friction measurements have been conducted by many automotive researchers. Furuhama *et al.* [13] carried out piston friction force measurement to obtain the effects of piston clearance, surface roughness, lubricant, ring size and contact pressure on the piston friction forces; they suggested that the piston friction is nearly proportional to the square root of the piston speed and the oil viscosity. Furuhama and Sasaki [14] introduced the movable bore with a pressure balancing device to measure the friction forces. With the aid of this movable bore method, Ku and Patterson [15] developed the fixed sleeve method to measure the instantaneous friction of the piston and ring assembly. The results show that the surface finish of the ring and cylinder wall affected friction significantly at TDC of the compression stroke. Uras and Patterson [16, 17] investigated the effect of the piston variables on piston ring assembly friction using an instantaneous IMEP method, and observed that during break-in, piston ring friction gradually reduces throughout the stroke. This suggests that some mixed or boundary friction exists throughout the stroke. Slone *et al.* [18] have developed a new bench tester for the laboratory simulation of the piston ring and cylinder wear; they observed that a lubricated surface was smoothed considerably when worn, while a unlubricated surface was further roughened. Simmons *et al.* [19] have at-

tempted to evaluate the fire ring wear as a function of fuel ignition quality. Fire ring wear was observed to increase rapidly as the ignition quality of the fuel dropped. The wear rate also increased for a given ignition quality fuel as the injection was advanced or retarded about the stock timing setting.

In addition to experimental research, numerous theoretical analyses on piston and ring assembly friction have been undertaken. From experimental data, Bishop [20] derived empirical equations which describe the magnitude of the most important factors determining the cycle efficiency and motoring friction of an engine. Ting and Mayor [21, 22] developed an analytical method for determining the inter-ring gas pressure, oil film pressure, and piston friction force for a reciprocating piston engine. This method has been used for predicting the bore wear pattern of actual engines. McGeehan [23] has presented an excellent review of piston and piston ring friction. It has been revealed that the piston ring friction is predominantly hydrodynamic with localized contact between the ring and cylinder wall at TDC firing during transient conditions, and under hydrodynamic conditions ring friction is proportional to the square root of the viscosity. Rohde [24] developed a ring model which allows the study of ring friction performance in the mixed lubrication regime. The dependences of the ring friction and power losses on surface topography, lubrication properties, and engine operating conditions have been investigated. Ting [25] reviewed some recent theoretical and experimental investigations related to piston ring tribology in the areas of friction determination, friction reduction, lubrication, and oil consumption. Patton *et al.* [26] have developed a friction model which predicts friction mean effective pressure for spark-ignition engines. This model provides reliable estimates of spark-ignition engine fmep, and offers a useful tool for understanding how the major engine design and operating variables affect individual component friction. Yagi *et al.* [27] suggested that frictional mean effective pressure is nearly proportional to a non-dimensional number given by piston stroke, mean equivalent crank diameter, and cylinder bore

through the experimental analysis of total engine friction.

The lubrication of the piston skirt is mainly hydrodynamic, while that of the ring assembly is partly in the mixed lubrication regime [17, 20, 28, 29], which is a transition state between hydrodynamic and boundary lubrication. In the hydrodynamic lubrication regime, where the fluid film is thick enough to prevent metallic contact between ring assembly and cylinder wall, friction is caused only by the viscous shear of the fluid film. However, as the thickness of the fluid film is reduced to the order of the surface roughness, metallic contact increases and boundary lubrication becomes dominant [28]. In contrast with hydrodynamic lubrication, long-term boundary lubrication results in wear.

2. 3 Lubrication and Oil Consumption

The junction between the piston ring and cylinder liner is subjected to exceptionally severe dynamic conditions, since the normal load, sliding velocity, and temperature, hence lubricant viscosity, all vary throughout the cycle. In addition, the shape of the junction might also change throughout the cycle due to elastic and thermal distortion and wear of the piston ring, the piston, and the cylinder liner [30]. Thus, effective lubrication has to be achieved with minimum oil consumption.

A number of valuable experimental and theoretical determinations of the oil film thickness between the piston rings and cylinder liner have been reported. Stewart and Selby [31] presented a comprehensive review of the published information on the substantial influence on engine performance of engine oil viscosity. Brown and Hamilton [32] have observed the large negative pressures in oil film lubricating a piston ring immediately after dead center position, and suggested that these pressures have the important effect of reducing the minimum film thickness. Dowson *et al.* [29] at-

tempted to predict the cyclic variation of film thicknesses generated between the ring and cylinder wall. This report confirmed the view that hydrodynamic lubrication is prevalent in most of the operating cycle. However, the predicted minimum film thickness, which generally occurs after TDC, indicated that these must be transition to boundary or mixed lubrication in this region. It has been known that when the engines are operated on hydrogen as the fuel, all carbon compounds in the exhaust gas (except for those already in the intake air) can be attributed to the burning of the lubricating oil. By using this principle, Furuhama and Hiruma [33] could measure the carbon dioxide (CO_2) in exhaust gas, and accurately measure the oil burned. Reipert and Buchta [34] presented new methods of piston design in relationship to oil consumption and blowby. Boisclair *et al.* [35] attempted to illustrate the time-dependent thermal environment around the top piston ring and lubricant; they observed that because of major transient effects, high lubricant temperature is experienced not only at top ring reversal but also down the liner to bottom ring reversal. By synthesizing recent technical papers, McGeehan [36] presented an outstanding review on the mechanical factors affecting oil consumption in four cylinder diesel and gasoline engines and the practical solutions achieved by design modifications. The progress in understanding hydrodynamic lubrication of piston rings has not yet led to a satisfactory procedure for a prediction of oil consumption in an engine, since the net transport of oil past a piston seal resulting from the presence of the lubricating film is only one component in the oil consumption mechanism [37]. Further realistic ring lubrication theory is expected to be developed.

2. 4 Types of Wear

Adhesive wear affects certain parts of the engine. In the upper cylinder, metal-to-metal contact between piston, rings, and cylinder walls takes place each time the engine is started because there is insufficient oil in the top portion of the engine. Oil with antiwear additives and low viscosity at low temperatures can provide some remedy [2].

Abrasive wear arises from the presence of atmospheric dust and metallic debris from corrosive and adhesive wear in the lubricating oil. Efficient air filtration is essential to eliminate the abrasive particle impurities [2].

Corrosive wear occurs when sliding takes place in a corrosive environment. In the absence of sliding, the products of corrosion form a film on the surfaces, which tends to slow down or even arrest the corrosion, but the sliding action wears the film away, so that the corrosive attack can continue [38]. Corrosive attack by acidic products of combustion is one of the chief causes of cylinder and ring wear. This effect is worse at low cylinder wall temperature [2]. It has been demonstrated that corrosion prevention is best accomplished through additive formulation designed to prevent the accumulation on the metal surface of the precursors to performic acid formation and to provide excellent dynamic anti-wear characteristics [39]. Nickel coating also has been proven as an effective and reliable technique to protect pistons from combustion knock erosion [40].

2. 5 Experimental Studies on Ring Wear Measurement

2. 5. 1 Ring Wear Measurement Using SLA

SLA (Surface Layer Activation), also called TLA (Thin Layer Activation) using radioactive ions has been used for extremely sensitive wear measurements of certain metallic surfaces. This wear study method, developed over a decade ago [41, 42], has proven to be a valuable diagnostic tool in evaluating piston ring wear without disassembling the engine [43 - 48]. Schneider and Blossfeld [49], and Konstantinov *et al.* [50] studied the rotational movement as well as the wear of piston rings with the aid of SLA. Particularly, Schneider *et al.* [51] investigated the effect of speed and power output on piston ring wear in a diesel engine using SLA. It has been shown that piston ring wear rates increase significantly with decreasing speed at constant power output, and it increases with increased power output at all speeds.

2. 5. 2 The Effect of Ion Implantation on Friction and Wear

Shepard and Suh [52] investigated the effects of ion implantation on the friction and wear behavior of metals and revealed that a significant reduction in friction and wear of the iron and titanium systems can be attributed to a hard layer formed during the ion implantation processes. This hard layer minimizes plowing and subsurface deformation and hence reduces the delamination wear process. Ion implantation research suggests that for high doses ($>10^{16}$ ions/cm^2) of heavy ions with low bombarding energies (typically several MeV or lower), a variety of material properties can be changed. These changes include amorphization, production of defect clusters, destruction of crystallinity or the production of a new phase, and surface hardness alteration. Such ion doses are comparable to the primary proton beam used in SLA, and are at least several orders of magnitude larger than that needed to produce a useful level of activity ($\sim 1\mu C_i$) by direct implantation. The lower mass of the proton beam

may not result in the damage absorbed by the MSU research group for the heavy ions [53].

2. 5. 3 Radioactive Ion Implantation Technique

Mallory *et al.* [54] have presented the feasibility of implanting a radioactive ion (e.g., ^{7}Be or ^{22}Na) in ceramic or metallic samples with a dose intensity suitable for viable wear studies. This Radioactive Ion Implantation (RII) technique could be applied to study piston ring wear. The activated piston ring emits a low-intensity γ-ray, which penetrates the cylinder wall. This γ-ray signature associated with wear particles is monitored with a NaI or Ge detector. The amount of wear for a given period of time can be evaluated with the γ-ray spectra since the wear is inversely proportional to the measured radiation. This technique can also be used to assess the performance of filtration systems [55].

The analysis of the measurement sensitivity is discussed in the Appendices for the purpose of providing reasonable estimates of the implantations needed to obtain in situ piston ring wear measurement using the RII technique. The polyenergetic TRIM simulation has been used to find an optimized energy of the implanting beam and a suitable set of absorbers necessary to produce a desired uniform dose-depth profile in the surface of a sample for RII studies.

Further detailed descriptions on the TRIM simulation and RII including measurement procedure can be found in Appendices

CHAPTER 3

GAS FLOW ANALYSIS

3. 1 Introduction

Small volumes formed at interfaces to connecting parts in an engine's combustion chamber are called the crevices. Gas flows into and out of these volumes during the engine operating cycle as the cylinder pressure changes. Total crevice volume is a few percent of the clearance volume, and the piston and ring crevices are the dominant contributors. When the engine is warmed up, dimensions including crevice volumes are changed.

The crevice processes occurring during the engine cycle are described as follows [2]: As the cylinder pressure rises during compression, the unburned mixture or air is forced into each crevice region. Since these crevices are thin, they have a large surface to volume ratio; the gas flowing into the crevice cools by heat transfer to close to the wall temperature. During combustion while the pressure continues to rise, the unburned mixture or air, depending on engine type, continues to flow into these crevice volumes. After the flame arrives at the crevice entrance, burned gases will flow into each crevice until the cylinder pressure starts to decrease. Once the crevice gas pressure is higher than the cylinder pressure, gas flows back from each crevice into the cylinder. The back-flow of gases into the combustion chamber can lead to excessive exhaust hydrocarbon and poor economy. For these reasons and others, understanding the processes involved in piston ring sealing are critical to a good engine design.

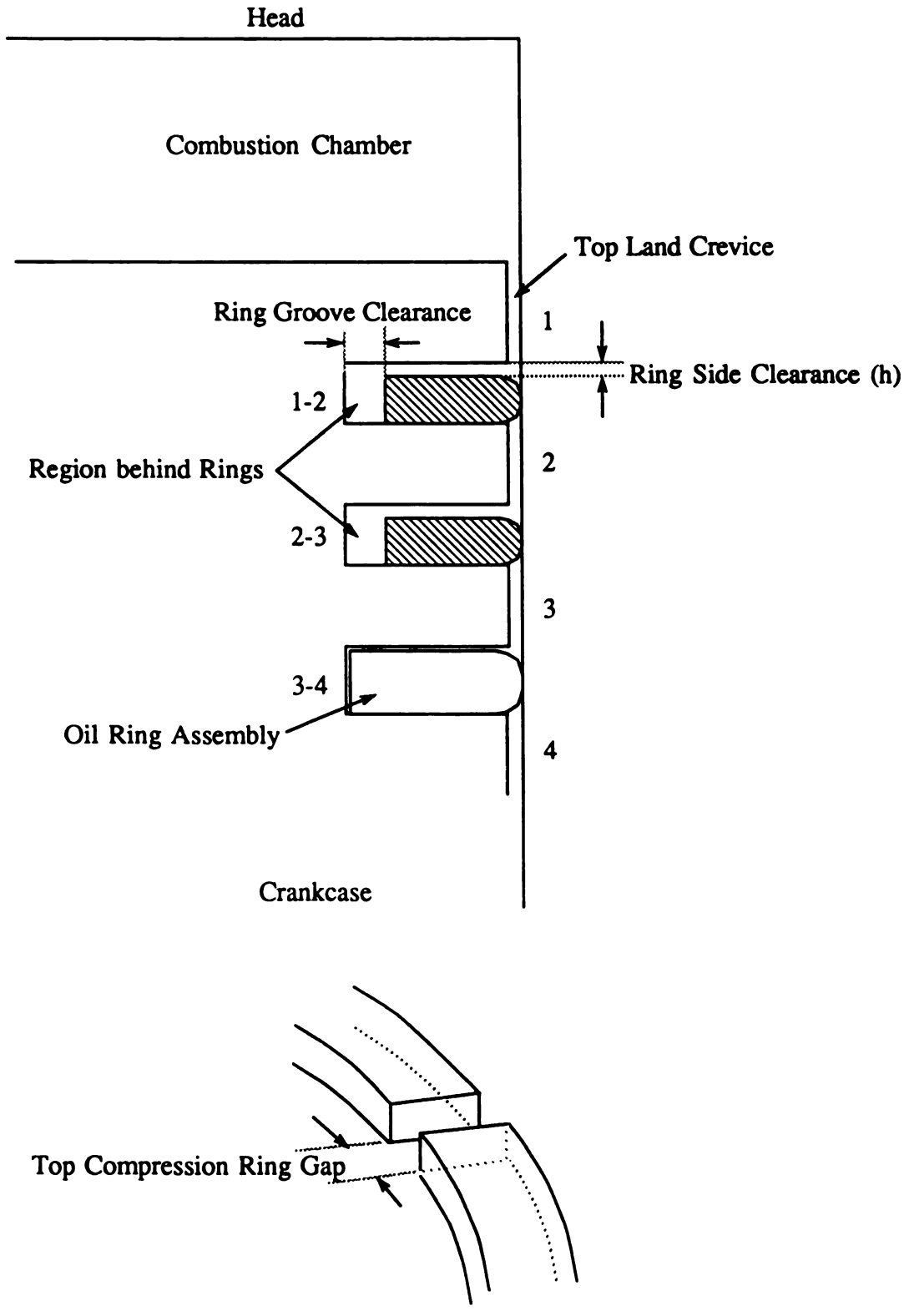

Figure 3.1 Detailed schematic of clearance volume in a piston engine

The volumes between the piston, piston rings, and cylinder walls are shown schematically in Figure 3.1. These crevices consist of a series of volumes (numbered 1, 1-2 etc.) connected by flow restrictions such as ring side clearance and ring gap. The geometry changes as each ring moves up and down in its ring groove, sealing either at the top or bottom ring surface. The gas flow, pressure distribution, and ring motion are therefore coupled [2]. The pressure distributions and ring motion can be determined by analyzing these crevices as volumes connected by passage ways, with a prescribed cylinder pressure versus crank angle profile coupled with a dynamic model for ring motion, and assuming that the gas temperature equals the wall temperature [56, 57].

The gas that flows from the combustion chamber past the piston rings into the crankcase is called the blowby. If there is good contact between the compression rings and the bore, and between the rings and the bottom of the grooves, then the only leakage path of consequence is the ring gap. Blowby of gases from the cylinder into the crankcase removes gas from these crevice regions and thereby prevents some of crevice gases from returning to the cylinder [2]. However, if the blowby is excessive, compression is reduced, emissions increase, and the lubricating film may deteriorate, affecting engine reliability and life.

Gas flow analysis has to be performed prior to the ring friction analysis since the gas pressures above and below a ring are used as boundary conditions in the calculation of the oil film pressures, and gas pressures behind the ring directly affect the ring friction force developed between the ring and cylinder bore. Ting and Mayor [21, 22] developed a method for computing the inter-ring gas pressure variations throughout the engine cycle. This analysis is reviewed and discussed with the assumptions and limitations of the theory.

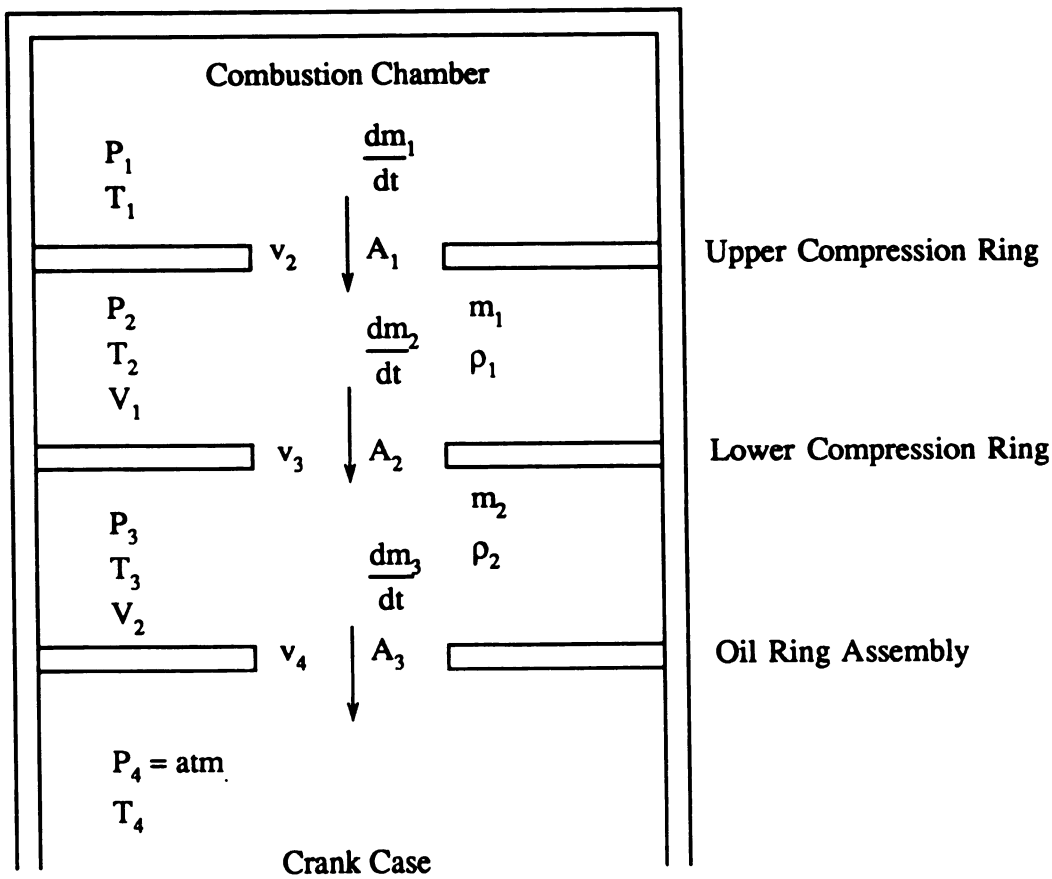

Figure 3.2 Orifice Volume Model of Ring Pack

3. 2 The Mass Flow Rate

The ring gap areas have been considered as the most important factors in determining the mass flow rate in an engine's crevices [21, 22]. The size of the ring gaps is increased due to the combined effects of ring and liner wear. Hence, the effect of ring gap area on the mass flow rate is critical in the ring design. The mass flow rate through each ring gap needs to be determined to calculate the inter-ring gas pressure. An orifice volume model of ring pack is shown in Figure 3.2. The volumes represent the inter-ring spaces that are formed by two adjacent rings, the intervening piston land, and the cylinder bore.

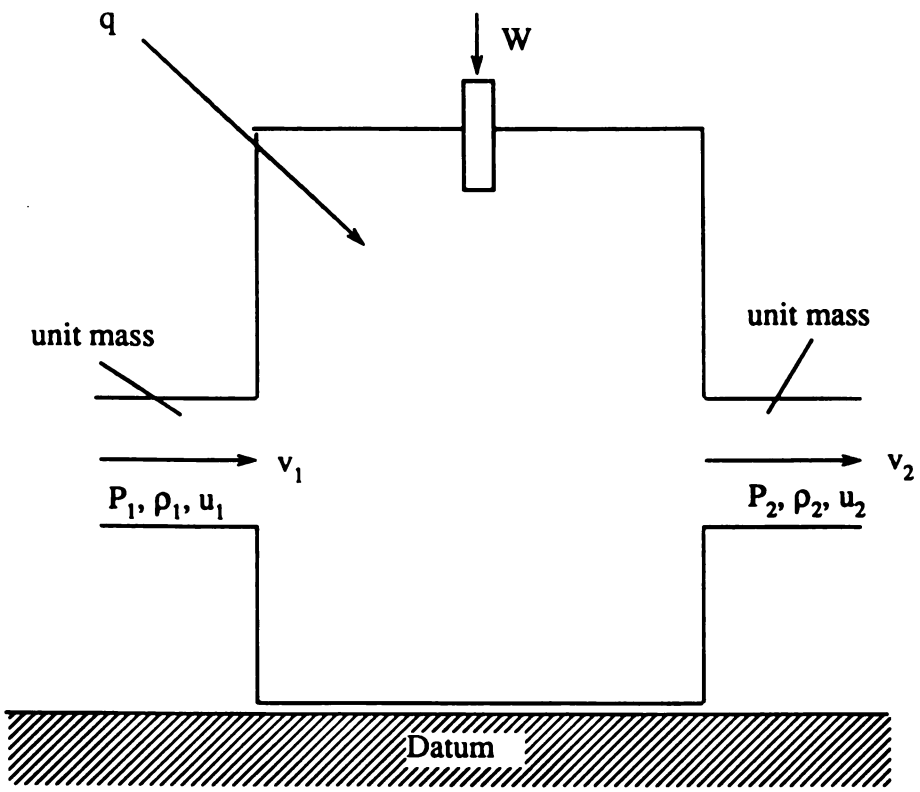

Figure 3.3 Schematic illustration of energy balance [28]

The following assumptions were made to model mass flow rate [21, 22]:

1) The ring gaps are the only gas leakage paths.
2) The rate of heat transfer is small, such that the gas flow through the ring pack is an unsteady adiabatic flow satisfying the perfect gas law.
3) The orifices are assumed to be equal in area to the effective leakage path formed by the ring gaps and the radial clearance between the piston and cylinder bore.
4) The gas flow is considered as a one-dimensional flow through the orifice with a constant discharge coefficient.
5) The friction effects are small such that the flow is isentropic.
6) The combustion chamber pressure remains unaffected despite the gas leakage.
7) The crankcase is considered to be at atmospheric pressure.

Consider a gas passing through a control volume as shown in Figure 3.3.

where W = the work done on or by the gas

q = the heat added per unit mass

v = velocity

u = internal energy per unit mass

P = pressure

ρ = gas density

and subscripts 1 and 2 denote each condition at the inlet and the exit, respectively.

For a unit mass, neglecting the potential energy changes, the Energy Equation is given as

$$q + P_1/\rho_1 - P_2/\rho_2 + W = u_2 - u_1 + (v_2^2 - v_1^2)/2 \qquad (3.1)$$

Because adiabatic flow has been assumed, q = 0. If, in addition, W = 0, then Equation (3.1) reduces to

$$P_1/\rho_1 - P_2/\rho_2 = u_2 - u_1 + (v_2^2 - v_1^2)/2 \tag{3.2}$$

For an ideal gas, the following relation is valid:

$$P = \rho RT \tag{3.3}$$

where T is the absolute temperature and R is the ideal gas constant.

The specific heat of a gas is the amount of heat required to change the temperature of a unit quantity of the gas one degree. For an ideal gas, the specific heat ratio is given by

$$\gamma = C_p / C_v \tag{3.4}$$

where C_p denotes the specific heat at constant pressure and C_v is the specific heat at the constant volume. Since the change in internal energy for a non flow constant volume process depends only on the temperature difference

$$u_2 - u_1 = C_v(T_2 - T_1) \tag{3.5}$$

For a constant pressure process

$$C_p = C_v + R \tag{3.6}$$

By combining Equations (3.4) and (3.6)

$$C_p = R/(\gamma - 1) \tag{3.7}$$

$$C_v = \gamma R/(\gamma - 1) \tag{3.8}$$

Therefore, for an isentropic, adiabatic process, the following relationship is valid:

$$P_1 / P_2 = (\rho_1 / \rho_2)^{\gamma} = (T_1 / T_2)^{\gamma/(\gamma-1)} \tag{3.9}$$

For a steady one dimensional gas flow, mass flow rate is given as

$$dm / dt = \rho A v \tag{3.10}$$

where m = the mass of gas

A = a cross-sectional area of flow

v = the velocity of gas

Then the mass flow rate passing through the upper compression ring gap as a function of crank angle can be expressed as

$$\begin{aligned} dm_1 / d\theta &= (dm_1/dt) / (d\theta/dt) \\ &= \rho_2 A_1 v_2 / \omega \end{aligned} \tag{3.11}$$

Since $v_1 = 0$, the velocity of the gas (v_2) through the ring gap can be found by substituting Equations (3.5) and (3.3) into Equation (3.2).

$$\begin{aligned} v_2 &= \{2 [P_1 / \rho_1 - P_2 / \rho_2 + C_v (T_1 - T_2)]\}^{1/2} \\ &= \{2 [R(T_1 - T_2) + R(T_1 - T_2) / (\gamma - 1)]\}^{1/2} \\ &= [2 \gamma R T_1 (1 - T_2 / T_1) / (\gamma - 1)]^{1/2} \end{aligned} \tag{3.12}$$

Again after substituting Equation (3.9) into Equation (3.12), the gas velocity becomes

$$v_2 = \{2\gamma RT_1[1 - (P_2/P_1)^{(\gamma-1)/\gamma}]/(\gamma - 1)\}^{1/2} \tag{3.13}$$

Accordingly, the mass flow rate passing through the top ring gap is given by

$$\begin{aligned} dm_1/d\theta &= A_1/\omega\{2\gamma RT_1\rho_2^2[1 - (P_2/P_1)^{(\gamma-1)/\gamma}]/(\gamma-1)\}^{1/2} \\ &= A_1/\omega\{2\gamma/(\gamma-1)\cdot(\rho_2/\rho_1)^2\cdot(\rho_1 P_1)\cdot[1 - (P_2/P_1)^{(\gamma-1)/\gamma}]\}^{1/2} \end{aligned} \tag{3.14}$$

Substituting Equation (3.9) into Equation (3.14), and using Equation (3.3) the mass flow rate for $P_1 > P_2$ is determined as

$$\begin{aligned} dm_1/d\theta &= A_1/\omega\{2\gamma/(\gamma-1)\cdot(P_2/P_1)^{2/\gamma}\cdot P_1^2/(RT_1)\cdot[1 - (P_2/P_1)^{(\gamma-1)/\gamma}]\}^{1/2} \\ &= A_1K_1\cdot(P_1/T_1^{1/2})\cdot(P_2/P_1)^{1/\gamma}\cdot[1 - (P_2/P_1)^{(\gamma-1)/\gamma}]^{1/2} \end{aligned} \tag{3.15}$$

where $K_1 \equiv \{2\gamma/[R(\gamma-1)]\}^{1/2}/\omega$

If $P_1 < P_2$

$$dm_1/d\theta = -A_1K_1\cdot(P_2/T_2^{1/2})\cdot(P_1/P_2)^{1/\gamma}\cdot[1 - (P_1/P_2)^{(\gamma-1)/\gamma}]^{1/2} \tag{3.16}$$

where the negative sign signifies the reverse gas flow.

Similarly, for $P_2 > P_3$

$$dm_2/d\theta = A_2K_1\cdot(P_2/T_2^{1/2})\cdot(P_3/P_2)^{1/\gamma}\cdot[1 - (P_3/P_2)^{(\gamma-1)/\gamma}]^{1/2} \tag{3.17}$$

If $P_2 < P_3$

$$dm_2/d\theta = -A_2 K_1 \cdot (P_3 / T_3^{1/2}) \cdot (P_2/P_3)^{1/\gamma} \cdot [1 - (P_2/P_3)^{(\gamma-1)/\gamma}]^{1/2} \qquad (3.18)$$

Also, for $P_3 > P_4$

$$dm_3/d\theta = A_3 K_1 \cdot (P_3 / T_3^{1/2}) \cdot (P_4/P_3)^{1/\gamma} \cdot [1 - (P_4/P_3)^{(\gamma-1)/\gamma}]^{1/2} \qquad (3.19)$$

If $P_3 < P_4$

$$dm_3/d\theta = -A_3 K_1 \cdot (P_4 / T_4^{1/2}) \cdot (P_3/P_4)^{1/\gamma} \cdot [1 - (P_3/P_4)^{(\gamma-1)/\gamma}]^{1/2} \qquad (3.20)$$

However, if the pressure downstream of the ring gap is less than the critical pressure, the pressure in the ring gap is always the critical pressure and the mass flow always equals the maximum value; whereas if the pressure downstream of the ring gap is greater than the critical pressure, the mass flow rate is determined by one of equations above according to the conditions [21, 22]. The critical pressure, where the mass flow rate reaches a maximum value, can be determined by differentiating this given equation with respect to P_i (where i = 2, 3, 4) and setting this result equal to zero. Consider Equation (3.15) as an example.

Defining $P_2/P_1 \equiv x$,

$$dm_1/d\theta = A_1 K_1 \cdot (P_1 / T_1^{1/2}) \cdot x^{1/\gamma} \cdot [1 - x^{(\gamma-1)/\gamma}]^{1/2}$$

$$= A_1 K_1 \cdot (P_1 / T_1^{1/2}) \cdot [x^{2/\gamma} - x^{(\gamma+1)/\gamma}]^{1/2} \qquad (3.21)$$

Differentiating Equation (3.21) with respect to x and setting the result equal to zero

gives

$$1/2 \cdot [x^{2/\gamma} - x^{(\gamma+1)/\gamma}]^{-1/2} \cdot [2/\gamma \cdot x^{2/\gamma - 1} - (\gamma+1)/\gamma \cdot x^{1/\gamma}] = 0$$

Since $[x^{2/\gamma} - x^{(\gamma+1)/\gamma}]^{-1/2} \neq 0$ for $C_p \neq C_v$

$$2/\gamma \cdot x^{(1-\gamma)/\gamma} - (\gamma+1)/\gamma = 0$$

Thus

$$x = [(\gamma+1)/2]^{\gamma/(\gamma-1)}$$

That is, the critical pressure is found to be

$$P_c = P_1[(\gamma+1)/2]^{\gamma/(\gamma-1)} \tag{3.22}$$

For combustion gases passing through the ring pack, γ is assumed to be 1.3 and the critical pressure is $0.546\, P_i$ (i = 1, 2, 3, 4) [21, 22].

Therefore, if $P_2 \leq 0.546\, P_1$, Equation (3.15) becomes

$$dm_1/d\theta = A_1 K_1 K_2 \cdot (P_1 / T_1^{1/2}) \tag{3.23}$$

where $K_1 \equiv \{2\gamma/[R(\gamma - 1)]\}^{1/2}/\omega$

$K_2 \equiv (0.546)^{1/\gamma} \cdot [1 - (0.546)^{(\gamma-1)/\gamma}]^{1/2}$

For $P_1 < P_2$, if $P_1 \leq 0.546\, P_2$

$$dm_1/d\theta = -A_1 K_1 K_2 \cdot (P_2 / T_2^{1/2}) \tag{3.24}$$

Similarly for $P_2 > P_3$, if $P_3 \leq 0.546\, P_2$

$$dm_2/d\theta = A_2 K_1 K_2 \cdot (P_2 / T_2^{1/2}) \tag{3.25}$$

For $P_2 < P_3$, if $P_2 \leq 0.546\, P_3$

$$dm_2/d\theta = -A_2 K_1 K_2 \cdot (P_3 / T_3^{1/2}) \tag{3.26}$$

For $P_3 > P_4$, if $P_4 \leq 0.546\, P_3$

$$dm_3/d\theta = A_3 K_1 K_2 \cdot (P_3 / T_3^{1/2}) \tag{3.27}$$

For $P_3 < P_4$, if $P_3 \leq 0.546\, P_4$

$$dm_3/d\theta = -A_3 K_1 K_2 \cdot (P_4 / T_4^{1/2}) \tag{3.28}$$

However, the actual mass flow rate through an orifice is less than the theoretical mass flow rates given by Equations (3.15) to (3.20) and Equations (3.23) to (3.28) because of the friction losses of the gas passing through the ring gap and the convergence of the gas streamlines as they pass through the ring gap [21, 22]. The actual mass flow rate through a ring gap is given by

$$(dm/dt)_{actual} = K_c(dm/dt)_{theoretical} \tag{3.29}$$

where K_c = orifice discharge coefficient

An orifice discharge coefficient of 0.65 has been taken for the calculation of inter-ring gas pressure since the ring gap was considered as a square-edge orifice [21, 22].

3. 3 The Determination of Inter-ring Gas Pressure

The mass of the gas bounded in the volume between the top and second ring shown in Figure 3.2 is given by

$$m_1 = \rho_1 V_1 \tag{3.30}$$

Substituting Equation (3.3) into Equation (3.30)

$$P_2(\theta) = m_1(\theta)RT_2/V_1 \tag{3.31}$$

At the crank angle of $\theta+\Delta\theta$, the pressure in the volume is given by

$$P_2+\Delta P_2 = RT_2/V_1\{m_1(\theta) + [dm_1/d\theta - dm_2/d\theta]\Delta\theta\} \tag{3.32}$$

Hence, the rate of pressure change is written as

$$dP_2/d\theta \approx RT_2/V_1(dm_1/d\theta - dm_2/d\theta) \tag{3.33}$$

Similarly

$$dP_3/d\theta \approx RT_3/V_2(dm_2/d\theta - dm_3/d\theta) \tag{3.34}$$

Therefore, the inter-ring gas pressure at each crank angle can be determined by marching through the cycle.

$$P_2(\theta+\Delta\theta) \approx P_2(\theta) + (d\theta/2)[(dP_2/d\theta)_\theta - (dP_2/d\theta)_{\theta+\Delta\theta}] \tag{3.35}$$

$$P_3(\theta+\Delta\theta) \approx P_3(\theta) + (d\theta/2)[(dP_3/d\theta)_\theta - (dP_3/d\theta)_{\theta+\Delta\theta}] \tag{3.36}$$

The convergence criteria for the calculation of the inter-ring gas pressure is critical. The iterations are continued until the convergent gas pressures are obtained.

Since the gas flow, pressure distribution, and ring motion are coupled as stated earlier, the axial movement of a piston ring in the ring groove needs to be considered to determine the pressure behind the top compression ring ($P_{1\text{-}2}$).

3. 4 The Axial Motion of the Fire Ring in the Groove

The axial motion of the ring can be predicted by using a simple force balance model [56, 57] with the same assumptions used in the evaluation of inter-ring gas pressures as follows:

The force due to the gas pressure acting on the ring is expressed as

$$F_p = \pi D_r \int_0^{W_r} P(x)dx \tag{3.37}$$

where D_r = diameter of the ring

W_r = width of the ring

x = coordinate in radial direction

P(x)=pressure distribution on the ring

Again assuming axial symmetry throughout the ring circumference, i.e., neglecting the twist, the rotation of the ring, and cylinder bore distortion; the pressure distribution on the ring can be found by considering the pressure below and above the ring with the substantial pressure drop across the ring.

$$P(x) \approx [P_1(\theta)+P_{1\text{-}2}(\theta)]/2 - [P_{1\text{-}2}(\theta)+P_2(\theta)]/2$$

$$= [P_1(\theta)-P_2(\theta)]/2 \qquad (3.38)$$

Equation (3.37) becomes

$$F_p \approx \pi D_r W_r [P_1(\theta)-P_2(\theta)]/2 \qquad (3.39)$$

While the inertia force is given by

$$F_i = m_r a_p \qquad (3.40)$$

where a_p denotes the acceleration of the piston. The direction of this force is dependent on the direction of piston motion. The friction force on the cylinder wall is usually neglected in the determination of the ring position in the groove since it is relatively small compared to the inertia and pressure force [28]. Also unlike Kuo *et al.* [57], an oil resistance between the ring and the groove is not included since there is too much

uncertainty concerning the presence and coverage of the oil film [58]. Therefore, the equation of the motion for the ring is found to be

$$\pi D_r W_r [P_1(\theta) - P_2(\theta)] /2 + m_r a_p = m_r (d^2h/dt^2) \qquad (3.41)$$

where h represents the ring side clearance. As long as the sum of the forces is positive, the ring seats in the bottom of the groove. But as the sum becomes negative, the ring moves upwards and finally settles on the top side of the groove. Equation (3.41) can be solved by applying the fourth order Runge-Kutta integration method. Thus, the pressure behind the fire ring can be determined considering the ring position in the groove.

3. 5 Results and Discussion

The specifications of the diesel engine used in this study are shown in Table 1. As a completed data set was not available, it has been pieced together based on available data for similar engine. The combustion gas pressures have been generated to give the same power output at each engine speed. Further detailed descriptions on IMEP and the power output follow in Section 4.2.

The procedure for the determination of inter-ring gas pressures at each engine speed is shown in Figure 3.4. The computer simulation has been performed using a ring dynamics analysis program, which has been under development for the past five years [28]. Figures 3.5 through 3.8 depict the gas pressures in each region determined from this analysis. The fire ring motion in the groove at each engine speed is shown in Figures 3.9 through 3.12. Comparing these Figures - Figures 3.5 and 3.9, Figures 3.6 and 3.10, Figures 3.7 and 3.11, and Figures 3.8 and 3.12 - it is found that

the gas pressure behind the ring depicted as the short-dotted line in each figure is definitely influenced by the ring motion in the groove. In other words, if the ring settles on the top side of the groove, the gas pressure behind the fire ring is the same as the gas pressure between the fire ring and lower compression ring, whereas if the ring seats at the bottom of the groove, it becomes the same as the combustion pressure.

Table 1 Specifications of the Engine

Engine Data

Engine Type : Diesel Engine

Engine Displacement : 12.7 L

Tested Engine Speed : 1200 rpm, 1500 rpm, 1800 rpm, 2100 rpm

Bore Diameter : 130 mm

Bore Surface Roughness : 0.15 μm

Stroke : 160 mm

Connecting Rod Length : 264.8 mm

Connecting Rod Weight : 4.704 kg

Engine Bore Temperature

9 mm from the Deck Top : 159 °C

22 mm from the Deck Top : 124 °C

165 mm from the Deck Top : 113 °C

Temperature Data

Mean Combustion Temperature : 326 °C

Upper Compression Ring Groove Temperature : 210 °C

Lower Compression Ring Groove Temperature : 177 °C

Oil Ring Groove Temperature : 135 °C

Second Land Temperature : 191 °C

Third Land Temperature : 149 °C

Sump Temperature : 121 °C

Table 1 (Cont'd)

Piston Data

Piston Diameter : 129.9 mm

Piston Height : 157 mm

Distance from the Deck to TDC : 1.5 mm

Piston Pin Weight : 1.828 kg

The Type of Oil

SAE 30

Stribeck Curve Data

Friction Coefficient : 0.1

The Nominal Minimum Oil Film Thickness for Mixed Lubrication (λ) : $1 \leq \lambda \leq 5$

Ring Gap Data

Upper Compression Ring Gap Area : 0.277 mm^2

Lower Compression Ring Gap Area : 0.245 mm^2

Oil Ring Gap Area : 0.865 mm^2

Upper Compression Ring Groove Area : 96 mm^2

Lower Compression Ring Groove Area : 105 mm^2

Oil Ring Groove Area : 147 mm^2

Land and Groove Volume Data

Upper Compression Ring Groove Volume : 991 mm^3

Lower Compression Ring Groove Volume : 952 mm^3

Oil Ring Groove Volume : 721 mm^3

Second Land Volume : 4180 mm^3

Third Land Volume : 689 mm^3

Table 1 (Cont'd)

Upper Compression Ring Data

Ring Thickness : 3.91 mm

Ring Width : 5.20 mm

Ring Diametral Tension : 51.59 N

Ring Weight : 0.045 kg

Ring Location : 29.8 mm

Surface Roughness : 0.127 μm

Groove Gap Width : 0.244 mm

Ring Face Type : Parabolic

Crown Height : 0.014 mm

Crown Offset : 0

Lower Compression Ring

Ring Thickness : 2.84 mm

Ring Width : 5.18 mm

Ring Diametral Tension : 44.48 N

Ring Weight : 0.035 kg

Ring Location : 47.4 mm

Surface Roughness : 0.127 μm

Groove Gap Width : 0.264 mm

Ring Face Type : Parabolic

Crown Height : 0.097 mm

Crown Offset : 1.143 mm

Oil Ring Data

Ring Thickness : 2.84 mm

Ring Width : 5.18 mm

Table 1 (Cont'd)

Ring Diametral Tension : 48.93 N

Ring Weight : 0.035 kg

Ring Location : 54.6 mm

Surface Roughness : 0.127 μm

Groove Gap Width : 0.373 mm

Ring Face Type : Parabolic

Crown Height : 0.082 mm

Crown Offset : 0.914 mm

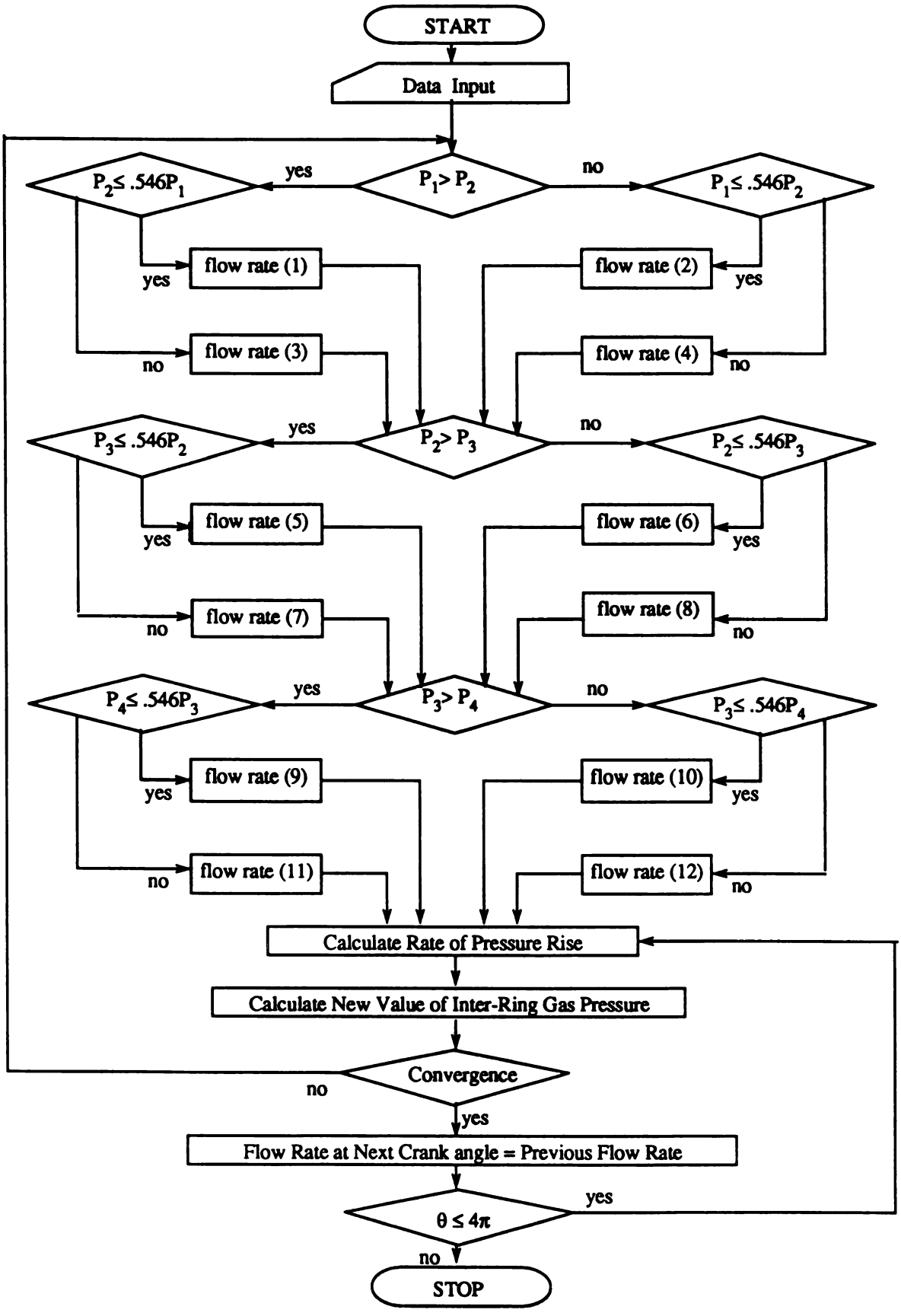

Figure 3.4 Procedure for the determination of inter-ring gas pressures

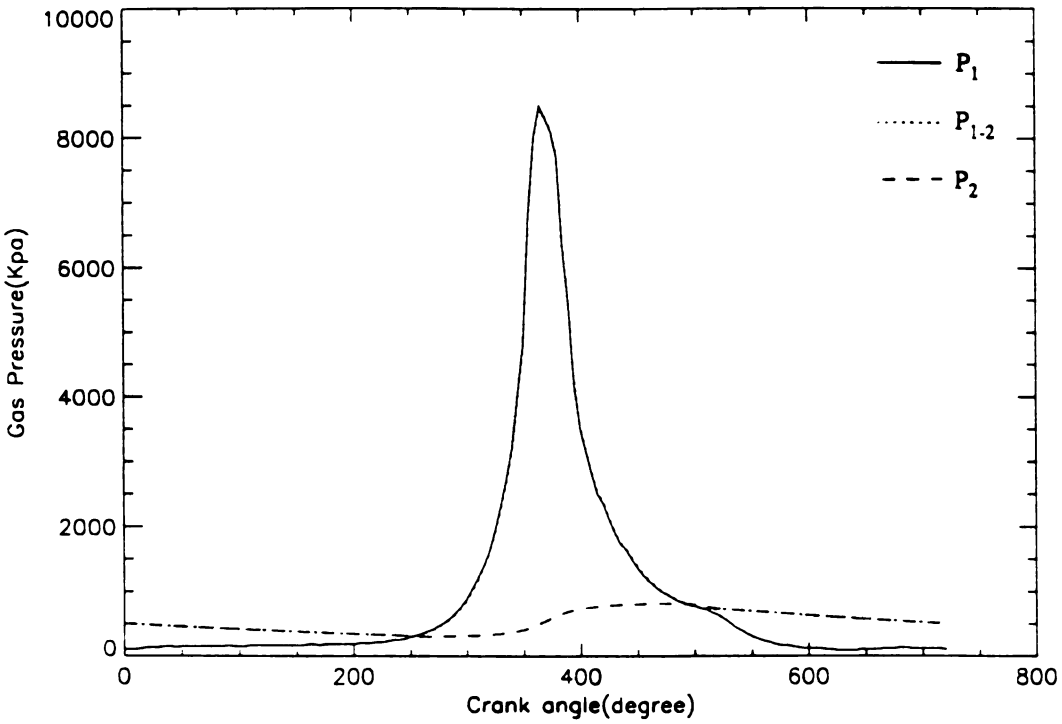

Figure 3.5 Gas pressure in each region at an engine speed of 1200 rpm

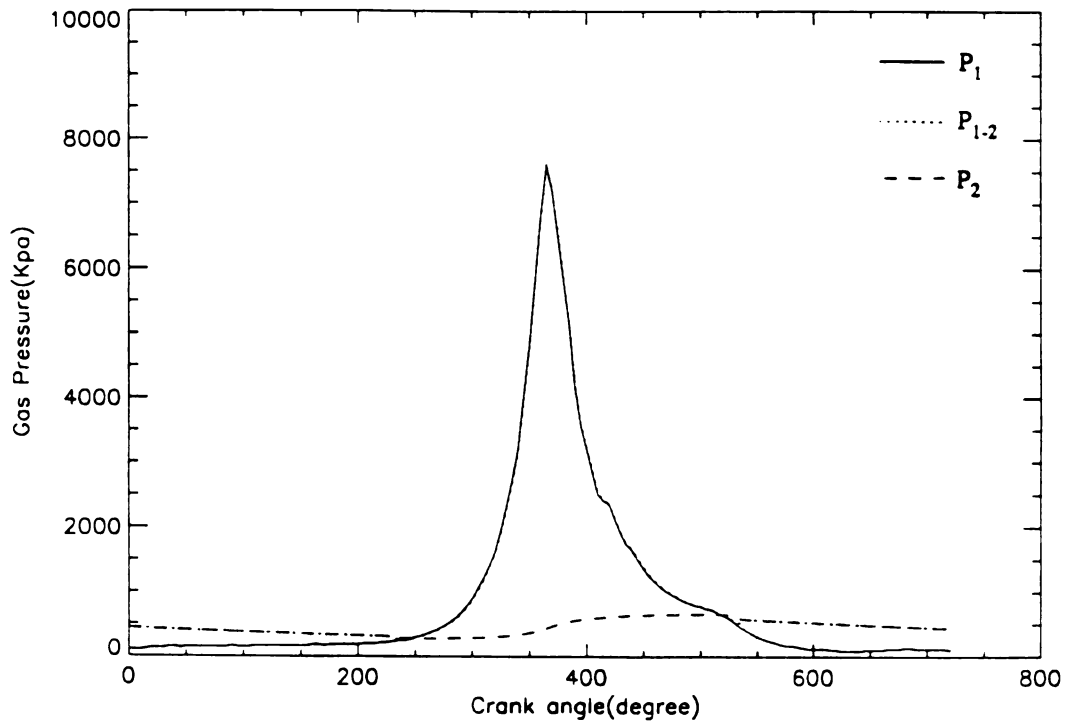

Figure 3.6 Gas pressure in each region at an engine speed of 1500 rpm

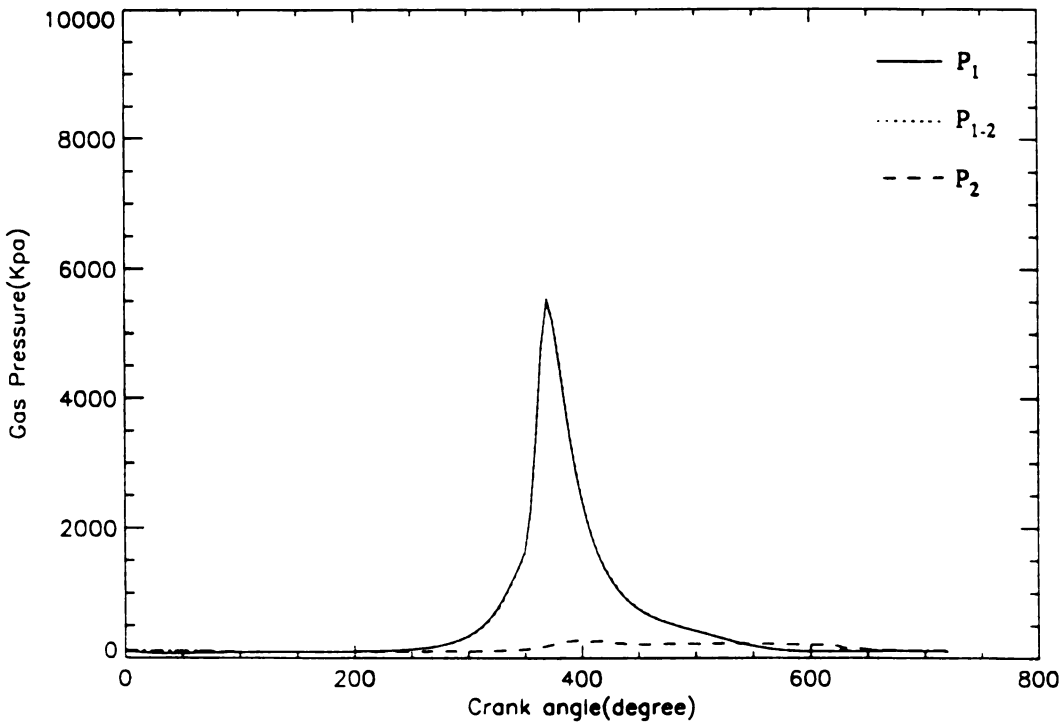

Figure 3.7 Gas pressure in each region at an engine speed of 1800 rpm

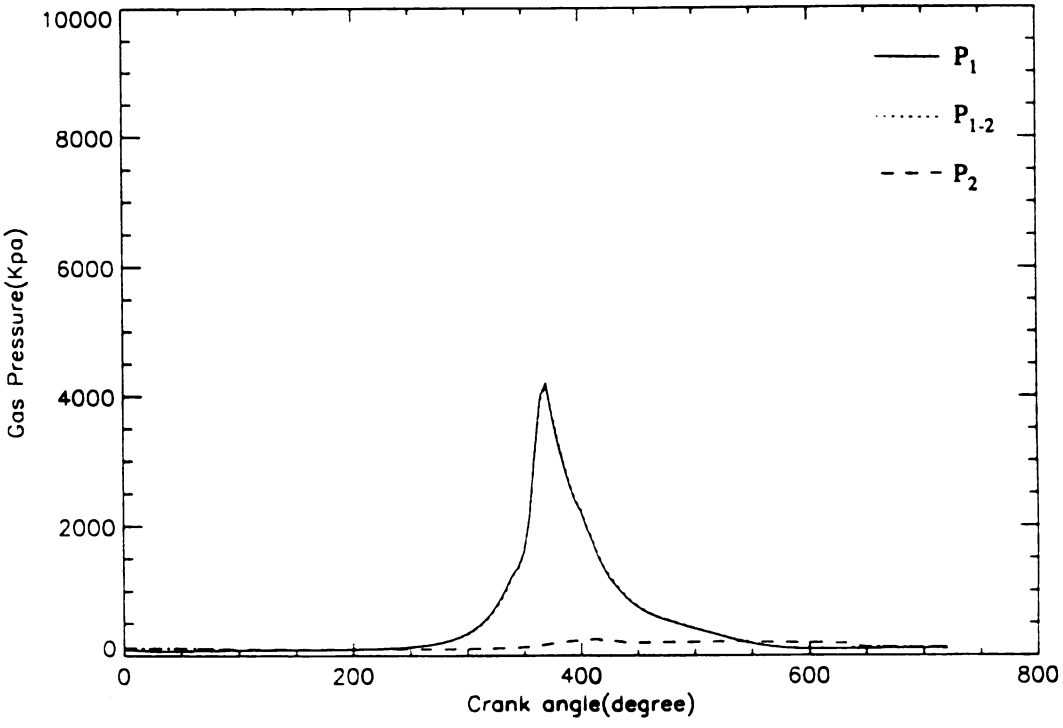

Figure 3.8 Gas pressure in each region at an engine speed of 2100 rpm

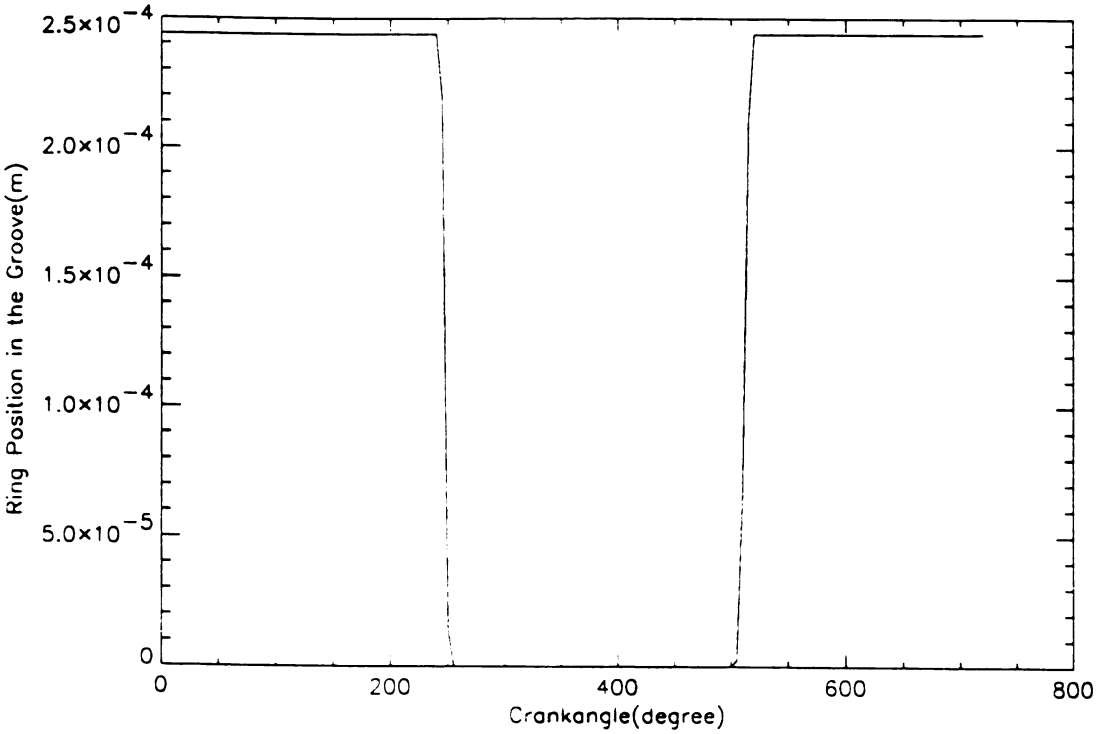

Figure 3.9 Ring position in the groove at an engine speed of 1200 rpm

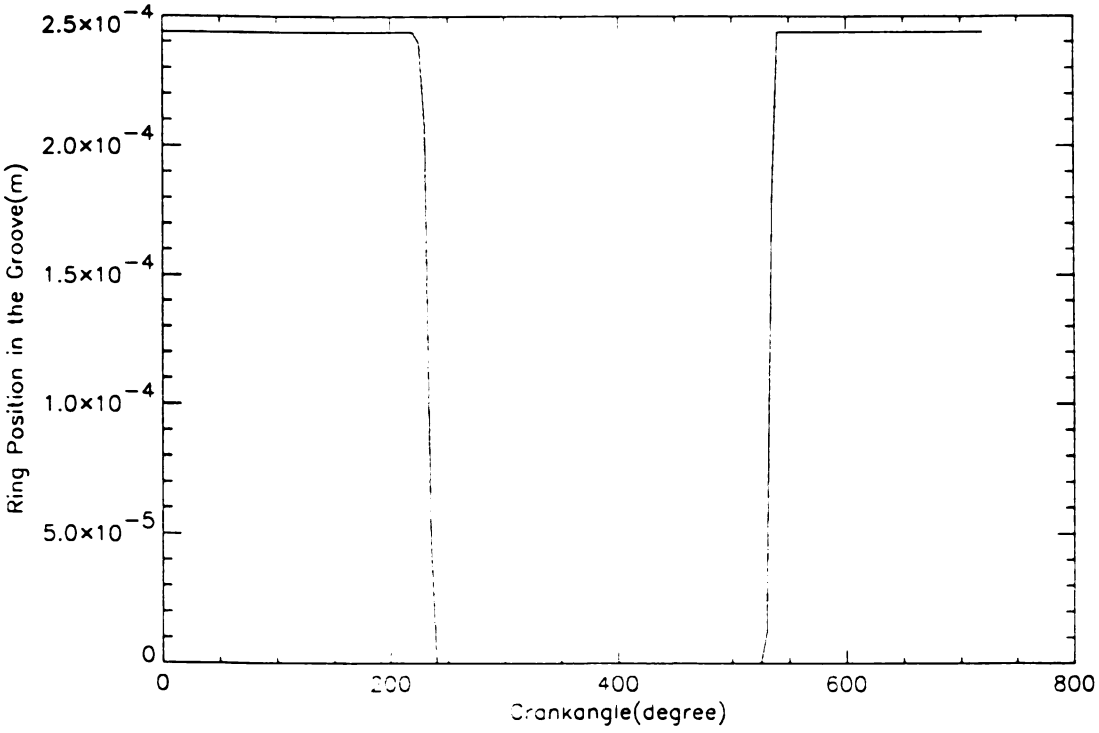

Figure 3.10 Ring position in the groove at an engine speed of 1500 rpm

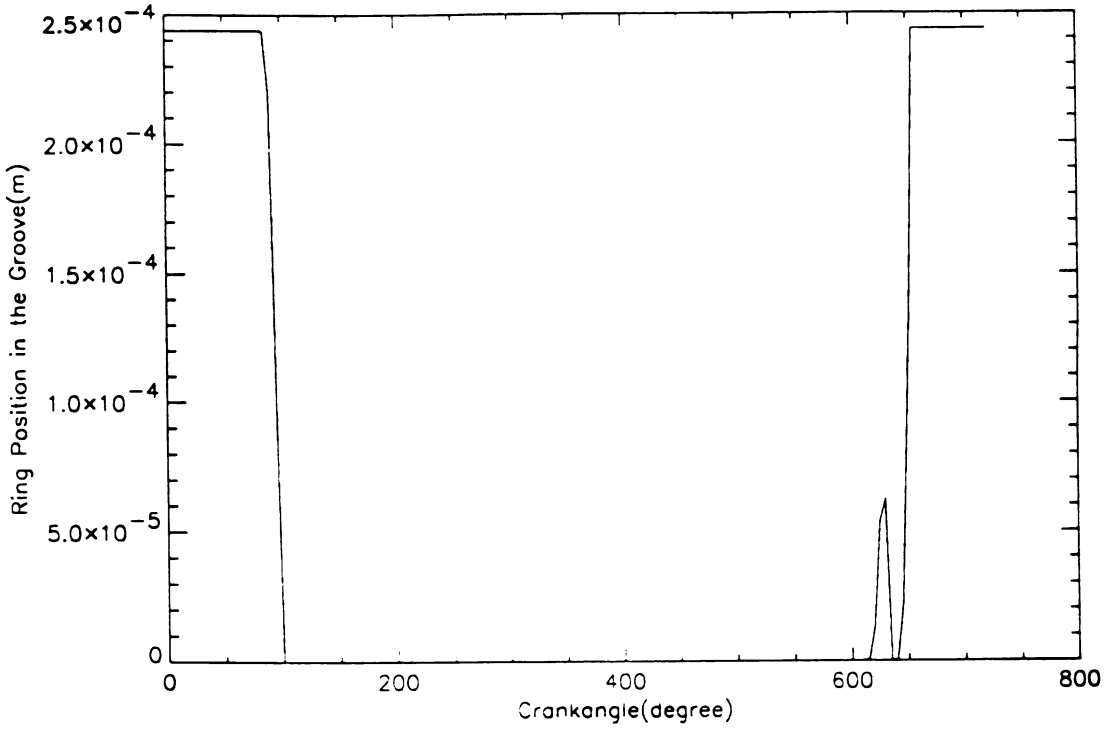

Figure 3.11 Ring position in the groove at an engine speed of 1800 rpm

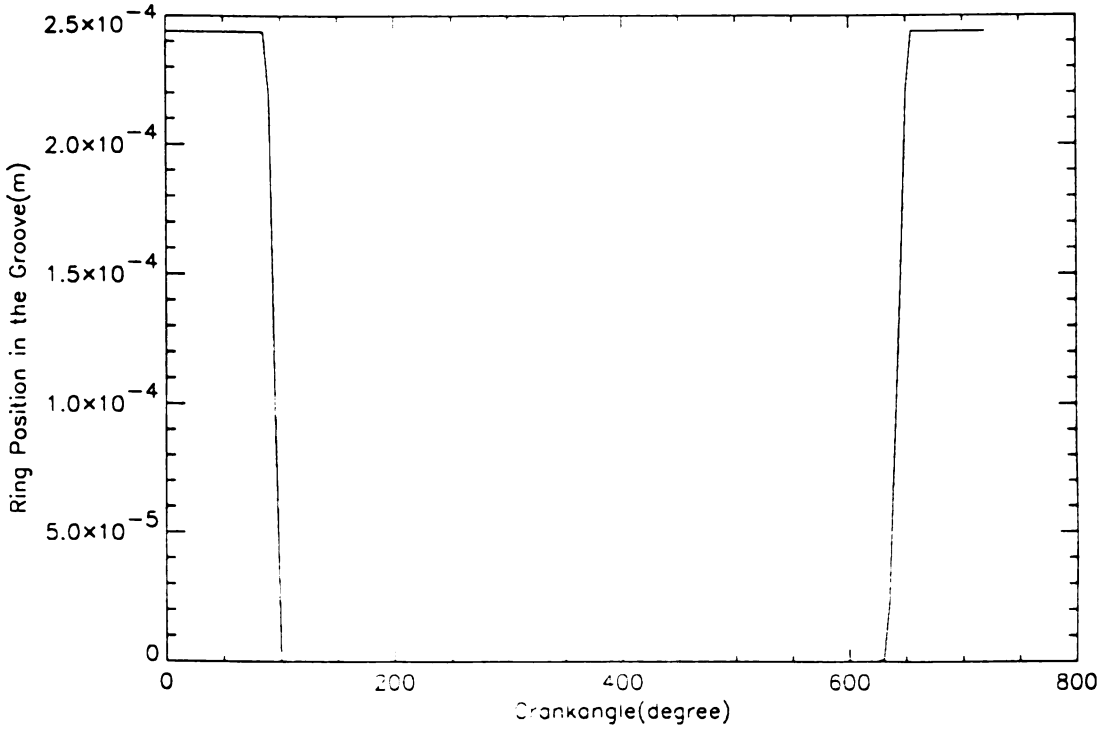

Figure 3.12 Ring position in the groove at an engine speed of 2100 rpm

CHAPTER 4

THE ANALYSIS OF FIRE RING FRICTION

The geometry of a piston in the cylinder bore and the velocity of a piston affect the lubrication conditions of the ring. Moreover, ring friction might be changed according to the engine speed and power output. These topics are reviewed prior to the ring friction analysis.

4. 1 Piston Kinematics

The basic geometries of a reciprocating engine are defined by the ratio of cylinder bore to piston stroke (R_{bk}); ratio of connecting rod length to a crank radius (R_{La}); and the compression ratio (r_c), which represents the ratio of maximum cylinder volume (V_c+V_d) to minimum cylinder volume (V_c) shown in Figure 4.1. In addition, the stroke and crank radius are related by

$$K = 2a \tag{4.1}$$

Typical values of these parameters are given as follows [2]:

1) r_c = 8 to 12 for SI (Spark-Ignition) engines, and r_c =12 to 24 for CI (Compression-Ignition) engines.
2) R_{bk} = 0.8 to 1.2 for small- and medium-size engines, decreasing to about 0.5 for large slow-speed CI engines.
3) R_{La} = 3 to 4 for small and medium-size engines, increasing to 5 to 9 for large slow-speed CI engines.

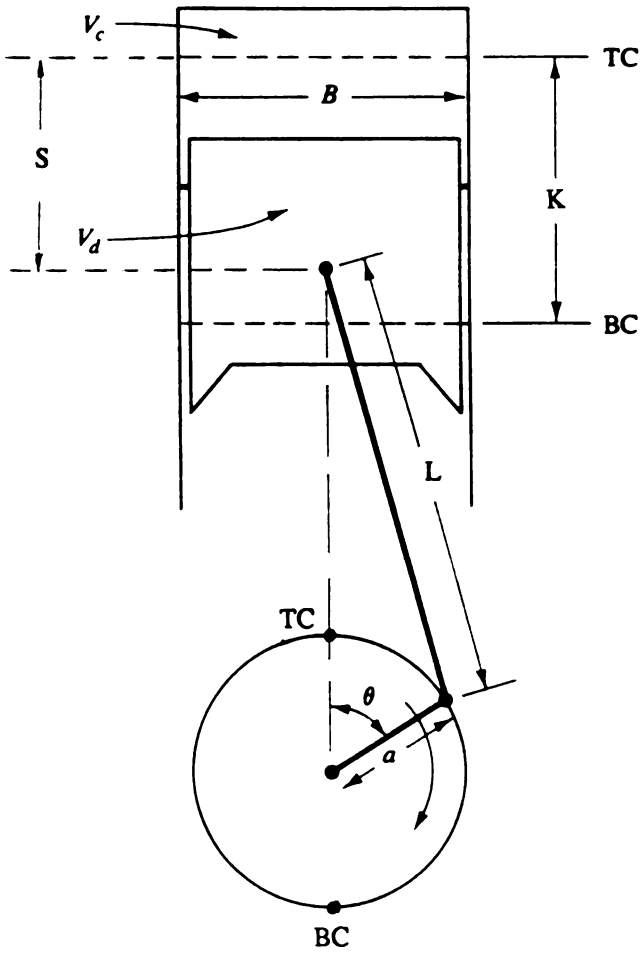

Figure 4.1 The geometry of a reciprocating piston engine, where B = bore, K = stroke, L = connecting rod length, a = crank radius, θ = crank angle[2]

The location of the piston depicted in Figure 4.1 can be determined as a function of crank angle as follows :

$$S(\theta) = L + a\,(1 - \cos\theta) - (L^2 - a^2 \sin^2\theta)^{1/2} \tag{4.2}$$

where the crank angle is defined as

$$\theta = \omega t \tag{4.3}$$

with the angular velocity, ω, obtained from

$$\omega = 2\pi N / 60 \tag{4.4}$$

where N is the rotational speed of the crank shaft in rev/min. Therefore, for one cycle of four-stroke engine operation

$$0 \le t \le 4\pi/\omega \tag{4.5}$$

Thus, the mean piston speed is expressed as

$$\begin{aligned} U_{mean} &= K / (\theta / \omega) \\ &= KN / 30 \end{aligned} \tag{4.6}$$

The instantaneous piston velocity is given by

$$\begin{aligned} U_p(t) &= [dS(\theta)/d\theta](d\theta / dt) \\ &= \omega[a \sin\theta + a^2 \sin\theta \cos\theta (L^2 - a^2 \sin^2\theta)^{-1/2}] \end{aligned}$$

$$= \omega[a \sin\omega t + (a^2/2)\sin 2\omega t\,(L^2 - a^2\sin^2\omega t)^{-1/2}] \qquad (4.7)$$

Differentiating Equation (4.7), the piston acceleration is found to be

$$\begin{aligned} a_p(t) &= \omega^2 a \cos\omega t + \omega^2 a^2 \cos^2\omega t \cdot (L^2 - a^2\sin^2\omega t)^{-1/2} \\ &\quad - \omega^2 a^2 \sin^2\omega t \cdot (L^2 - a^2\sin^2\omega t)^{-1/2} \\ &\quad + \omega a^2 \sin\omega t \cos\omega t(-1/2)\cdot(L^2 - a^2\sin^2\omega t)^{-3/2}\cdot(-2\,a^2\sin\omega t\cos\omega t\cdot\omega) \\ &= \omega^2 a \cos\omega t + \omega^2 a^2 \cos 2\omega t \cdot (L^2 - a^2\sin^2\omega t)^{-1/2} \\ &\quad + \omega^2 a^4 \sin^2\omega t \cos^2\omega t\cdot(L^2 - a^2\sin^2\omega t)^{-3/2} \end{aligned} \qquad (4.8)$$

4. 2 The Indicated Mean Effective Pressure and Brake Power

One of the most significant indicators of the performance of internal combustion engine is the IMEP (Indicated Mean Effective Pressure). IMEP is defined as an average work delivered at the piston face during a complete engine cycle.

From a thermodynamic analysis, the work performed on or by a chemical system during a volumetric change in state is

$$W = \int_v P\,dV \qquad (4.9)$$

where W = work

P = cylinder pressure

V = cylinder volume

IMEP is obtained by normalizing this indicated work with the total cylinder displacement volume [59].

$$IMEP = (1/V_D) \int_v P\, dV$$

$$= (1/V_D) \int_0^{4\pi} P\, (dV/d\theta) d\theta \qquad (4.10)$$

where V_D denotes the total cylinder displacement volume. Brake mean effective pressure is determined as

$$BMEP = \eta_e \cdot IMEP \qquad (4.11)$$

where η_e denotes a mechanical efficiency. A mechanical efficiency of 90% has been assumed in this analysis. Therefore, the brake power is obtained from

$$BP = BMEP \cdot V_D \cdot N_{max} / n_R \qquad (4.12)$$

where N_{max} represents the maximum rated engine speed obtained for a maximum mean piston speed, and n_R is the number of crank revolutions for each power stroke per cylinder (two for four-stroke cycles, one for two-stroke cycles). These definitions are used with the data available in the literature to develop pressure-crank angle information for the conditions at which the power output is known.

4. 3 Reynolds Equation

The oil film thickness developed between the ring assembly and cylinder bore needs to be determined in order to predict oil consumption and friction loss. However, the minimum oil film thickness cannot be determined easily since it can be taken as a function of the surface roughness [28]. It has been observed that the ring can tilt, rotate, or move axially up and down in the groove throughout the engine cycle [49, 56, 57, 60, 61]. However, here the ring motion in the groove is neglected since it is negligibly small compared to piston motion, and thus has little effect on the ring friction [62].

Therefore, for two dimensional flow of an incompressible lubricant, the Navier-Stokes equation for the liquid film motion reduces to a Reynolds equation of the form [2, 29, 30, 63]

$$\partial/\partial x[(h^3/\mu)\cdot(\partial p/\partial x)] + \partial/\partial y[(h^3/\mu)\cdot(\partial p/\partial y)] = -6U_p(\partial h/\partial x) + 12(\partial h/\partial t) \qquad (4.13)$$

where h = oil film thickness

μ = oil viscosity

p = oil film pressure

U_p= piston velocity

x = coordinate in the axial direction

y = coordinate in the circumferential direction

t = time

The following assumptions were made to model hydrodynamic lubrication for the piston ring [21, 22, 28]:

1) The oil film between the ring and cylinder bore is sufficient for hydrodynamic lubrication, thus body forces are ignored.

2) The oil viscosity does not change around the ring face but may change with temperature at different positions along the bore.

3) The lubricant is Newtonian and incompressible.

4) The flow is laminar.

5) There is no slip at the boundaries.

The lubrication of piston rings in firing engines is periodic with a period of $4\pi/\omega$ for a four-stroke engine. Hence

$$p(t) = p(t+4\pi/\omega)$$
$$h(t) = h(t+4\pi/\omega) \qquad (4.14)$$

If axial symmetry is assumed such that there is no flow of lubricant in the circumferential direction between the ring and cylinder bore, and the lubricant is assumed to be an incompressible fluid having a mean viscosity (μ) throughout the oil film at any specified crank angle, then Reynolds equation can be expressed as

$$\partial/\partial x[h^3(\partial p/\partial x)] = -6\mu U_p(\partial h/\partial x) + 12\mu(\partial h/\partial t) \qquad (4.15)$$

A first integration of Equation (4.15) leads to an expression for the axial pressure gradient in the lubricant film

$$dp/dx = -6\mu U_p/h^2 + 12\mu(x/h^3)(\partial h/\partial t) + C_1/h^3 \qquad (4.16)$$

where C_1 is the integration constant. Therefore, the pressure distribution of the lubricant between the ring and cylinder bore can be found by numerically integrating Equation (4.16).

$$p = -6\mu U_p I_1 + 12\mu(\partial h/\partial t)I_2 + C_1 I_3 + C_2 \tag{4.17}$$

where $I_1 = \int dx/h^2$

$I_2 = \int x/h^3 dx$

$I_3 = \int dx/h^3$

C_2 = an integration constant

The geometry of lubricated junction between a piston ring and cylinder bore is shown in Figure 4.2. Hence, the boundary conditions are given by

$$p = P_1 \quad \text{at } x=0$$
$$p = P_3 \quad \text{at } x=T_r \tag{4.18}$$

where P_1 and P_3 represent the pressure above and below the top ring, respectively, and T_r is the thickness of the ring. These conditions enable the integration constants C_1 and C_2 to be determined.

Since $dy = rd\theta$, the normal load on the top ring is expressed as

$$F_n = \int_0^{2\pi}\int_0^{T_r}(P_2 + P_{ten})rdxd\theta \tag{4.19}$$

where P_2 denotes the pressure behind the top ring, P_{ten} represents the pressure due to the radial tension of the ring, and r is the outside radius of the ring. Since axial sym-

metry has been assumed, the load equation is then written as

$$\int_0^{T_r} (P_2 + P_{ten}) r dx = \int_0^{T_r} p(x) r dx \tag{4.20}$$

where p(x) denotes the axial pressure distribution between the ring and the cylinder bore shown in Equation (4.17). Along with the geometry of the ring face profile, the cylinder bore temperatures at the ring locations for any crank angle has to be defined since the oil viscosity is greatly dependent on the temperature. By solving Equation (4.20) with Equation (4.17), oil film thickness and oil film pressure distribution can be determined. Further detailed discussion on the determination of the viscosity is followed in the next section.

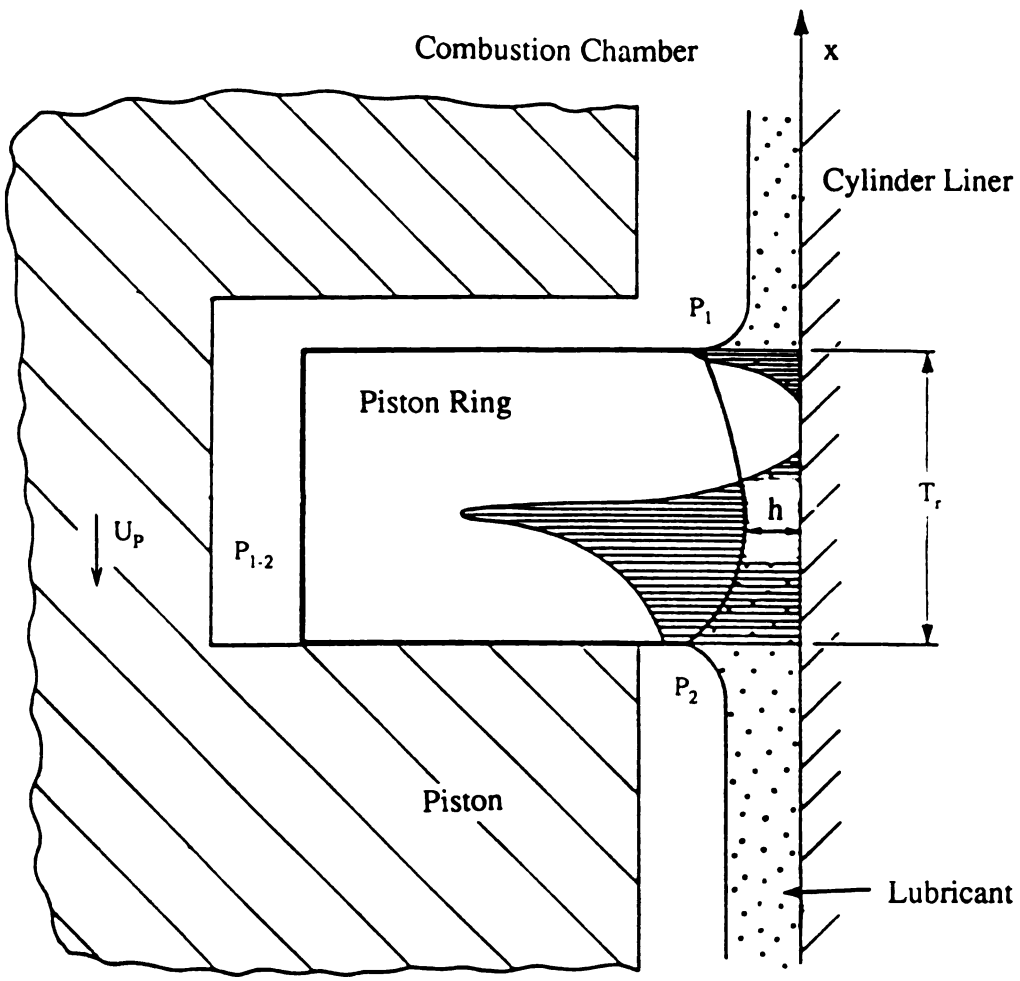

Figure 4.2 Geometry of lubricated junction between a piston ring and cylinder bore

4. 4 Lubrication

The lubricant between the ring and the cylinder bore reduces the frictional resistance of the engine to a minimum to ensure maximum mechanical efficiency, protects the ring and the bore against the wear, and also contributes to cooling the piston and the cylinder where the friction work is dissipated.

The temperature of the oil and engine parts it contacts, the presence of oxygen, the characteristics of the metal surfaces and debris, and the products of the fuel combustion influence the oxidation of the hydrocarbon components in lubricating oil [2]. Of these, high temperature is the primary factor. The top ring groove, where the temperature easily reaches 250°C is the most critical region. The lubricating oil under these conditions contributes to deposit formation. These deposits eventually lead to ring sticking, which results in excessive blowby [2].

The viscosity, which is the most important property of a lubricant is a function of temperature and pressure [28]. Generally, both friction and film thickness increase with increasing viscosity under normal engine operating conditions. The density of oil is little affected unless turbulent motion exists between the ring and the cylinder bore. The effect of temperature on the oil viscosity is much greater than its effect on any other physical properties. The viscosity of lubricating oils decreases with increasing temperature. Following is the one of the most frequently used viscosity and temperature relations.

$$\mu = a \cdot \exp[b/(T+c)] \tag{4.21}$$

where a is the viscosity at $T = \infty$. The constants in this equation have been determined from the known viscosity values at the specific temperature. They are shown in Table 2. The unit of viscosity is N-sec/m^2.

Table 2 Constants in the Vogel Viscosity Equation

SAE Grade	Vogel Constants		
	a	b	c
5 W	0.05567	900.0	110.8
10 W	0.04082	1066.0	116.5
15 W	0.06681	902.0	100.2
20 W	0.02370	1361.0	123.3
20	0.04987	1028.0	108.0
30	0.02370	1361.0	123.3
40	0.07227	1396.0	121.7
50	0.01963	1518.0	122.6

4. 5 Fire Ring Friction

The ring may undergo the different lubricated conditions depending on the effective oil film thickness and joint effective surface roughness between the ring and the cylinder bore.

The coefficient of friction can be expressed as [2]

$$f_0 = \alpha \cdot f_b + (1-\alpha) f_h \tag{4.22}$$

where f_b denotes the boundary friction coefficient of the metal-to-metal contact, f_h is the hydrodynamic friction coefficient, and α represents the metal-to-metal contact constant varying between 0 and 1. As $\alpha \rightarrow 1$, the lubrication regime approaches the

boundary regime, while as $\alpha \rightarrow 0$, it approaches the hydrodynamic regime. Here the lubricant film is sufficiently thick to separate completely the surfaces in relative motion. The mixed lubrication regime can be found where the transition between these regimes occurs. The lubrication regimes are determined from the Stribeck diagram [6, 23, 24] shown in Figure 4.3 by using the ratio of minimum oil film thickness to joint effective surface roughness.

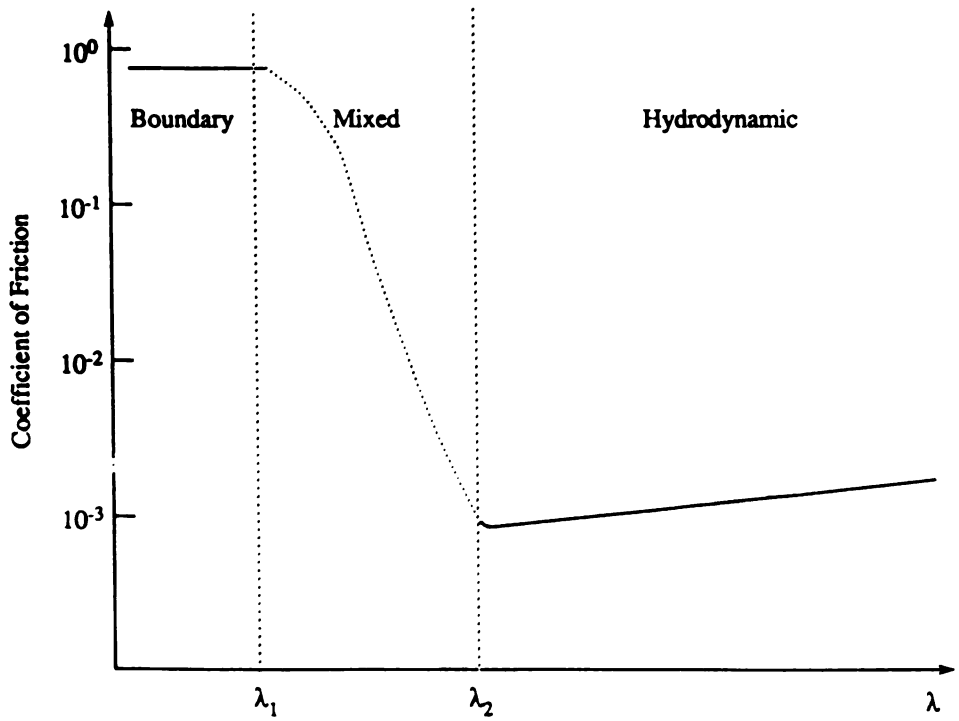

Figure 4.3 Stribeck diagram for a piston ring

(λ = nominal minimum film thickness)

4.5.1 Hydrodynamic Lubrication

If the ratio of effective oil film thickness to the joint effective surface roughness is large enough, then friction is caused by the viscous shear of the lubricant and the pressure gradient through the lubricant. Since the lubricant is assumed to behave as a Newtonian fluid, the shear stress is proportional to the velocity gradient across the film. Therefore, the hydrodynamic friction force per unit area of the sliding surface in the axial direction is defined as [28]

$$f_x = h/2(dp/dx) + \mu U_p/h \tag{4.23}$$

where dp/dx = pressure gradient in the axial coordinate

x = coordinate in the axial direction

h = oil film thickness

μ = oil viscosity

U_p= piston speed

The evaluation of the oil film thickness and pressure gradient in the axial coordinate have been discussed already in Section 4.3. Here the hydrodynamic friction force can be determined by integrating Equation (4.23) over the nominal contact area between the ring and cylinder bore [28].

$$F_f = \int_0^{2\pi}\int_0^{T_r} f_x \, r dx d\theta \tag{4.24}$$

where T_r denotes the thickness of the fire ring, and r is the radius of the ring. Since the axial symmetry throughout the circumference of the ring has been assumed, Equation (4.24) can be written as

$$F_f = 2\pi \int_0^{T_r} f_x \, r \, dx \tag{4.25}$$

Again, the geometry of the ring face profile needs to be defined in order to perform this integration numerically.

4. 5. 2 Mixed and Boundary Lubrication

A mixed lubrication occurs when the ratio of the elastohydrodynamic oil film thickness to the joint effective surface roughness is relatively small. To the hydrodynamic friction is then added metal-to-metal solid friction at the peaks of the asperities. Both hydrodynamic and boundary conditions coexist. The surface texture controls this transition from hydrodynamic to mixed lubrication, and load or speed variations or mechanical vibration may cause this transition to occur [2].

Boundary lubricated friction is calculated from [28]

$$F_f = f_0 F_n \tag{4.26}$$

where f_0 is the friction coefficient determined from the Stribeck diagram, and F_n is the normal load applied on the piston ring and the cylinder bore.

4. 6 Results and Discussion

The instantaneous piston locations of the Diesel engine used in this study is shown in Figure 4.4. Figures 4.5 and 4.6 illustrate the piston velocities and accelerations, respectively, at each engine speed. IMEP has been calculated in order to obtain the same power output under different engine speeds. Through the use of the P-V diagrams shown in Figures 4.7, 4.8, 4.9, and 4.10; computer simulations have been carried out to generate the combustion gas pressures that give the same power output used in the experimental study [51]. Table 3 shows the IMEP and power output at each engine speed calculated through this analysis.

Table 3 IMEP and Power Output under different engine operating conditions

Engine Speed (rpm)	Peak Pressure (kPa)	N_{max} (rev/sec)	IMEP (kPa)	Power Output (kW)
1200	8500	31.4	1356	244
1500	7600	39.3	1165	262
1800	5530	47.1	972	262
2100	4200	55.0	834	263

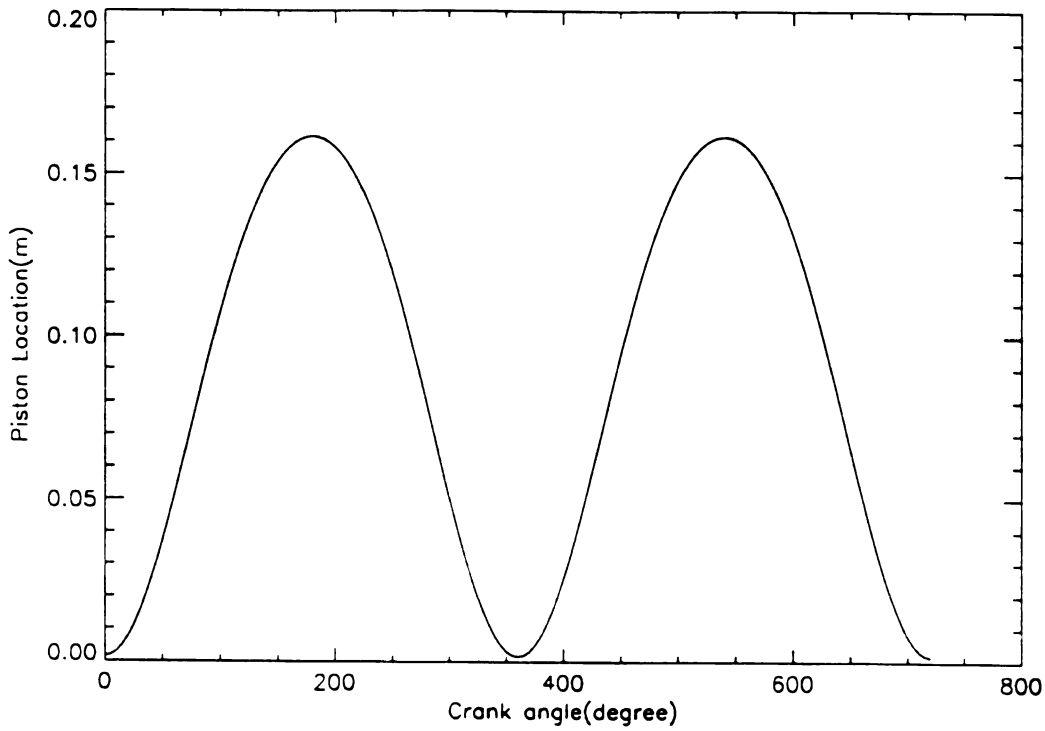

Figure 4. 4 Piston location of a Diesel engine

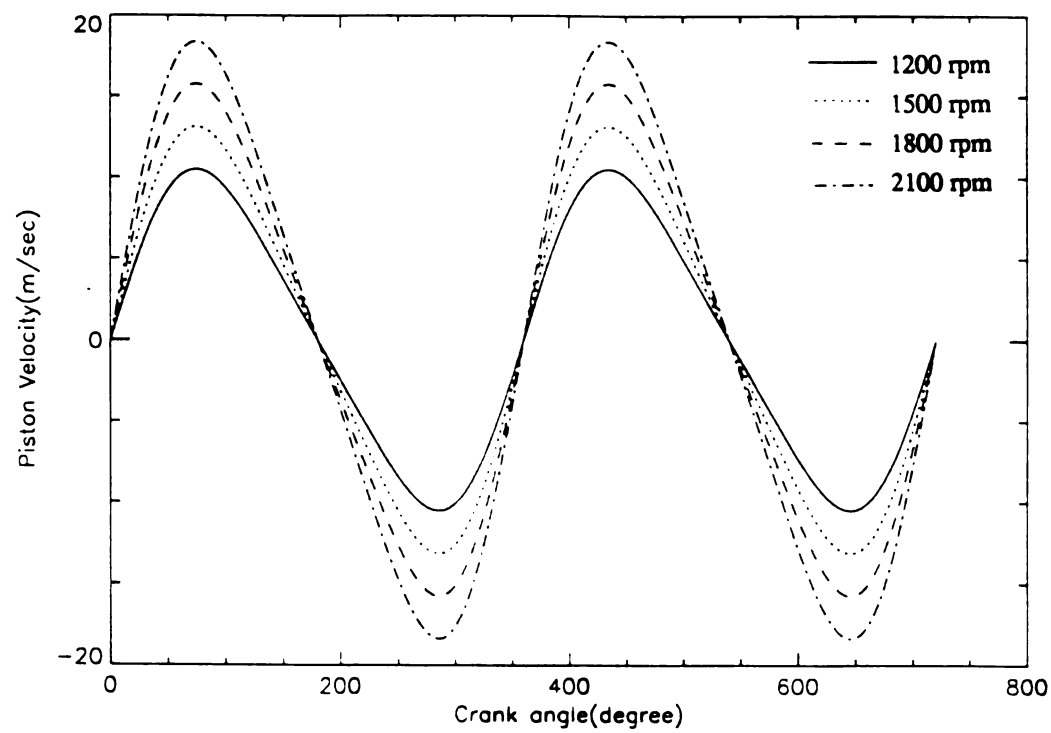

Figure 4.5 Piston velocity at each engine speed

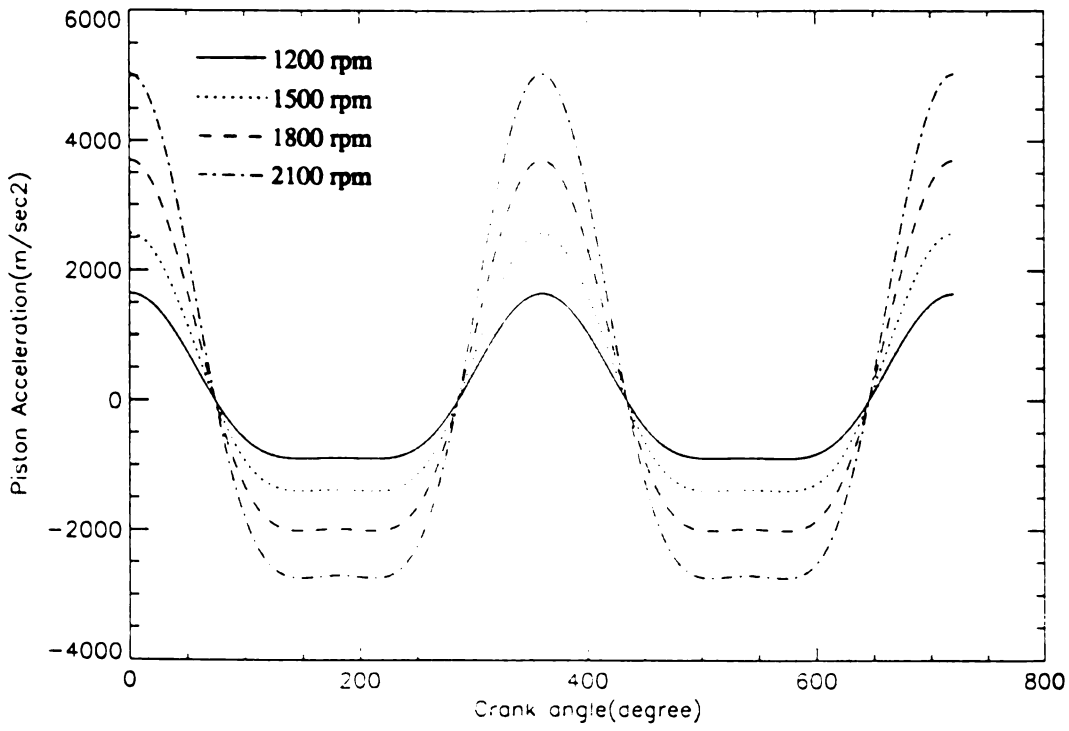

Figure 4.6 Piston acceleration at each engine speed

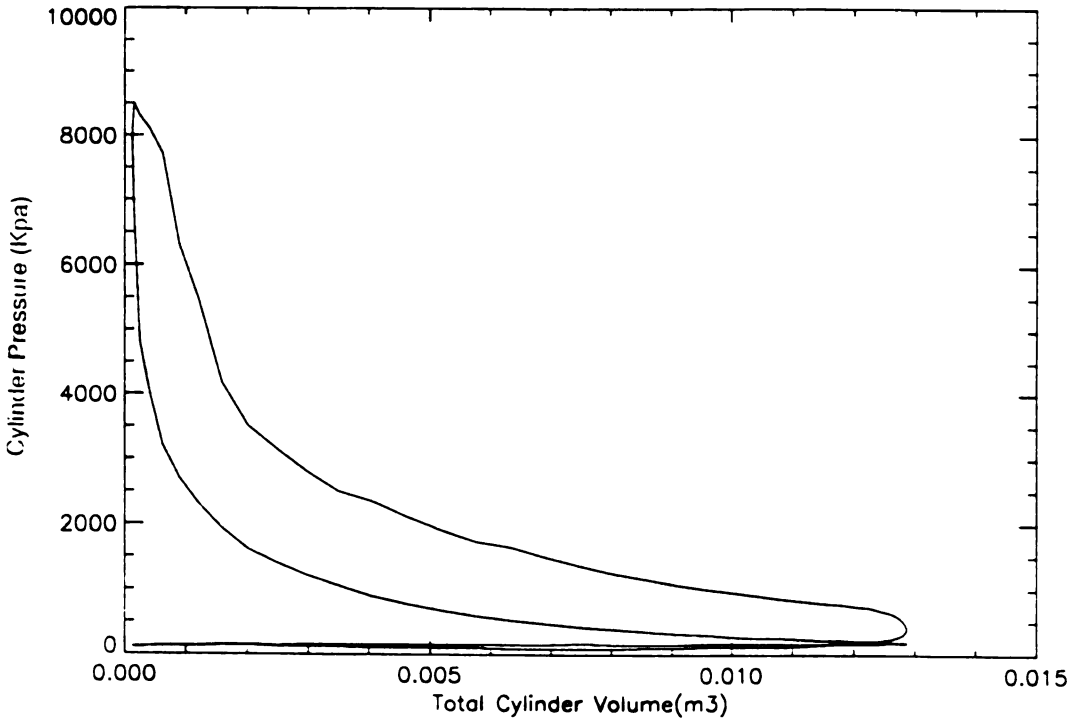

Figure 4.7 P-V diagram at an engine speed of 1200 rpm

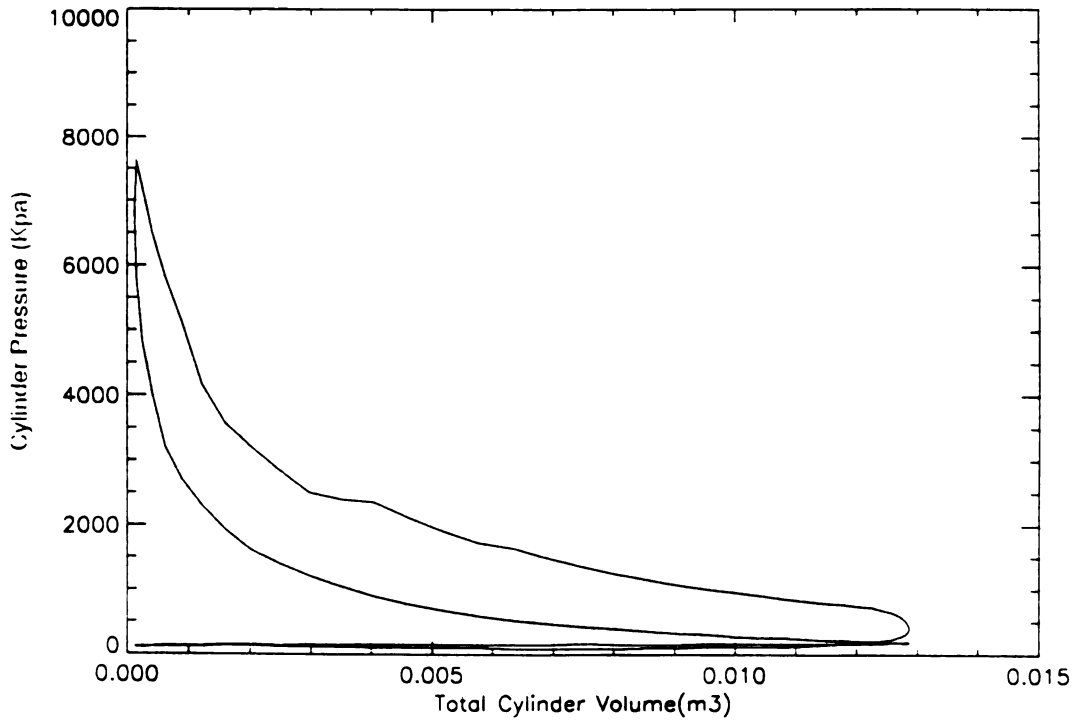

Figure 4.8 P-V diagram at an engine speed of 1500 rpm

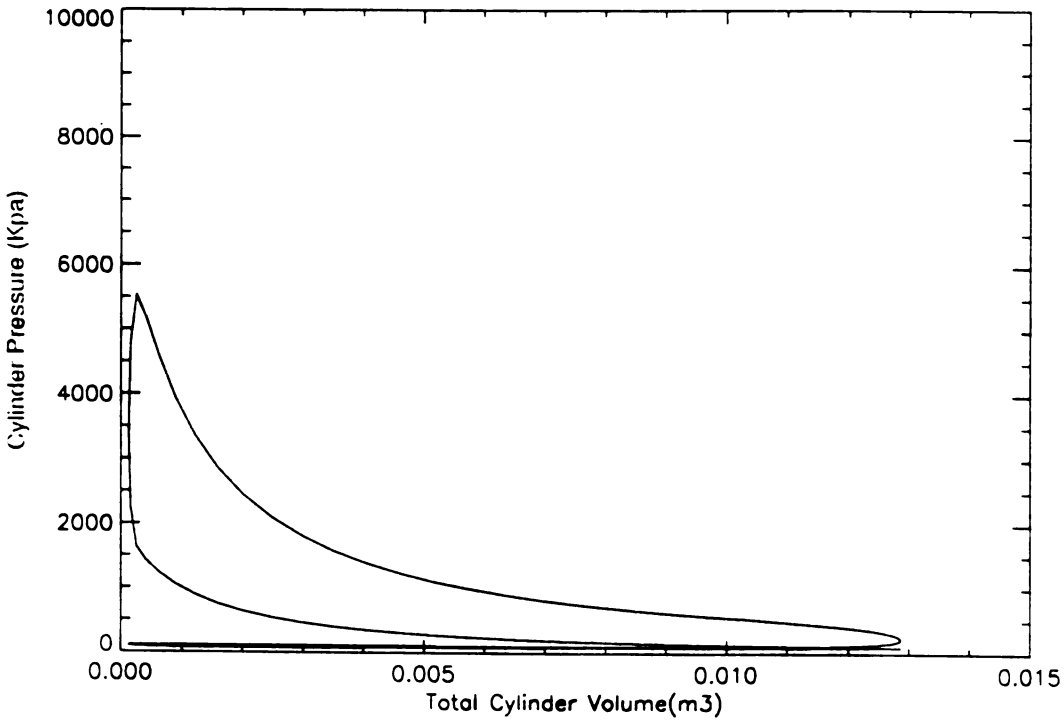

Figure 4.9 P-V diagram at an engine speed of 1800 rpm

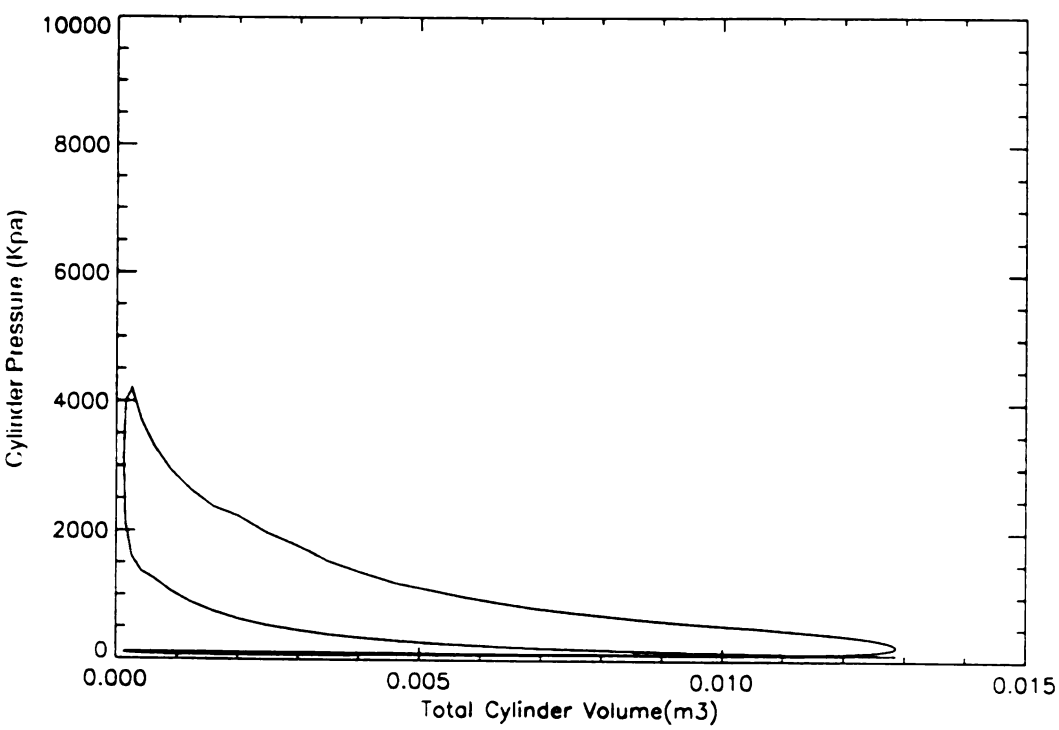

Figure 4.10 P-V diagram at an engine speed of 2100 rpm

It has been assumed that hydrodynamic lubrication begins at the nominal minimum film thickness, λ=5, while boundary lubrication begins at λ=1. Also, assuming axial symmetry throughout the circumference of the ring, the minimum oil film thicknesses shown in Figures 4.11 through 4.14 have been obtained with the aid of the ring dynamics analysis program. Some unexpected changes in the curve in the middle of the stroke are presumed to be due to the ring motion in the groove. As shown in these figures, the minimum oil film thicknesses tend to be lower just after each TDC and BDC. These are likely to be the points where the piston ring undergoes metallic contact with the cylinder wall. It seems that these effects are more prominent at the lower engine speeds than at the higher engine speeds since the combustion gas pressures are relatively higher at lower engine speeds, provided that the power outputs are the same. At the beginning of intake, and also at the end of exhaust, as shown in Figures 4.13 and 4.14, the minimum oil film thicknesses do not approach the level at which the mixed or boundary lubrication occurs. Presumably it would be due to the relatively small difference between the pressure behind the fire ring and the combustion gas pressure at these points. In other words, if this pressure difference is not large enough, the fire ring pushes the cylinder wall with a relatively lower load, and thus it results in the larger oil film thickness, which leads to hydrodynamic lubrication.

The ring friction forces are illustrated in Figures 4.15 through 4.18. As already expected from the results of the minimum oil film thicknesses, it is clear that the higher the engine speed, the lower the ring friction forces at the same power output.

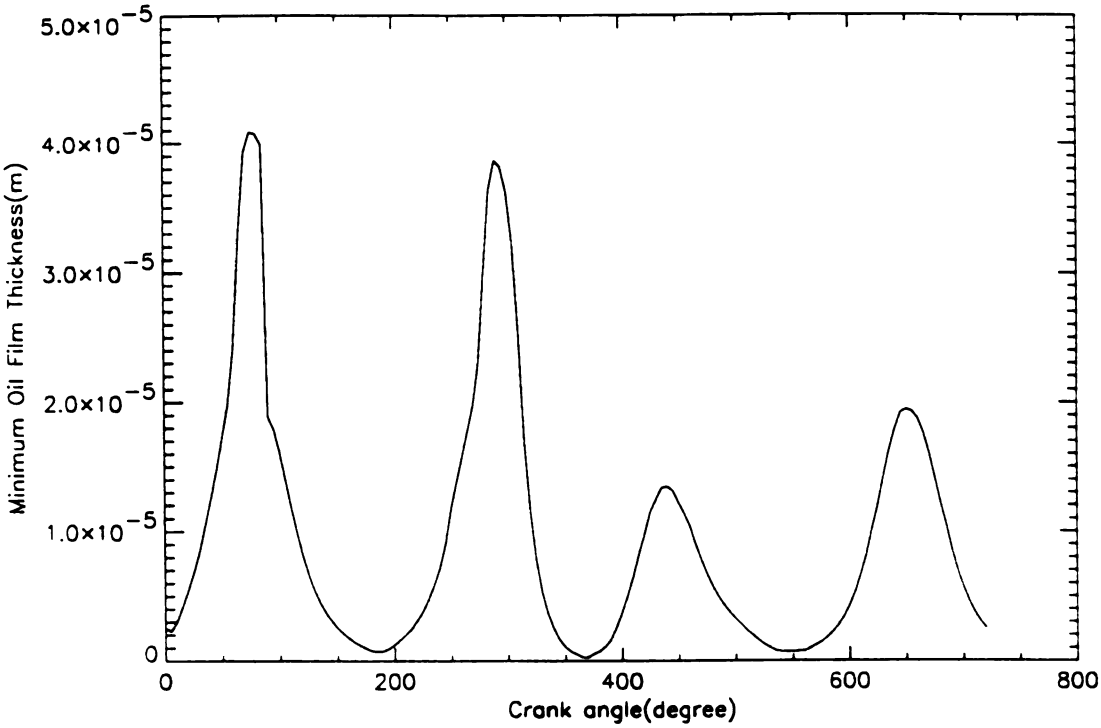

Figure 4.11 Minimum oil film thickness at an engine speed of 1200 rpm

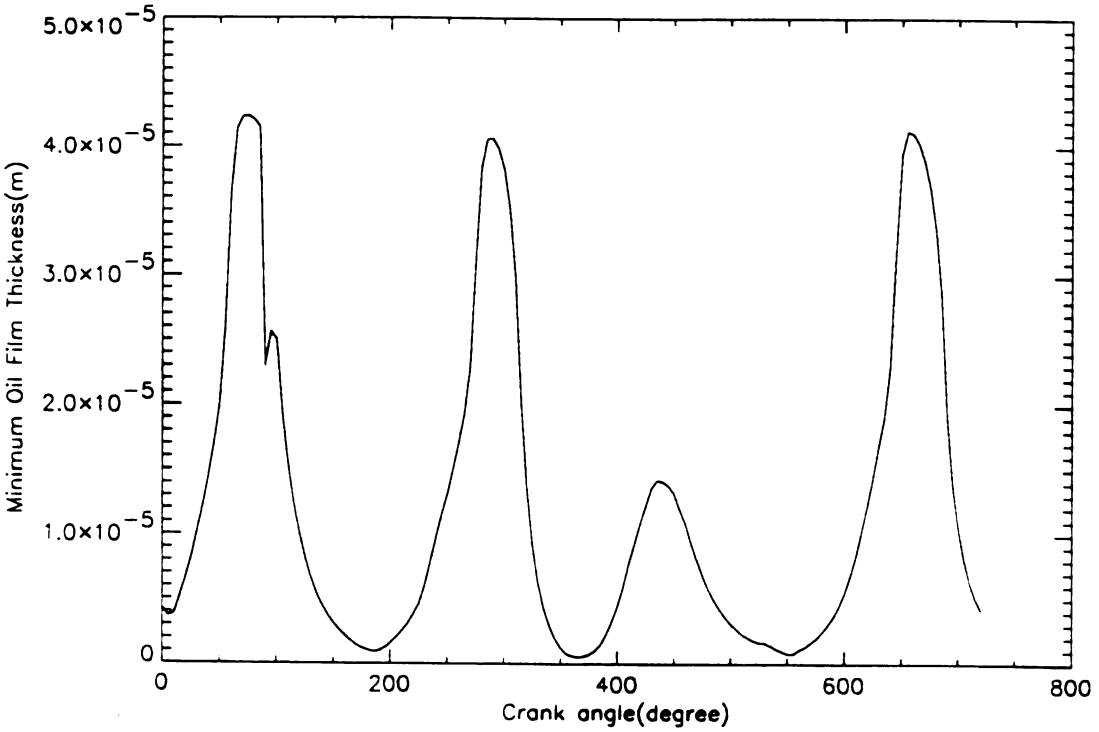

Figure 4.12 Minimum oil film thickness at an engine speed of 1500 rpm

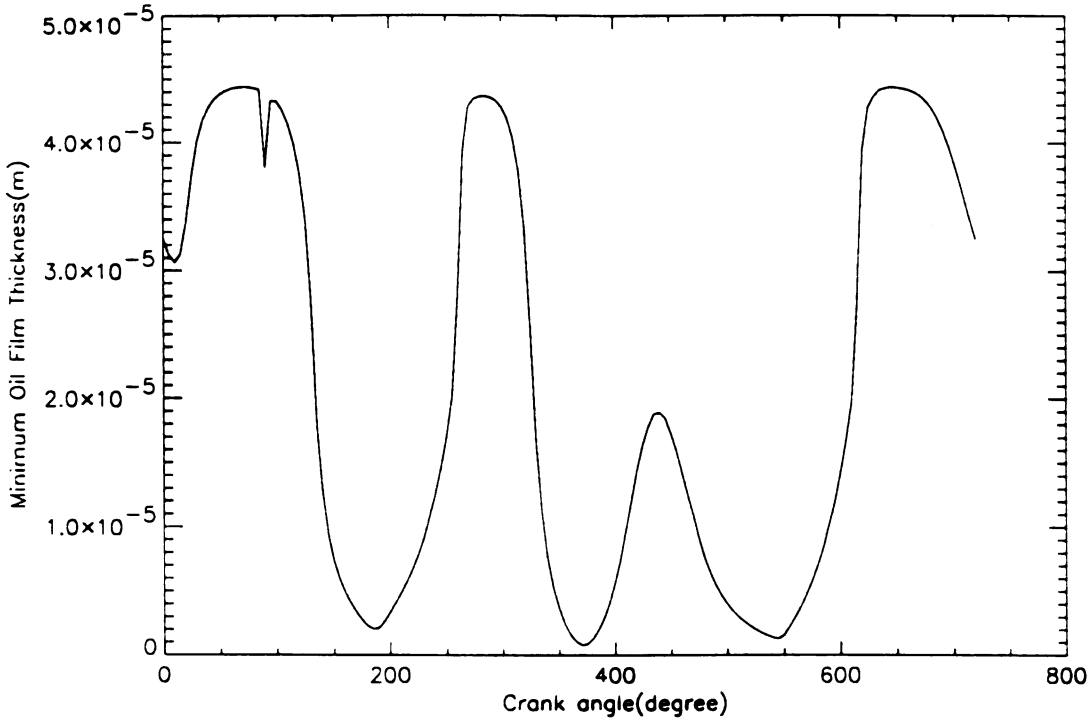

Figure 4.13 Minimum oil film thickness at an engine speed of 1800 rpm

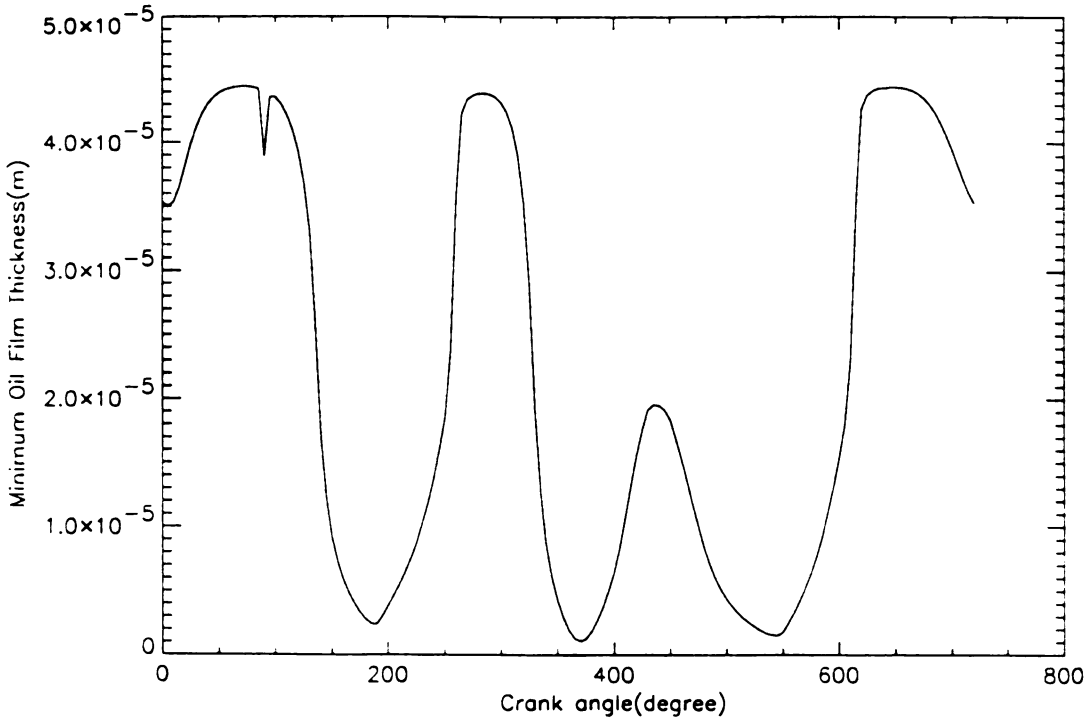

Figure 4.14 Minimum oil film thickness at an engine speed of 2100 rpm

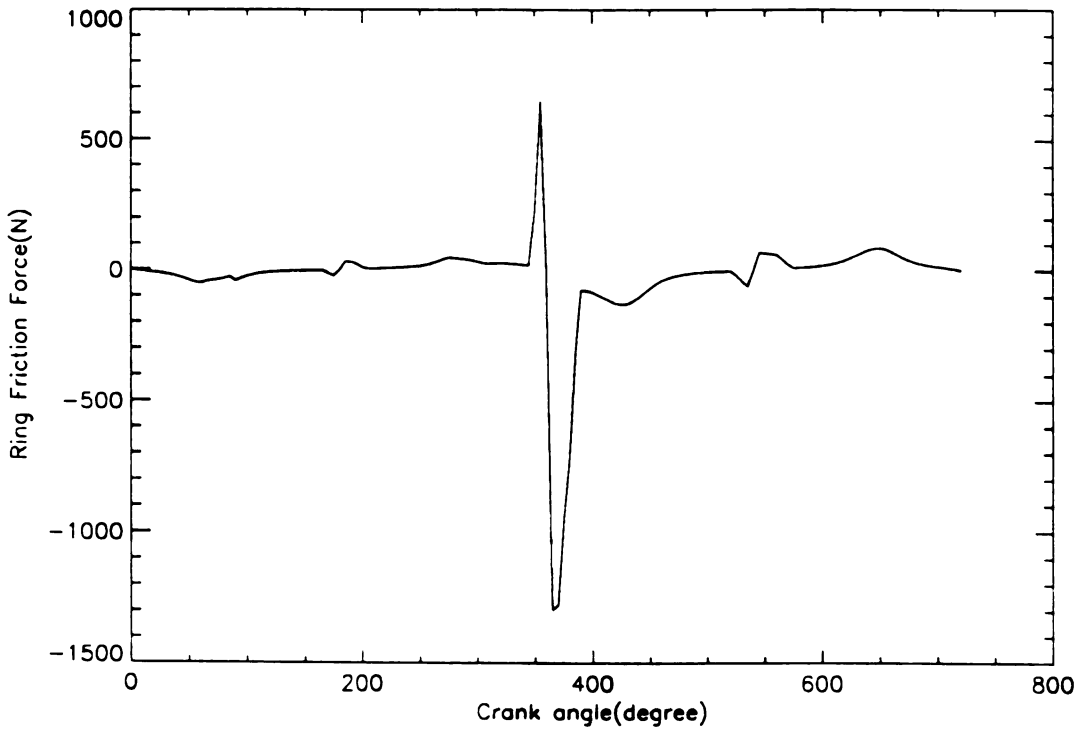

Figure 4.15 Ring friction force at an engine speed of 1200 rpm

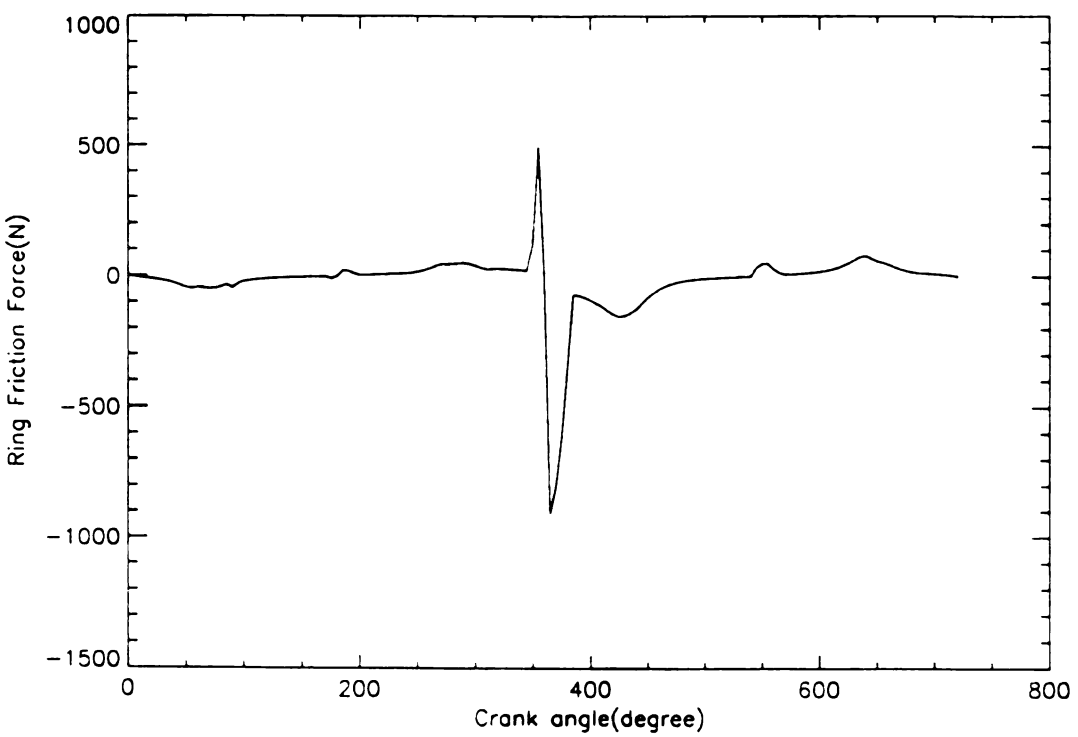

Figure 4.16 Ring friction force at an engine speed of 1500 rpm

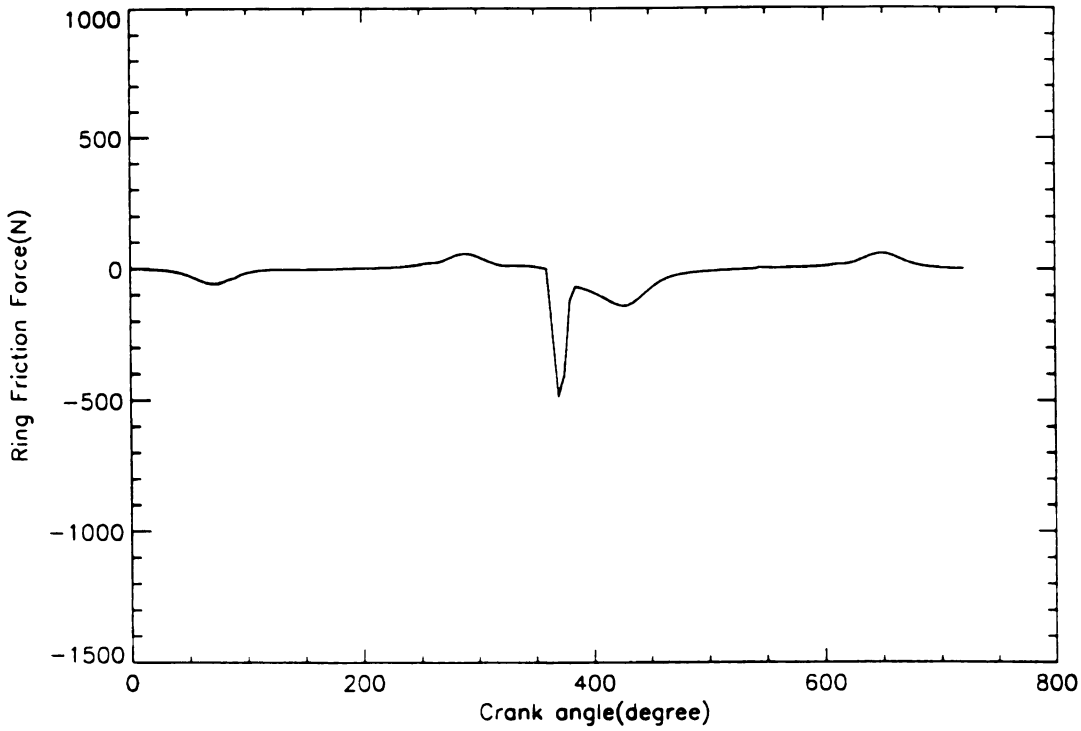

Figure 4.17 Ring friction force at an engine speed of 1800 rpm

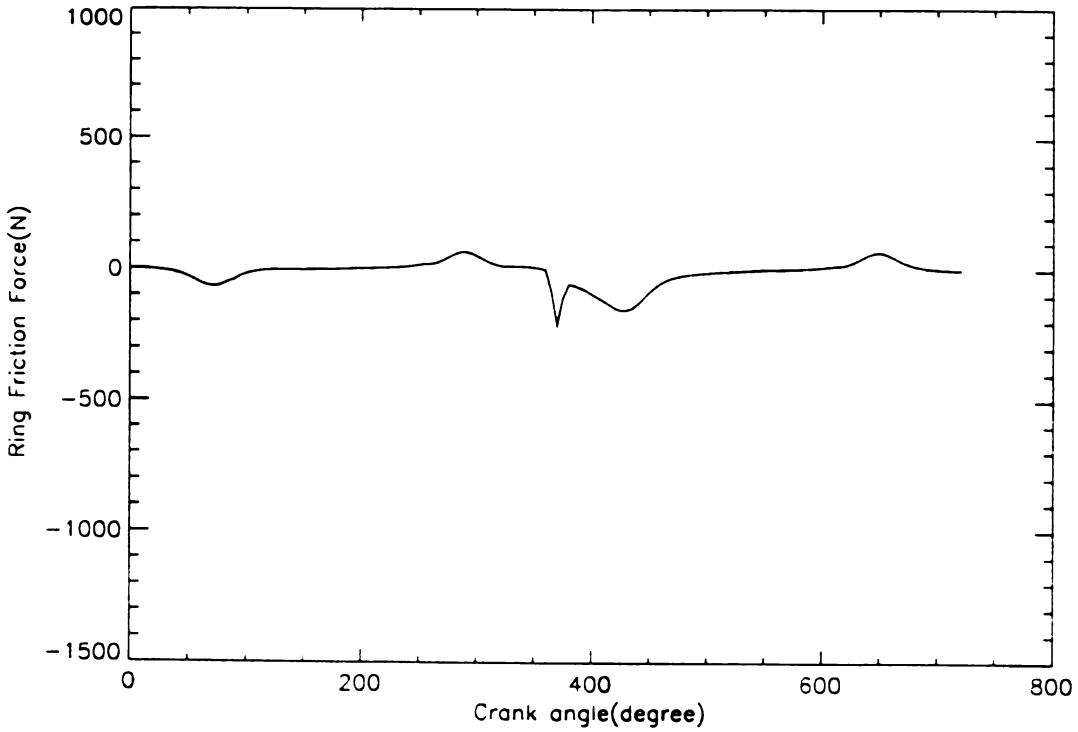

Figure 4.18 Ring friction force at an engine speed of 2100 rpm

CHAPTER 5

THE APPROXIMATE MODEL OF FIRE RING WEAR

5. 1 Relationship between Friction and Wear

There is no universal relationship between friction and wear. Relationships can be obtained only on a case-by-case basis since both friction and wear are interfacial phenomena [64, 65].

A high, steady friction coefficient may not result in high wear, but a high friction coefficient is a good indication of substantial wear. Frictional changes can be indicators of changes in wear mode, so even though the friction coefficient may not correlate in a predictive way with wear rate, it may still be an indicator of wear transitions. On the other hand, if the pre- and post- wear transition wear rates are known for a given tribosystem, then the total wear volume of a sliding system can be predicted by proportioning it in accordance with the wear process transition signaled by the frictional record. This is an indirect but potentially useful technique for monitoring tribosystems whose mild and severe wear rates are already known [65].

The presence of third bodies, transfer layers, and film are particularly relevant to the friction and wear relationship. It has been reported that the friction force would change over time as deposited interfacial media assume a greater role in sliding behavior, particularly when the interfacial wear product removal processes in the system are inefficient [65].

5. 2 Fire Ring Wear Model

The analysis of fire ring friction has been discussed in Chapter 4 through the use of the Reynolds equation, the load equation, and the Stribeck diagram. Here the procedure for determining the fire ring wear from known friction forces is presented.

An instantaneous friction work applied on the fire ring can be obtained from the ring friction force as follows:

$$\delta W_f = F_f \cdot \delta S \tag{5.1}$$

where F_f denotes the friction force calculated in Section 4.5 and δS is an instantaneous sliding distance on the cylinder bore. While, an instantaneous adhesive volume loss of the fire ring can be defined as [66, 67, 68]

$$\delta V_w = \eta F_n \delta S \tag{5.2}$$

where F_n represents the normal load applied on the fire ring, and η is the wear coefficient which characterizes the wear behavior of the fire ring on the cylinder wall. Equation (5.2) suggests that the wear coefficient (η) has the inverse dimension of hardness or the dimension of volume over energy.

The following assumptions were made to model fire ring wear:

1) The lateral motion of the piston and the ring motion in the groove are neglected, such that the ring friction forces are assumed to be parallel to the piston motion.
2) Axial symmetry is assumed throughout the circumference of the ring, such that cylinder bore distortions [69, 70] are not allowed in this model.
3) Fire ring wear is achieved by the plastic deformation of ring material.

4) Wear occurs only in the mixed or boundary lubrication regime [71] where the hydrodynamic film breaks down.

5) In the mixed or boundary lubrication regime, the amount of volume loss that occurs on the ring surface is proportional to the friction work applied on the ring.

In order to find a functional form for the wear coefficient, it is necessary to investigate the factors that affect ring wear. Particularly under mixed or boundary lubricated conditions, wear between the ring and the cylinder bore in relative motion is determined by the surface and lubricant properties, as well as the applied load and the sliding distance. The important parameters that might need to be included in Equation (5.2) are the effective nominal minimum film thickness, ring face profile, the ratio of true contact area to the nominal contact area, oil viscosity, and the hardness of the ring [2, 68]. Hence, it can be deduced that the wear coefficient would be a function of these system variables.

$$\eta = \eta(\zeta, \mu, \lambda, \kappa, \xi) \tag{5.3}$$

where ζ = ring face profile

μ = oil viscosity

$\lambda = h_f/\sigma$ = effective nominal minimum film thickness

$\sigma = (\sigma_1+\sigma_2)^{1/2}$

= joint effective surface roughness of the two contacting surface

h_f = elastohydrodynamic oil film thickness on the cylinder bore

$\kappa = A_t/A_0$

A_t = true contact area

A_0 = nominal area of contact

$\xi = H_c/H_r$

H_r = hardness of the ring

H_c = hardness of the cylinder

The oil film thickness under condition of hydrodynamic lubrication cannot be easily determined since it depends upon the topography of surfaces and the height of the asperities. Thus, the elastohydrodynamic oil film thickness that indicates the minimum oil film thickness from the surface roughness parameter and the effective nominal minimum film thickness (λ) have been introduced previously [72, 73].

O'Callaghan and Provert [74] reported that the true contact area between two abutting solids is only a fraction of the nominal area of contact as shown in Figure 5.1.

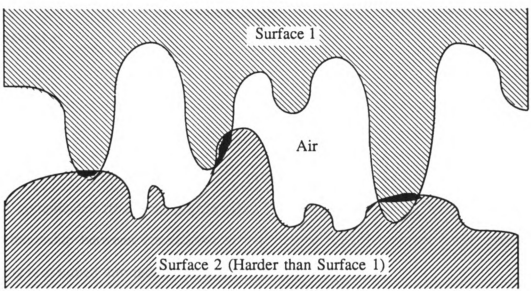

Figure 5.1 Schematic illustration of true area of contact

For the wear of minimally lubricated sliding system, Lee and Ludema [73] have observed that the true contact area is linearly related to the nominal minimum film thickness, and the nominal minimum film thickness is proportional to the wear rate.

$$\ln(\delta V_w / \delta t) \propto -\ln(\lambda) \tag{5.4}$$

$$\ln(\kappa) \propto -\ln(\lambda) \tag{5.5}$$

Since $(\delta V_w / \delta t) \propto \eta$, Proportionality (5.4) and Proportionality (5.5) become

$$\eta \propto (1/\lambda) \tag{5.6}$$

$$\kappa \propto (1/\lambda) \tag{5.7}$$

Also, it has been proposed that the adhesive wear volume is inversely proportional to the hardness of the softer material [38, 67, 75]. Hence, using Proportionality (5.6) and Proportionality (5.7) with the hardness ratio, the wear coefficient can be expressed as

$$\eta \propto \kappa \xi / \lambda \tag{5.8}$$

However, Proportionality (5.8) still presents difficulties for the quantitative analysis of complicated ring wear phenomena. Therefore, to model the fire ring wear, a linear relationship between the amount of volume loss and the friction work applied on the ring is assumed throughout the engine operation. That is,

$$\delta V_w \propto \delta W_f \tag{5.9}$$

Then, Proportionality (5.9) leads to the following expression:

$$\eta \propto f_0 \tag{5.10}$$

where f_0 is the friction coefficient determined from Section 4.5.

It has been reported that during normal engine operation, the edge of the ring face profile is quickly worn away, allowing for the generation of a small hydrodynamic film thickness [28]. Also, in the lubricated wear test, it has been observed that joint effective surface roughness is decreased during running-in [76]. Thus, it can be deduced that the wear coefficient would be decreased during running-in. Sarkar [67, 75] deduced an expression for the running-in wear of the machine part as an exponential function of the sliding distance, and by using the SLA technique, Schneider *et al.* [51] observed that the wear rate of the piston ring is given by the exponential function of the time. Hence, by using Equation (5.10) with these observations and reports, we can define mean wear coefficient for mixed or boundary lubricated condition as

$$\eta \equiv f_0 [\alpha \cdot \exp(-\beta S) + \gamma] \tag{5.11}$$

and for hydrodynamic lubricated condition as

$$\eta \equiv 0 \tag{5.12}$$

where $\alpha = (\eta_0 - \eta_\infty)/ f_0$

$\gamma = \eta_\infty / f_0$

η_∞= wear coefficient at steady state

Steady state means the condition of a given tribosystem wherein the average wear coefficient, wear rate, and other specified parameters have reached and maintained a relatively constant level.

However, in this study coefficients α, β, and γ are evaluated from previously published information since the wear coefficients, η_0 and η_∞, cannot be explicitly determined from Proportionality (5.8) due to the lack of information.

Therefore, Proportionality (5.2) can be written as

$$\begin{aligned}\delta V_w &= f_0[\alpha\cdot\exp(-\beta S) + \gamma]\, F_n \delta S \\ &= [\alpha\cdot\exp(-\beta S) + \gamma]\, F_f \delta S \end{aligned} \tag{5.13}$$

where F_f denotes the friction force calculated in Section 4.5. Rewriting Equation (5.13) in terms of real time for mixed or boundary lubricated conditions

$$\delta V_w = [\alpha\cdot\exp(-\beta U_p t) + \gamma]\, F_f U_p \delta t \tag{5.14}$$

and for hydrodynamic lubricated condition

$$\delta V_w \approx 0 \tag{5.15}$$

Thus, considering the effective nominal minimum film thickness, accumulated wear of the fire ring can be evaluated by numerically integrating Equations (5.14) and (5.15)

the fire ring can be evaluated by numerically integrating Equations (5.14) and (5.15)

5. 3 Results and Discussion

The decrease in the wear rate of the piston ring has been accounted for as follows: The surface under the counterformal contact creates a situation where the load is concentrated on a parallel narrow band of highly stressed metal. Under combined normal and tangential stresses, the softer member of the couple flows plastically, and the junction area grows, which results in decrease in the wear rate [75, 78]. Barber and Ludema [77] have reported that the roughness, which would be needed in the early stage of engine operation to enhance the removal or wearing off of the cylinder wall and ring material, would possibly contribute to an initial high wear rate. It has also been reported [67, 75] that gross surface flow occurs when sliding commences even at a moderate load causing an increase in the hardness of the interface. A work hardened zone also forms below the surface, and there is evidence of formation strongly adherent oxides which protect machine parts from gross distress in services. For instance, electron diffraction has revealed that the run-in surfaces of grey cast iron piston rings and cylinder possess an oxide layer and graphite flakes which are oriented with their cleavage planes parallel to the sliding distance [75].

5. 3. 1 Other Work related to Wear Studies

Some previous papers containing useful concepts and information for the analysis of ring wear are reviewed and discussed.

Suh and Saka [79] have demonstrated that the adhesive wear rate is proportional to the normal load applied at the junctions for the same sliding distances.

Wang *et al.* [80] presented the mathematical model for unlubricated piston rings shown below.

$$dW/dt = 0.25\, K_w K_t P_m V_m \tag{5.16}$$

where K_w = wear coefficient (Mpa^{-1})

$K_t = T_{suction}/T_{discharge}$ = temperature difference factor

P_m = the mean effective pressure (Mpa)

V_m= the mean velocity (m/sec)

However, Equation (5.16) cannot be used to calculate the ring wear for the one cycle of engine operation because mean effective pressure and mean velocity have been used. Moreover, the wear coefficient has been considered as a constant throughout the engine cycles.

Sarkar [67, 75] has deduced a mathematical expression for running-in wear of the machine part as follows :

$$V_w = V_0[1 - \exp(-ns)] \tag{5.17}$$

where V_w = volume loss at sliding distance s

V_0 = initial volume available at the junctions

n = proportional constant which might depends on the applied load

s = sliding distance

However, Sarkar failed to consider properly the load effect on the wear.

From empirical results, Schneider *et al.* [51] have presented the following

wear rate equation for the piston ring :

$$(dW/dt)_{emp} = a \cdot \exp(-bt) + c \tag{5.18}$$

where a = the wear rate at 0 hours due to break-in

b = the time dependence of break-in

c = the wear rate after break-in is complete

5. 3. 2 Error Estimation and Discussion of Predicted Results

Here error estimation needs to be conducted since the coefficients α, β, and γ used in this study were not calculated but obtained from another study [51]. Consider that the worn volume of the ring is determined from

$$V_w \approx \pi D_r T_r W_w \tag{5.19}$$

where D_r = ring diameter

T_r = ring thickness

W_w = worn width of the ring

Equation (5.14) then becomes

$$\delta W_w / \delta t = [\alpha \cdot \exp(-\beta U_p t) + \gamma] F_f U_p / (\pi D_r T_r) \tag{5.20}$$

where α, β, and γ are the coefficients dependent on the ring face profile, the oil viscosity, the effective nominal minimum film thickness, the ratio of the true contact

area over the nominal contact area, and the ratio of the cylinder bore hardness over the ring hardness as mentioned in Section 5.2. In order to estimate these coefficients, Equation (5.18) with known coefficients a, b, and c is used in this study. Thus

$$\alpha = \pi a D_r T_r / (F_f U_p) \tag{5.21}$$

$$\beta = b/U_p \tag{5.22}$$

$$\gamma = \pi c D_r T_r / (F_f U_p) \tag{5.23}$$

The uncertainties in the coefficients α, β, and γ can then be related to the uncertainties involved in each parameter as follows [81] :

$$d\alpha = |\partial\alpha/\partial a|da + |\partial\alpha/\partial D_r|dD_r + |\partial\alpha/\partial T_r|dT_r + |\partial\alpha/\partial F_f|dF_f + |\partial\alpha/\partial U_p|dU_p \tag{5.24}$$

$$d\beta = |\partial\beta/\partial b|db + |\partial\beta/\partial U_p|dU_p \tag{5.25}$$

$$d\gamma = |\partial\gamma/\partial c|dc + |\partial\gamma/\partial D_r|dD_r + |\partial\gamma/\partial T_r|dT_r + |\partial\gamma/\partial F_f|dF_f + |\partial\gamma/\partial U_p|dU_p \tag{5.26}$$

Evaluating each partial derivative and substituting these into Equations (5.24), (5.25), and (5.26),

$$d\alpha/\alpha = da/a + dF_f/F_f + dU_p/U_p + dD_r/D_r + dT_r/T_r \tag{5.27}$$

$$d\beta/\beta = db/b + dU_p/U_p \tag{5.28}$$

$$d\gamma/\gamma = dc/c + dF_f/F_f + dU_p/U_p + dD_r/D_r + dT_r/T_r \tag{5.29}$$

Therefore, by specifying the uncertainties in each parameters as 10%, the uncertainties in the coefficients α, β, and γ are estimated to be

$$d\alpha/\alpha = \pm 0.5 \tag{5.30}$$

$$d\beta/\beta = \pm 0.2 \tag{5.31}$$

$$d\gamma/\gamma = \pm 0.5 \tag{5.32}$$

Attempts have been made to generate the same engine operating conditions with the same specifications of the Diesel engine used in the experimental study [51]. Assuming a mechanical efficiency of 90%, similar power outputs compared with experimental data were obtained from IMEP analysis. Therefore, the coefficient β can be determined from Equation (5.22) with the mean piston speed. However, the coefficients α, and γ cannot be evaluated explicitly from Equations (5.21) and (5.23) since the friction forces depend on the lubricated condition. Thus, these coefficients need to be determined by following procedure :

1) At the steady state, the amount of ring wear for one cycle of engine operation at each engine speed is evaluated from the experimental study [51] by assuming quasi-static equilibrium.
2) For one cycle of engine operation at each engine speed, iterations are necessary to obtain the convergent wear coefficient γ.
3) Similarly, the coefficient α can be determined by considering the initial break-in period from the experimental data.

The coefficients α, β, and γ determined from these analysis are shown in Table 4. Ring wear rate at each engine speed is evaluated with the average coefficients shown in this table. Figures 5.2 through 5.5 indicate that the ring wear rates at each engine speed for one cycle of engine operation at steady state. Accumulated ring wear in each cases are illustrated in Figure 5.6.

Table 4 Wear Coefficients

Engine Speed	Power output	α	β	γ
1200 rpm	242 kW	$6.2*10^{-16}$	$5.2*10^{-7}$	$1.3*10^{-16}$
1500 rpm	262 kW	$7.7*10^{-16}$	$6.2*10^{-7}$	$1.7*10^{-16}$
1800 rpm	262 kW	$9.5*10^{-16}$	$3.2*10^{-7}$	$2.6*10^{-16}$
2100 rpm	263 kW	$22.0*10^{-16}$	$4.9*10^{-7}$	$5.2*10^{-16}$
Average coefficient		$(11.3\pm5.7)*10^{-16}$	$(4.9\pm1.0)*10^{-7}$	$(2.7\pm1.4)*10^{-16}$

Figure 5.7 illustrates the average ring wear rate at each engine speed and power output. The results show that the higher the engine speed the wear rates are reduced at the same power output. These trends correspond to the experimental results [51] shown in Figure 5.8. However, as shown in these figures, the theoretical ring wear rate does not completely comply with the experimental observations. Presumably, this is due to the fact that the theoretical combustion gas pressures generated by the computer simulation are not exactly the same as the experimental data, even though each power output at each engine speed is the same. Furthermore, it was not feasible to assign the identical values of the ring geometry, the ring face profile, the oil viscosity, temperature distributions in the cylinder bore, and the surface roughness of the ring and the cylinder bore used in the experiment due to the lack of information. The selection of the point of the nominal minimum film thickness, where the mixed lubrication begins, was estimated, so this might be an another factor which caused errors. Also, the conversion error included in the empirical equation obtained from experimental data cannot be neglected. As shown in Table 4, all of the data for coefficients α and γ are within the error boundary except at 2100 rpm, and the data for 1500 rpm and 1800 rpm for coefficient β are out of the error boundary. However, an

order of one in the specific wear rate calculation is acceptable because too much uncertainties are involved in present analysis. Although the results shown in Figure 5.7 and Table 4 are not perfect, this is the first model of piston ring wear which includes ring dynamics.

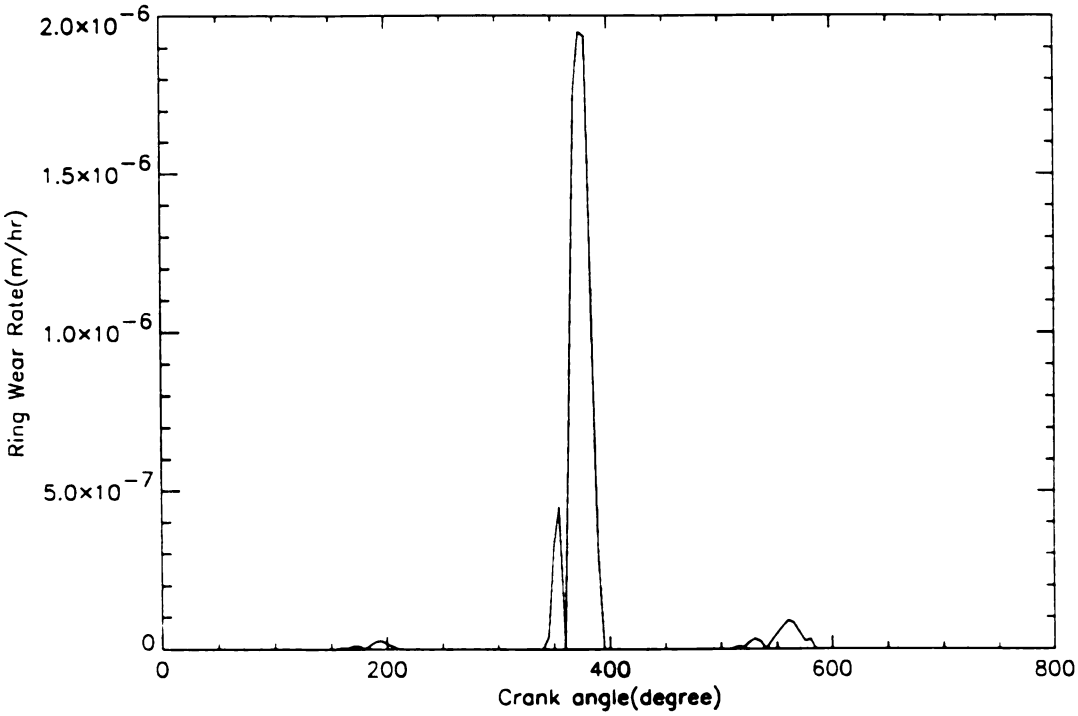

Figure 5.2 Ring wear rate for one cycle of engine operation at 1200 rpm

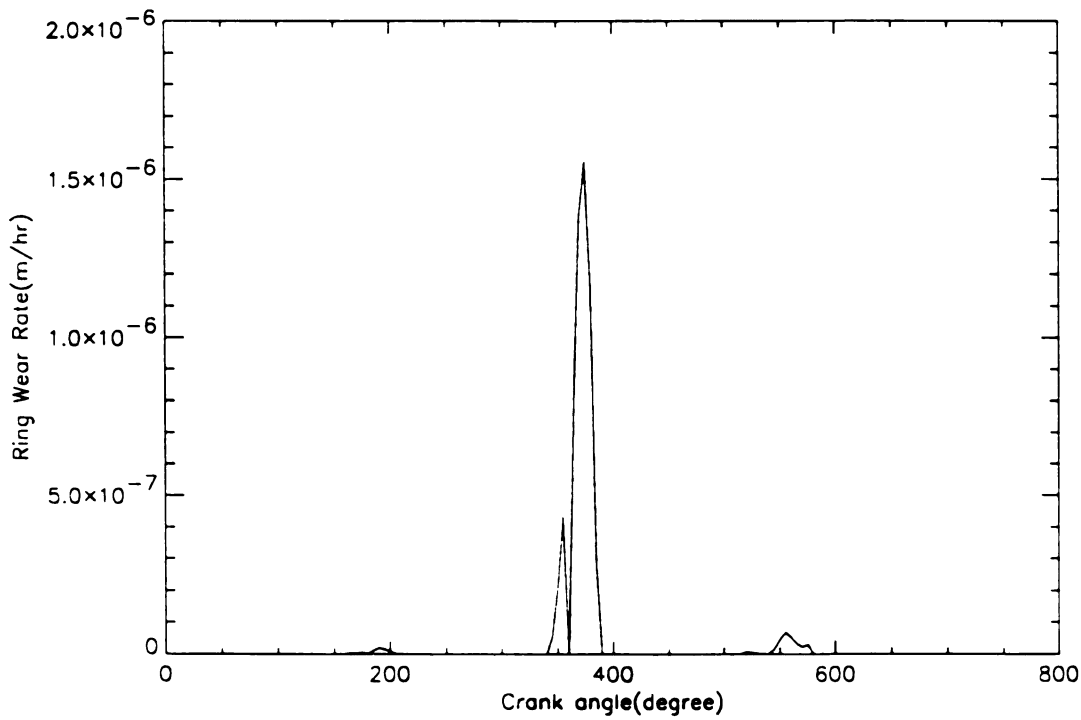

Figure 5.3 Ring wear rate for one cycle of engine operation at 1500 rpm

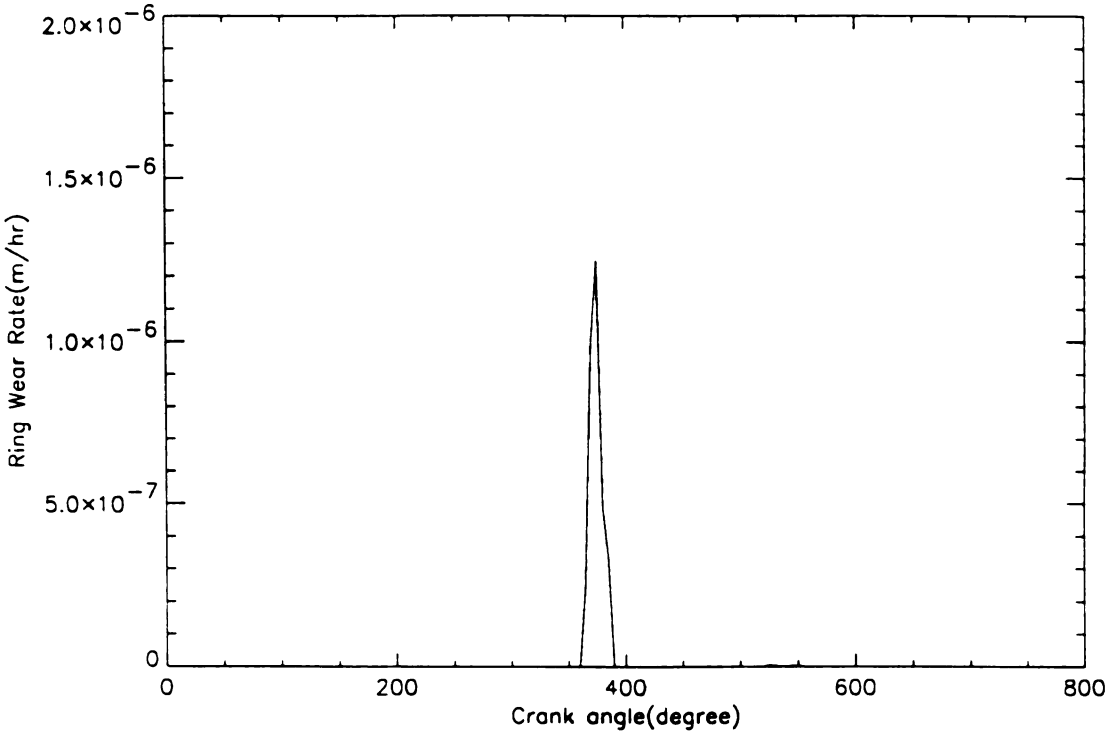

Figure 5.4 Ring wear rate for one cycle of engine operation at 1800 rpm

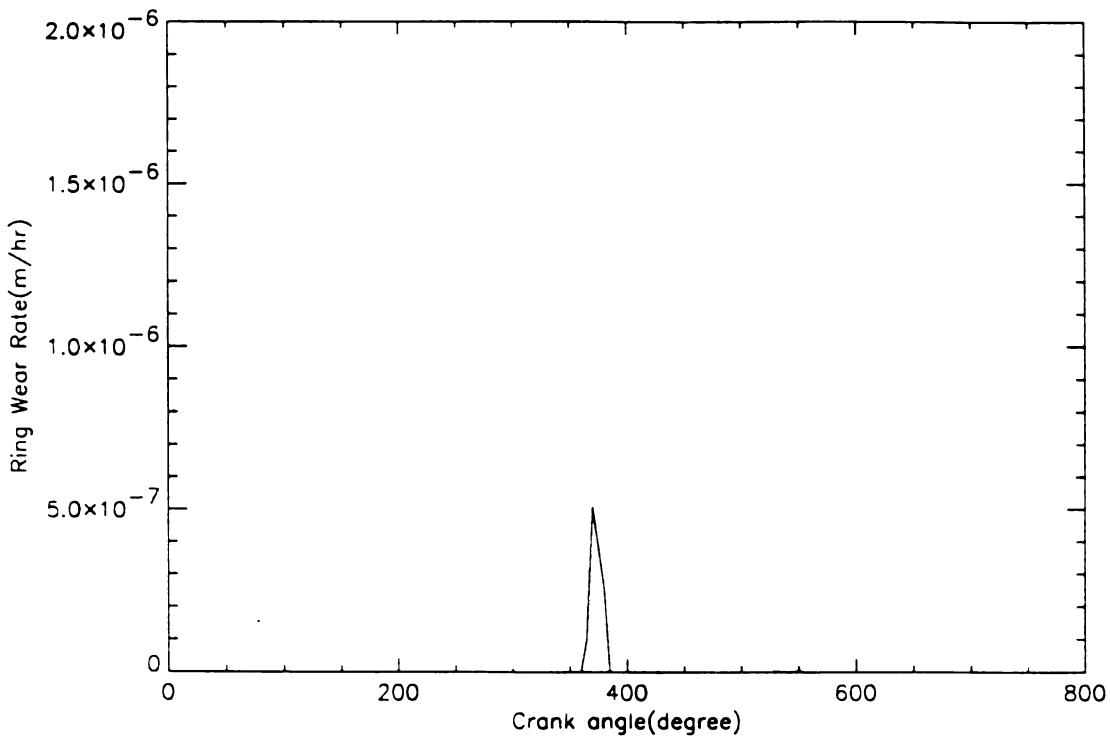

Figure 5.5 Ring wear rate for one cycle of engine operation at 2100 rpm

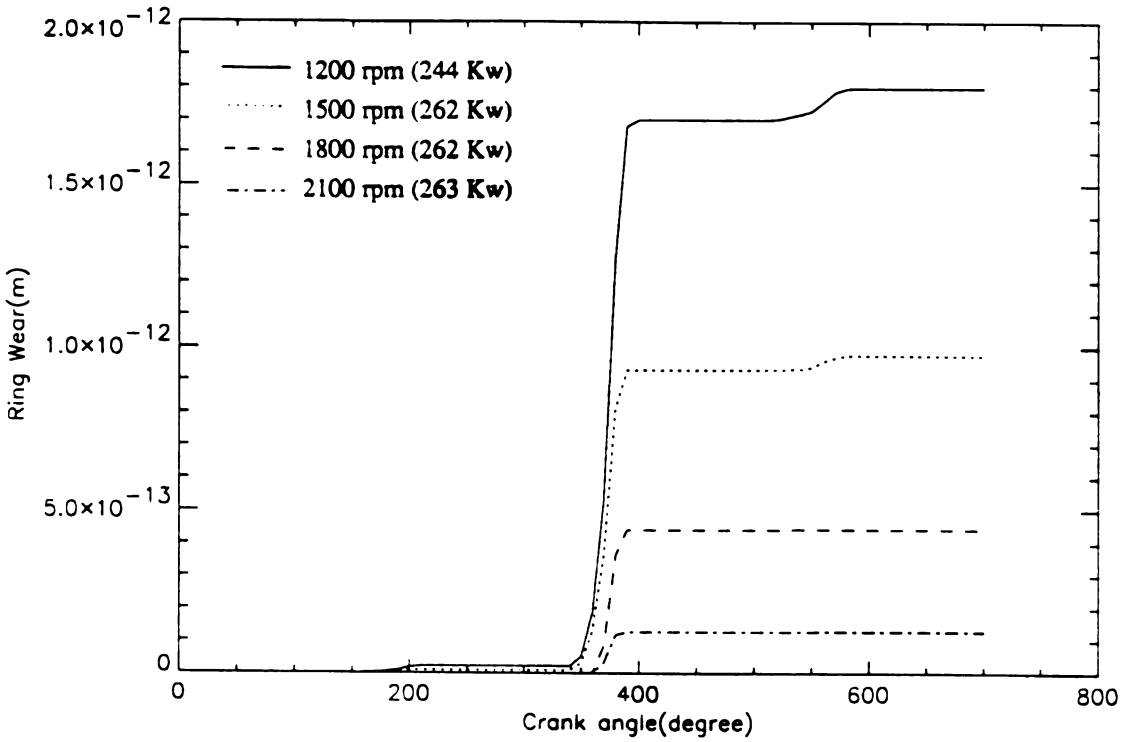

Figure 5.6 Accumulated ring wear for one cycle of engine operation

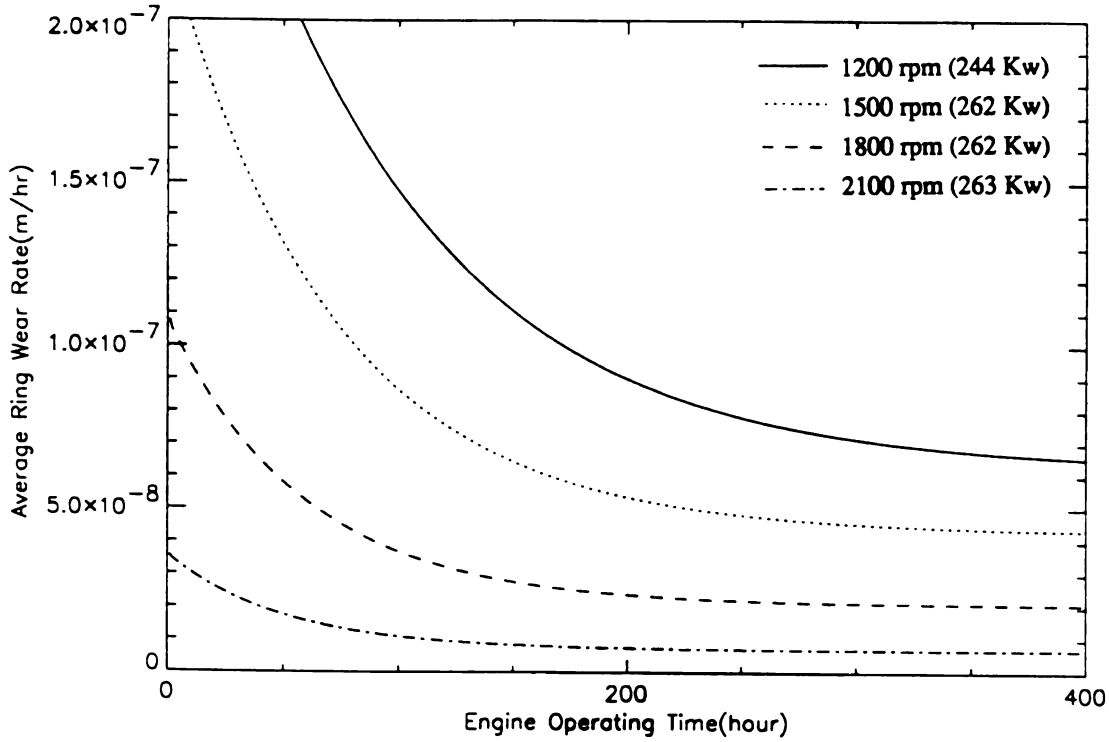

Figure 5.7 Theoretical average ring wear rate at each engine speed

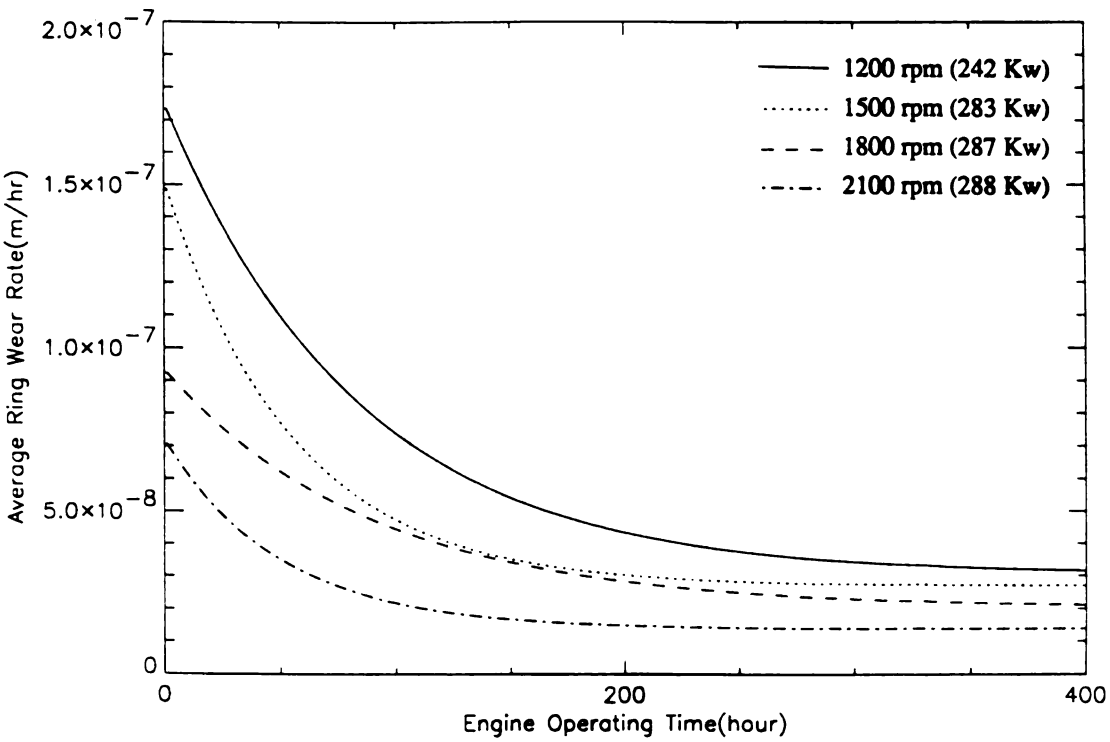

Figure 5.8 Experimental average ring wear rate at each engine speed

CHAPTER 6

SUMMARY AND CONCLUSIONS

The flow chart shown in Figure 6.1 summarizes the entire procedure for the fire ring wear analysis, which have been discussed so far.

A piston ring wear model has been developed through the use of the ring friction analysis with the assumption of a linear relationship between the ring wear and the friction work applied on the surface of the ring. It was also assumed that ring wear occurs only in the mixed or boundary lubrication regime, where the hydrodynamic film breaks down. The lubrication regimes were separated by considering the nominal minimum film thickness. The ring dynamics analysis program has been used to investigate the gas pressure distributions, axial motion of the ring in the groove, the minimum oil film thickness on the cylinder wall, and the ring friction force under different engine operating conditions assuming axial symmetry throughout the circumference of the ring. Gas flow analysis shows the coupling phenomena between the ring motion in the groove and the gas pressure distributions as predicted. Ring friction analysis demonstrates that the minimum oil film thicknesses at each engine speed tend to be lower just after TDC and BDC. Probably, these are the points where the piston ring undergoes metallic contacts with the cylinder wall. It seems that these effects are more prominent at the lower engine speeds than at the higher engine speeds since the combustion gas pressures are relatively higher at the lower engine speeds provided that the power outputs are the same. As a result, the higher the engine speed at the same power output, ring friction force is reduced.

The wear rate equation for the piston ring, which is empirically obtained from the experiment, is generalized by introducing an analytic expression in terms of ring friction work and the wear coefficient. This ring wear analysis clearly shows that the higher the engine speed, the wear rates are decreased when compared to the lower speeds at the same power output. This result is consistent with the experimental observations. It seems that increasing the engine speed and maintaining the power output by reducing the combustion gas pressure, if it is possible, would provide a good protection from an unexpected failure of the piston ring due to excessive friction. Increased engine speeds may result in other problems, however. The effects of change in ring face profile on the ring wear was also studied. The results shows that the ring friction force on the parabolic face ring is less than that of barrel face ring, which generally results in less wear. Presumably, because the minimum oil film thickness produced on the parabolic face ring is higher than that on barrel face ring.

For a boundary lubricated condition, Verbeek [68] calculated the wear coefficient of the piston ring, obtaining 10^{-17} m^2N^{-1}. Also, Childs and Sabbagh [71] have performed boundary lubricated pin-on-ring test with cast iron materials to produce specific wear rates of 10^{-19} to 10^{-16} m^2N^{-1}. As shown in Table 4, the average wear coefficient at steady state (γ) drawn from this analysis has yielded close to the maximum value of these experimental wear rate. Again, considering the uncertainties involved in this analysis, it seems that this result is quite reasonable, since usually the ring wear rate of a Diesel engine is much higher than that of an SI engine.

Though present analysis is employed locally in the Diesel engine, the model developed in this study can be applied to any piston engine, as long as the specifications of the engine such as the oil viscosity, temperature distributions in the cylinder bore, the ring geometry, the ratio of cylinder bore hardness over ring hardness, and the ring face profile are given as the same. This is the first model of piston ring wear

which includes ring dynamics, and is intended to provide a framework for a general model which can include the factors mentioned above.

This ring wear model should be a useful research tool in developing new material and lubrication strategies to combat the detrimental effects of piston ring wear. A further development of this analysis would be to generalize the model and couple it with the experimental results of the radioactive ion implantation technique which has been developed at MSUERL or the SLA technique developed by KFK.

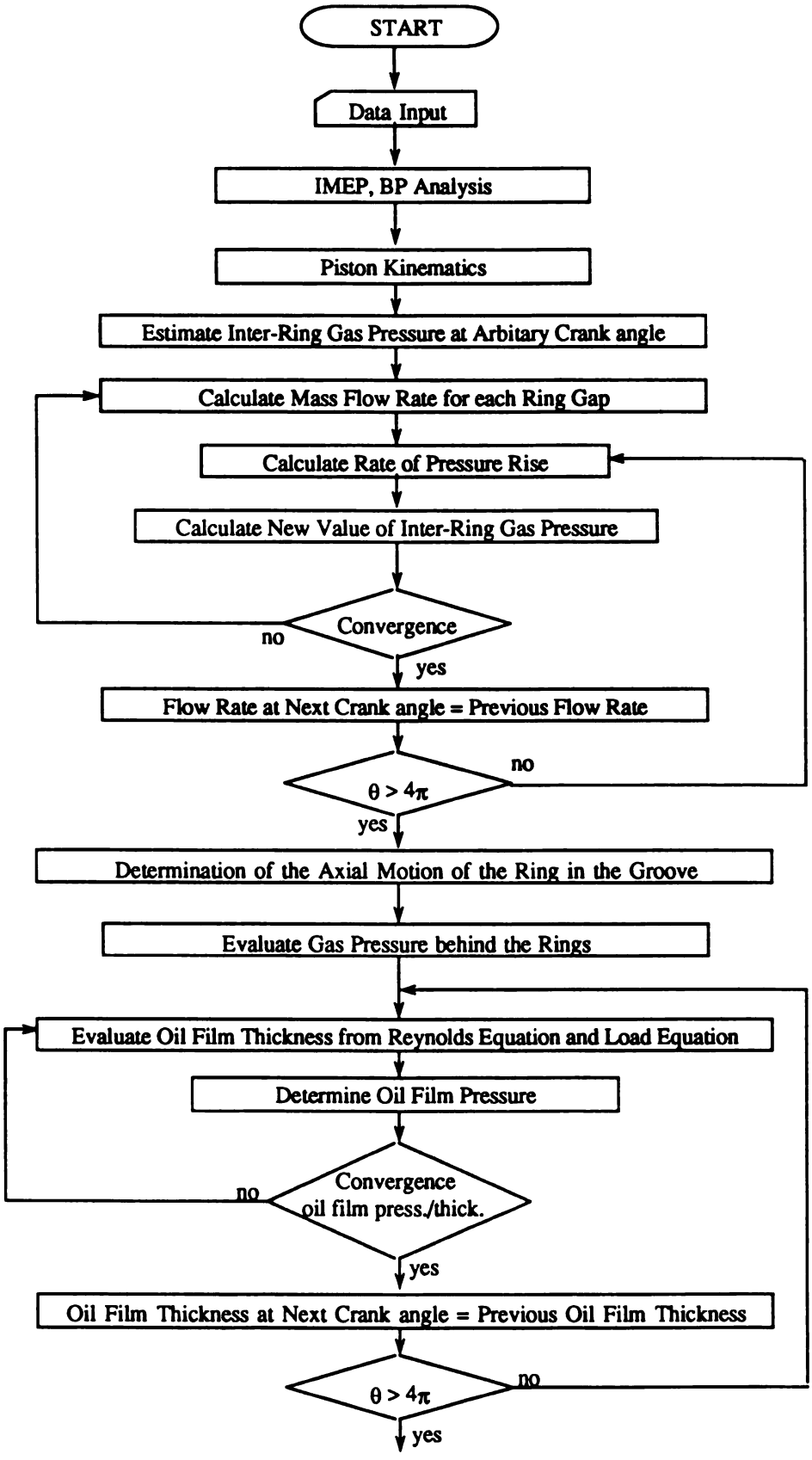

Figure 6.1 Procedure for fire ring wear analysis

Figure 6.1 (Cont'd)

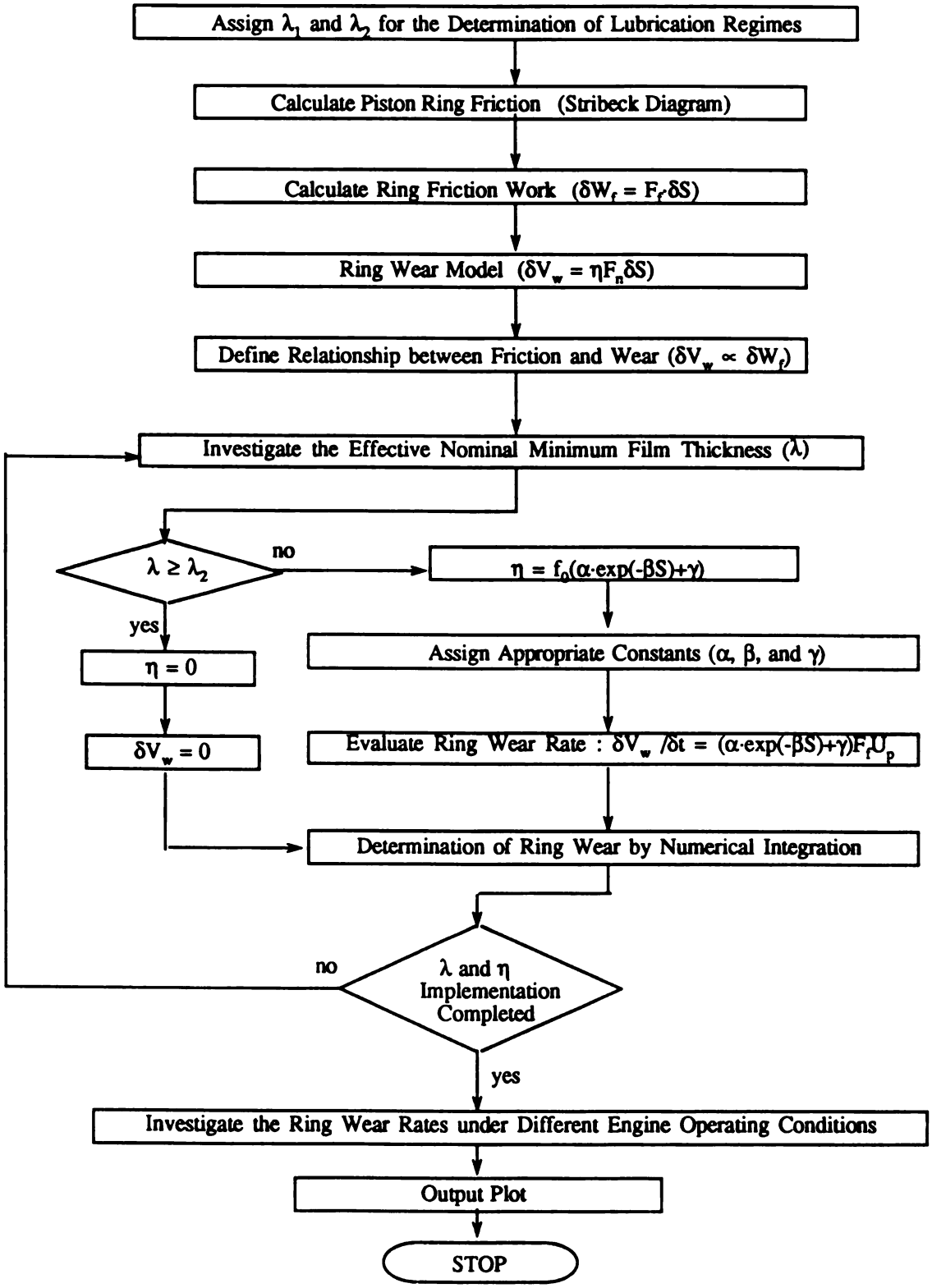

CHAPTER 7

RECOMMENDATIONS

7. 1 The Limitation of the Model

Axial symmetry has been assumed throughout the circumference of the ring in this analysis. However, realistically the fire ring wears more towards the top side than the bottom side producing an asymmetrical barrel form probably comprising two flats or tapers [82]. This experimental result suggests that it would be possible to predict this effect through the use of a three-dimensional model. Also, fatigue, chemical reaction, and corrosive wear were not included in this ring wear model. Such complicated phenomena cannot be accounted for using this simple ring wear model.

7. 2 Recommendations for Future Research

The theoretical and experimental results indicated that a mechanism for piston ring wear is governed by a large number of interrelated factors and should be a field for further intensive research. Advanced analytical development work is needed in the following areas :

1) The effect of ring design variables such as ring width and the position of the ring groove as well as the ring face profile on the ring wear.
2) Piston ring and bore surface finish data which can provide the surface roughness characteristics for a more reasonable estimate of the average piston ring face wear in an engine with different cylinder liners.
3) Further realistic piston ring lubrication theory, including lubricant flow through the

ring gaps, net transport of lubricant within the film between the rings and cylinder wall, and the complex movement of lubricant associated with ring lift.

4) A more sophisticated three-dimensional ring wear model including fatigue, abrasion and corrosive wear as well as axial, twist and rotational motion of the ring, and cylinder bore distortion.

5) Innovative and reliable experimental methods to confirm predictions from these models such as local ring wear, pressure behind the piston ring, ring location and motion.

APPENDICES

APPENDIX A

THE APPLICATION OF RADIOACTIVE ION IMPLANTATION TECHNIQUES FOR PISTON RING WEAR MEASUREMENT

A. 1 The Advantages of RII over SLA

SLA (Surface Layer Activation) is limited to certain materials, e.g., iron and chromium, where proton, deuteron, or helium ion bombardment can produce an isotope with a reasonable half-life and an identifiable radiation. Hence, large classes of materials such as plastics, rubbers, and ceramics, (which are presently being developed for engine parts and materials with atomic number $Z < 24$) are not accessible to this technique. In addition, it has been suggested that SLA can be more destructive to target materials. Calculations using TRIM [1] indicate that more vacancies are created in the SLA process than in the ion implantation for a given amount of activity [83].

Implantation of the radioactive ion for wear analysis represents a significant advancement over the presently available SLA. The principle advantage of this technique over SLA is that instead of bombarding the target with a high energy proton beam to change the atomic nature of the material, a heavy ion cyclotron beam is used to implant ions into the surface. The material retains its original atomic structure, and conveniently long-lived nucleus can be implanted. This means that a wide class of materials including non-metallic ceramics, graphite composites, plastics and rubber compounds, which cannot be easily studied using SLA, can be studied using radioactive ion implantation [54, 84]. The half-life of typical radionuclides produced using SLA on such materials are too short to be useful for wear measurements.

Another unique feature of this method is that only the radioactive ion is im-

planted, and nuclear reactions do not take place in the wear sample. This eliminates the problem of unwanted background radiation. As wear is measured in situ, this technique can be used to monitor wear rates associated with many different modes of engine operation without disassembly of the engine. This method is repeatable, and transient wearing behavior can be detected with a sensitivity of wear rate measurement of nm/hr.

A. 2 The Measurement Procedure of Piston Ring Wear

The wear rate of the piston ring is measured in the following way:

1) The optimized energy of the beam and a suitable set of absorbers necessary to produce a desired uniform dose-depth profile in the surface of piston ring are obtained using the polyenergetic TRIM simulation, which is descibed in Appendix B.

2) As shown in Figure A.1, the outer surface of the piston ring is activated using condition provided from the polyenergetic TRIM simulation. It is then installed in the piston engine.

3) The initial radiation level of the piston ring is measured by using the NaI or Ge detector before the break-in. Similarly, the final radiation level is also detected after the break-in period. Subtraction of the final activity measured from the initial activity measured gives the activity removed.

4) Assuming that the wear rate is uniform throughout the circumference of the piston ring, it can be determined from the detector counts removed - if it is measurable - since the radioactivity is linearly proportional to its implantation depth [45], assuming a uniform dose-depth distribution shown in Figure A.2.

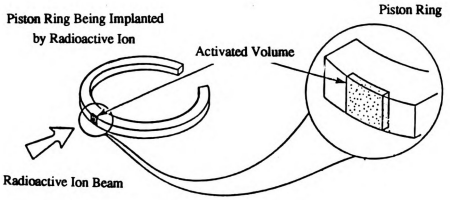

Figure A.1 Activation of the piston ring by radioactive ion beam

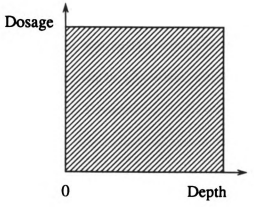

Figure A.2 Idealized uniform dose-depth distribution

A. 3 Radioactivity

The number of radioactive nuclei present at time t can be determined as

$$N = N_0 e^{-\lambda t} \tag{A.1}$$

where N_0 is the total number of radioactive nuclei at time t = 0, and λ is the decay constant. The half-life of a radioactive nucleus is then defined as the time $t_{1/2}$ during which the number of nuclei reduces to one-half the original value. Using Equation (A.1)

$$1/2 = e^{-\lambda t_{1/2}}$$

which gives

$$\lambda = \ln 2 / t_{1/2} \tag{A.2}$$

This decay constant, along with the type of decay and the energy of decay, characterizes a given radioactive nucleus and can be regarded as one of its signatures [84].

The polyenergetic TRIM simulation would be able to provide an optimized energy of the beam and a suitable set of absorbers to produce a uniform dose-depth profile in the surface of piston ring. However, a problem arises concerning how many particles should be implanted into the surface of piston ring to produce a desired radiation level. To prevent a health hazard, it should not exceed certain dosages. Suppose it is limited within a radioactivity of α μC_i with the intensity per decay (branching ratio) of $\gamma(\%)$, then the number of particles to be implanted is determined as follows. The disintegration per second for α μC_i of this radioactive ion is

$$R = \alpha(3.7 * 10^{10})(10^{-6})\gamma \qquad \text{(dis/sec)}$$
$$= (3.7 * 10^{4})\,\gamma\alpha \qquad \text{(dis/sec)} \qquad \text{(A.3)}$$

Since the decay constant of a given radioisotope is given by Equation (A.2), the number of particles to be implanted is determined by

$$N = R / \lambda$$
$$= (3.7 * 10^{4})\gamma\alpha / (\ln 2 / t_{1/2})$$
$$= (5.34 * 10^{4})\,\gamma\alpha t_{1/2} \qquad \text{(particles)} \qquad \text{(A.4)}$$

where γ, α, and $t_{1/2}$ denote an intensity per decay, activity, and half-life of the given radioactive ion, respectively. Therefore, to produce a maximum radioactivity of α μC_i for a specific radioisotope, the maximum number of particles allowed for implantation are $(5.34 * 10^4)\,\gamma\alpha t_{1/2}$ particles.

In addition, the detector efficiency needs to be calibrated to estimate an amount of radioactivity for a given detector count. Figure A.3 shows a calibrated detector efficiency [85].

Consider the radioisotope implanted into the surface of a piston ring with a depth of d μm and a dosage of α μC_i. By using Equation (A.3) with a detector efficiency of ε, the mean detector count is expressed as

$$C_m = \varepsilon\,(3.7 * 10^4\,\gamma\alpha) \qquad \text{(counts/sec)} \qquad \text{(A.5)}$$

Thus the time needed to reach desired counts, C_d, is given by

$$t_d = C_d / C_m$$
$$= (2.70 * 10^{-5})\,C_d / (\gamma\alpha\varepsilon) \qquad \text{(sec)} \qquad \text{(A.6)}$$

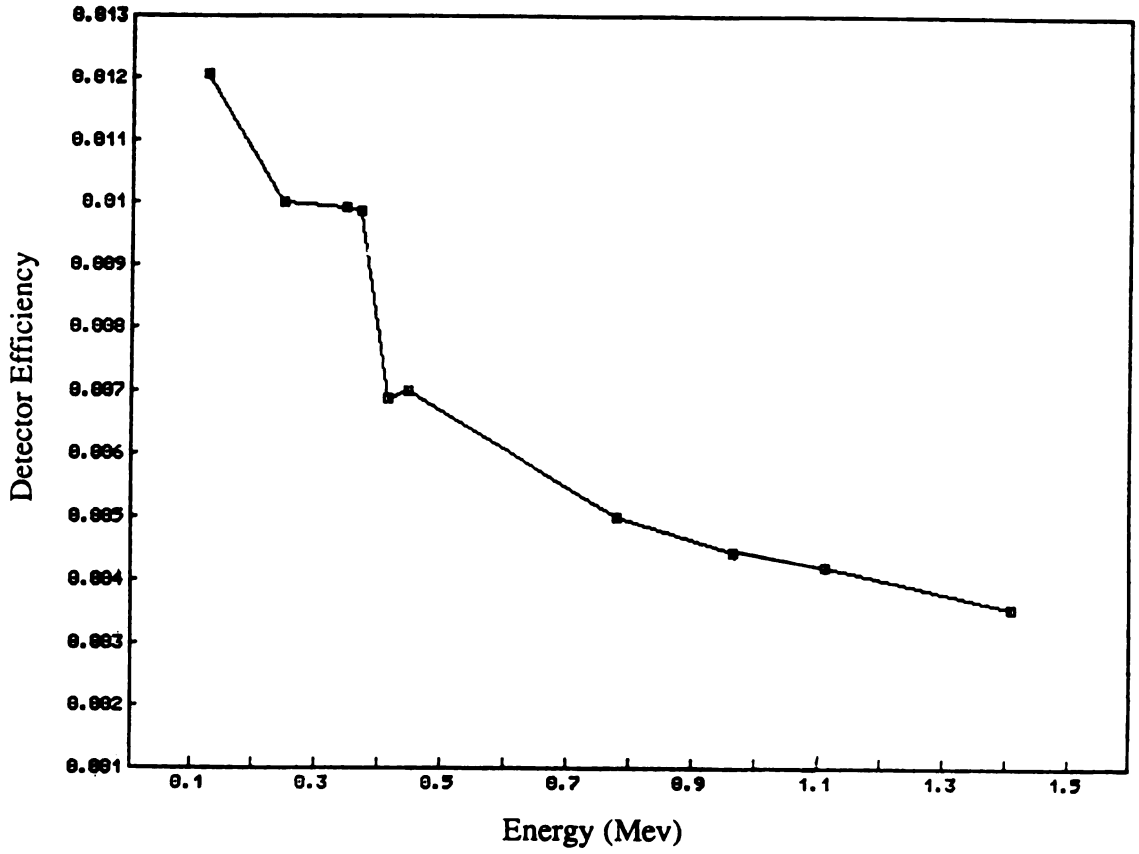

Figure A.3 Detector Efficiency Calibration

A. 4 The Sensitivity of Measurement

As stated in Section A.2, an initial and final detector count are measured for the same period of counting time. However, these measurements involve inevitable errors. The sensitivity related with these measurements is discussed in this Section.

Suppose that the initial detector count is measured as C_i and the final detector count is C_f for the same period of counting time after an hour of break-in; counts removed is then given by

$$C_{rm} = C_i - C_f \tag{A.7}$$

Thus radioactivity removed becomes

$$\alpha_{rm} = \alpha_0(C_i - C_f) / C_i \tag{A.8}$$

where α_0 represents an initial radioactivity.

By applying the linear relationship between dosage and depth, a depth removed for an hour of break-in is expressed as

$$\begin{aligned} d_{rm} &= d_0\alpha_{rm} / \alpha_0 \\ &= d_0(C_i - C_f) / C_i \end{aligned} \tag{A.9}$$

where d_0 denotes an initial implantation depth in μm.

Reconsidering Equation (A.7) with probable error to check the sensitivity of the measurement

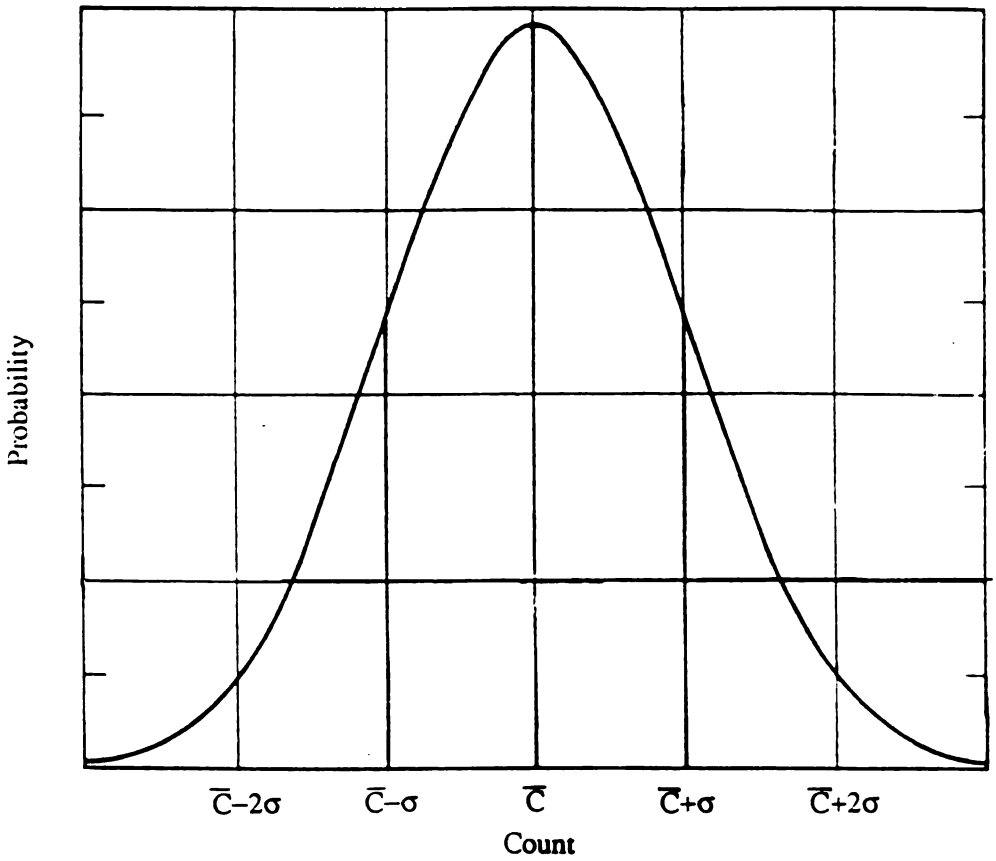

Figure A.4 Normal distribution

$$C_{rm} = (C_i \pm \delta C_i) - (C_f \pm \delta C_f) \qquad \text{(A.10)}$$

where

$$\delta C_i = 2\sigma_i \qquad \text{(A.11)}$$

with a reliability of 95 % as shown in Figure A.4. The standard deviation, σ_i is then given by

$$\sigma_i = C_i^{1/2} \tag{A.12}$$

for counts measured, C_i [86]. Therefore, Equation (A.10) becomes

$$C_{rm} = (C_i - C_f) \pm 2(C_i^{1/2} + C_f^{1/2}) \tag{A.13}$$

with a reliability of 95 %. However, this wear measurement is valid only if

$$C_i - C_f \geq 2\,(C_i^{1/2} + C_f^{1/2}) \tag{A.14}$$

for a given period of counting time. That is,

$$(C_i^{1/2} + C_f^{1/2})(C_f^{1/2} - C_i^{1/2} + 2) \leq 0 \tag{A.15}$$

since $C_i^{1/2}+C_f^{1/2} > 0$

$$C_f^{1/2} - C_i^{1/2} + 2 \leq 0 \tag{A.16}$$

This yields

$$C_f \leq (C_i^{1/2} - 2)^2 \tag{A.17}$$

Therefore, the maximum measurable value of the final detector count is found to be $(C_i^{1/2}-2)^2$ for a given initial detector count, C_i.

In addition, in order to calibrate the detector efficiency at each energy level more accurately, errors need to be considered. A detector efficiency at each energy is

defined by

$$\varepsilon = C_d / C_t \tag{A.18}$$

where C_d is a detector count, and C_t is a true count in 4π steradians. While the probable error in Equation (A.18) is written as

$$\begin{aligned} \delta\varepsilon &= \delta(C_d / C_t) \\ &= \delta C_d / C_t - C_d \, \delta C_t / C_t^2 \end{aligned}$$

Therefore

$$\begin{aligned} \delta\varepsilon / \varepsilon &= (\delta C_d / C_t - C_d \, \delta C_t / C_t) / (C_d / C_t) \\ &= \delta C_d / C_d - \delta C_t / C_t \end{aligned} \tag{A.19}$$

By applying Equation (A.11) and Equation (A.12) into Equation (A.19)

$$\delta\varepsilon / \varepsilon = 2 \left((1 / C_d)^{1/2} + (1 / C_t)^{1/2} \right) \tag{A.20}$$

with a reliability of 95%. Rewriting Equation (A.18) with error involved

$$\varepsilon = C_d / C_t \pm 2 \, C_d / C_t \left((1 / C_d)^{1/2} + (1/C_t)^{1/2} \right) \tag{A.21}$$

with a reliability of 95%.

Therefore, experimental studies for in situ ring wear measurement using RII technique expect to be performed with these estimates.

APPENDIX B

THE TRIM SIMULATION

B. 1 Introduction

A Monte-Carlo computer simulation that calculates the slowing down and scattering of energetic ions in amorphous targets has been developed for obtaining the most realistic range and damage profiles in any complex target [1].

This Monte-Carlo method called TRIM (Transport of Ions in Matter) as applied in simulation techniques has a number of distinct advantages over present analytical formulations based on transport theory [1, 87]. It allows the explicit consideration of surfaces and interfaces, the rigorous treatment of elastic scattering with any number of different target atoms in multi-atomic targets, and finally it yields the full distribution function rather than a few segments of such distributions. The TRIM program provides information on reflection and transmission properties of planar targets, as well as ion range and collisional damage characteristics. It is also easy to include recoil cascades, which in turn yield all the information on sputtering, ballistic mixing, and defect production.

Several ion transport procedure based on the Monte Carlo method have been reported [88, 89]. Aside from considering crystalline or amorphous targets, their major differences lie in their treatment of electronic energy losses or nuclear scattering. Since energetic ions undergo many collisions in the process of slowing down, the method used to evaluate the scattering integral is critically important in terms of its relative computer efficiency. Therefore, the TRIM simulation has made use of a new analytical scheme that very accurately reproduces scattering integral results for realistic potentials.

B. 2 Physical Assumptions used in TRIM

The TRIM program follows a large number of individual ion or particle histories in a target. Each history begins with a given position, direction, and energy of the ion. The particle is assumed to change direction as a result of a sequence of collisions with the target atom and move in straight free-flight paths between collisions. The particle's energy is reduced after each free-flight path by the amount of electronic energy loss and then (after the collision) by the nuclear energy loss, which is the result of transferring momentum to the target atom in the collision [87]. Each ion's history is terminated either when the energy drops below a pre-specified value or when the position of the particle has moved out of the front or rear surface of the target. The target is considered amorphous with atoms at random locations, which means that any directional properties of the crystal lattice are ignored [1]. Thus, it actually describes implantation into amorphous materials and neglects channelling effects that may become important at low-dose low-energy implantation, which a fraction of the ions may get steered through open passage (planar or axial) along certain directions in crystalline structures [87, 90]. Also nuclear reactions are not included. The nuclear and electronic energy losses or stopping powers are assumed to be independent. Therefore, particles lose energy in discrete amounts in nuclear collision and lose energy continuously from electronic interactions. In most cases for energies below 1 MeV/amu, the electronic straggling of ion was found to be of little importance for their projected range profiles [91]. However, electronic stopping becomes more dominant than nuclear stopping in higher energy.

The TRIM simulations are based on the binary collision model, and thus the ion history is determined by a series of subsequent binary encounters with the target atoms [1]. This assumption may break down at very low energies where deflections

may occur even at large separations from the target nucleus. In this case the ion may interact with more than one target atom at the same time and errors may be introduced by treating such collisions separately with very small free-flight paths in between [87]. However, a quantitative study of the amount of error introduced this way has not been performed so far.

B. 3 Preliminary Simulations and Results

Though the time integral was found to be of little importance in all cases except for the very low energy, according to the simulation conducted, it has been observed that a minimum of 1000 particles are required to get statistically reasonable and normalized data [92]. For the heavier ion or the ion having higher energy, more particles might need to be simulated to produce a normalized distribution since the projected range and straggling is increased with the energy of the implanted ion.

A simulation of monoenergetic ^{20}Ne beam into silicon nitride (Si_3N_4) has been performed to check the ion concentrations and radiation damages [92]. Silicon nitride was chosen because it is considered as one of the standards for advanced ceramic material research. Figure B.1 represents the 2.5 MeV/amu ^{20}Ne ion dose-depth profile implanted into Si_3N_4, while its radiation damage is shown in Figure B.2.

In order to produce an uniform dose-depth profile on an implanted surface, it is necessary to superpose the monoenergetic beam degrading their intensity by a suitable set of absorbers. To simulate a polyenergetic ion implantation profile from a monoenergetic ^{20}Ne beam, gold foils of varying thickness were used as degraders in front of Si_3N_4. In addition, in order to perform a polyenergetic simulation, it is necessary to optimize the window size of an ion range profile to achieve the desired spartial resolution. If the window is too small, some of the ions might not be included in this window due to the deflection of the ion trajectory, while if the window is too wide,

although the area of interest remains the same, the spatial resolution becomes relatively coarse. A spatial resolution of 50 nm has been achieved using a 5 μm window. Figure B.3 shows the 2.5 MeV/amu ^{20}Ne ion implanted into Si_3N_4 using different thickness of gold foil. Six separate degrader foils having a 6 to 8.5 μm thickness of gold foils with an interval of 0.5 μm were modeled in this polyenergetic simulation.

The simulation of a nonradioactive ^{20}Ne ion was chosen since this beam is easily produced at the NSCL (National Superconducting Cyclotron Laboratory), and ion ranges and damage produced by this beam are expected to be similar to that of the ^{22}Na beam because of its proximity in atomic number [92]. Further studies of the production mechanism will provide guidance for realistic model development regarding the ^{22}Na beam.

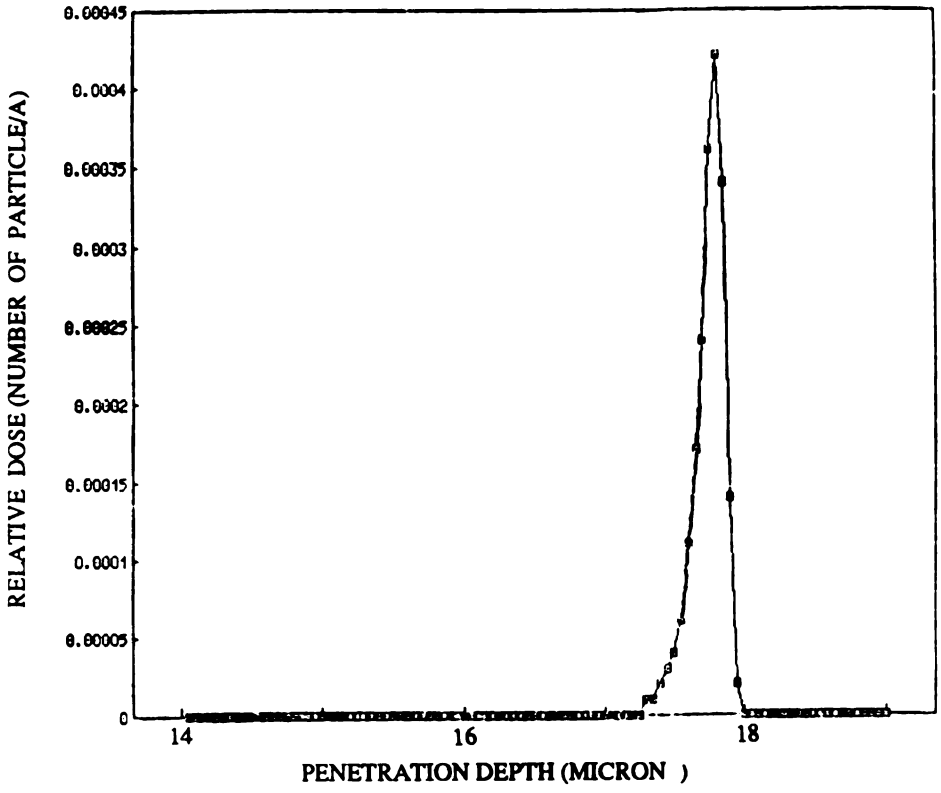

Figure B.1 The ion range profile of a 2.5 MeV/amu ^{20}Ne beam implanted onto Si_3N_4

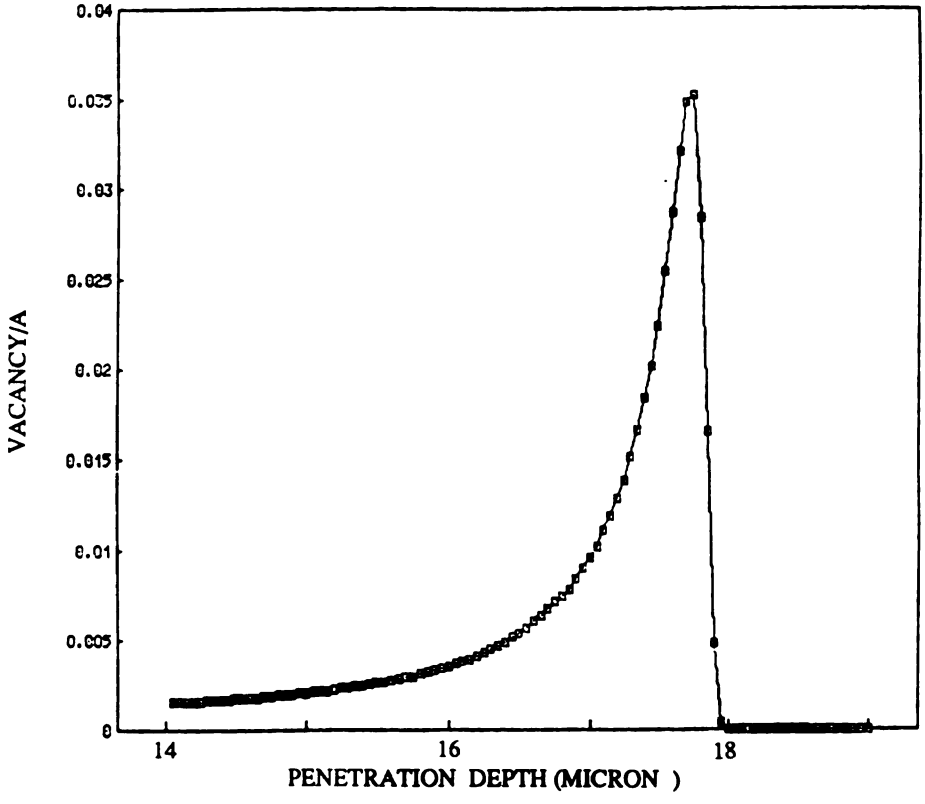

Figure B.2 The radiation damage of Si_3N_4 for a 2.5 MeV/amu ^{20}Ne beam

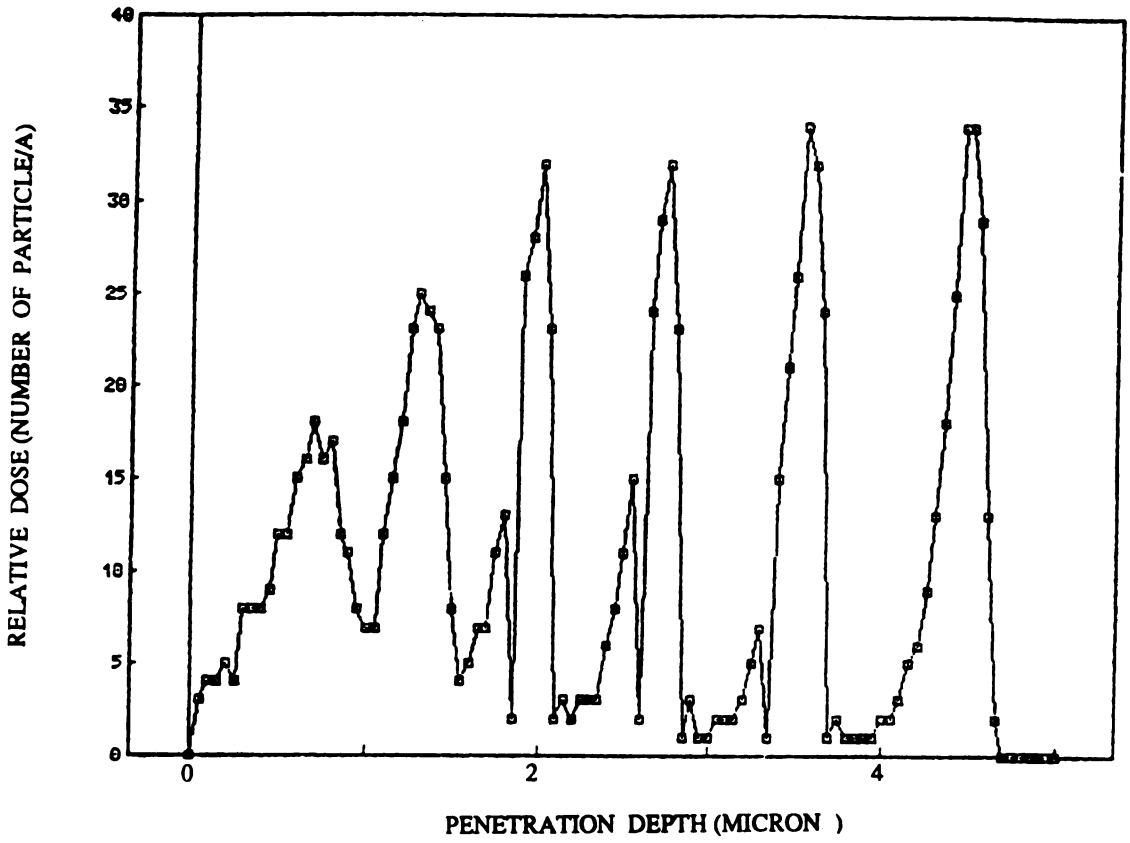

Figure B.3 Polyenergetic profile for a 2.5 MeV/amu ^{20}Ne beam degraded by stacked gold foils

BIBLIOGRAPHY

BIBLIOGRAPHY

1) Ziegler, J. F., Biersack, J. P., and Littmark, U., Vol.1, *The Stopping Power and Range of Ions in Solids*, Pergamon Press, NewYork (1985).

2) Heywood, J. B., *Internal Combustion Engine Fundamentals*, McGraw-Hill Company, NewYork (1988).

3) Taylor, C. F., *The Internal Combustion Engine in Theory and Practice*, M.I.T. Press, Cambridge (1985).

4) McCormick, H. E., Anderson, R. D., Mayhew, D. J., and Rychlewski, W. J., "New Developments in Piston Ring for the modern Diesel Engine", *SAE Paper* 750769 (1975).

5) Prasse, H. F., McCormick, H. E., and Anderson R. D., 'New Piston Ring Innovations to Help Control Automotive Engine Emissions", *SAE paper* 730006 (1973).

6) Sunden, H., and Schaub, R., "The Manufacture of Piston Rings for Slow and Medium Speed Diesel Engines", *Tribology International*, Vol.12, No.1, pp.3-14, 1979.

7) Taylor, B. J., Eyre, T. S., "A Review of Piston Ring and Cylinder Liner Materials", Tribology International, Vol.12, No.2, pp.79-89 (1979).

8) Hill, S. H., and Newman, B. A., "Piston Ring Design for Reduced Friction", *SAE Trans*. 841222 (1984).

9) Holt, J. W., and Murray, E. J., "A Two Ring Piston for Gasoline Engine", *SAE Trans*. 860248 (1986).

10) Young, W. B., and McComb, J. A., "New Piston Ring Face Coating Using Design of Experiments", *SAE Trans*. 900588 (1990).

11) Yoshida, H., Kusama, K., and Sagawa, J., "Effects of Surface Treatment on Piston Ring Friction Force and Wear", *SAE Trans*. 900589 (1990).

12) Jeng, Y. -R., "Friction and Lubrication Analysis of Piston Ring Pack", *SAE Paper* 920492 (1992).

13) Furuhama, S., and Takiguchi, M., Tomizawa, K., "Effect of Piston and Piston Ring

Designs on the Piston Friction Forces in Diesel Engines", *SAE Trans.* 810977 (1981).

14) Furuhama, S., and Sasaki, S., "New Device for the Measurement of Piston Frictional Forces in Small Engines", *SAE Trans.* 831284 (1984).

15) Ku, Y. G., and Patterson, D. J., "Piston and Ring Friction by the Fixed Sleeve Method", *SAE Trans.* 880571 (1988).

16) Uras, H. M., and Patterson, D. J., "Effect of Some Lubricant and Engine Variables on Instantaneous Piston and Ring Assembly Friction", *SAE Trans.* 840178 (1984).

17) Uras, H. M., and Patterson, D. J., "Effect of Some Piston Variables on Piston and Ring Assembly Friction", *SAE Trans.* 870088 (1987).

18) Slone, R., Patterson, D. J., Morrison, K. M., and Schwartz, G. B., "Wear of Piston Rings and Liners by Laboratory Simulation", *SAE Trans.* 890146 (1989).

19) Simmons, R. A., Dymock, K. R., and Webster, G. D., "Fire Ring Wear Assessment on a 6V92TA Detroit Diesel Engine", *SAE Trans.* 890420 (1989).

20) Bishop, I. N., "Effect of Design Variables on Friction and Economy", Paper 812A presented Jan. 1964 at *SAE congress* (1964).

21) Ting, L. L., and Mayer, J. E., "Piston Ring Lubrication and Cylinder Bore Wear Analysis, Part I - Theory", *ASME trans., Journal of Lubrication Technology*, 73-Lub-25,1974.

22) Ting, L. L., and Mayer, J. E., "Piston Ring Lubrication and Cylinder Bore Wear Analysis, Part II - Theory Verification", *ASME trans., Journal of Lubrication Technology*, 73-Lub-27, 1974.

23) McGeehan, J. A., "A Literature Review of the effect of Piston and Ring Friction and Lubricating Oil Viscosity on Fuel Economy", *SAE Trans.* 780673 (1978).

24) Rohde, S. M., "A Mixed Friction Model for Dynamically Loaded Contacts with Application to Piston Ring Lubrication", *Surface Roughness Effects in Hydrodynamic and Mixed Lubrication, Winter Annual Meeting of ASME*, pp.19-50, November, 1980.

25) Ting, L., "A Review of Present Information on Piston Ring Tribology", *SAE Trans.* 852355 (1985).

26) Patton, K. J., Nitschke, R. G., and Heywood, J. B., "Development and Evaluation of a Friction Model for Spark-Ignition Engines", *SAE Trans.* 890836 (1989).

27) Yagi, S., Ishibasi, Y., and Sono, H., "Experimental Analysis of Total Engine Friction in Four Stroke S.I. Engines", *SAE Trans.* 900223 (1990).

28) Brombolich, L. J., "Effect of Cylinder Distortions and Piston Ring Effects on Oil Consumption and Friction Losses in Automobile Engines", Tribology Project Research Report, Argonne National Laboratory, 1989.

29) Dowson, D., Economu, P. N., Ruddy, B. L., Strachen, P. J., and Baker, A. J. S.,"Piston Ring Lubrication-Part II : Theoretical Analysis of a Single Ring and a Complete Ring Pack", from "Energy Conservation through Fluid Film Lubrication Technology : Frontiers in Research and Design", *Winter Annual Meeting of ASME*, Dec 1979, pp.23-52.

30) Dowson, D., "Non-Steady State Effect in EHL", NASA Conference Publication 2300, *Tribology in the 80's*, Vol.1 (1984).

31) Stewart, R. M., and Selby, T. W., "The Relationship Between Oil Viscosity and Engine Performance - A Literature Search", *SAE Trans.* 770372 (1977).

32) Brown, S. R., and Hamilton, G. M., "Negative Pressure Under a Lubricated Piston Ring", *Journal of Mechanical Engineering Science*, Vol. 20, No.1, pp49-57, 1978.

33) Furuhama, S., and Hiruma, M., "Some Characteristics of Oil Consumption Measured by Hydrogen Fueled Engine", *ASLE Trans*, Vol.34, No.12 (1977).

34) Reipert, P., and Buchta, R., "New Design Methods for Pistons", *SAE Paper* 810933, 1981.

35) Boisclair, M. E., Hoult, D. P., and Wong, V. W., "Piston Ring Thermal Transient Effects on Lubricant Temperatures in Advanced Engines", *ASME Conference and Exhibition*, Jan. 1989, 89-ICE-2.

36) McGeehan, J. A., "A Survey of the Mechanical Design Factors Affecting Engine Oil Consumption", *SAE Trans.* 790864 (1979).

37) Economou, P. N., Dowson, D., and Baker, A. J. S.,"Piston Ring Lubrication - Part I : The Historical Development of Piston Ring Tribology", *ASME Trans.*, Vol.104, January, 1982.

38) Rabinowicz, E., *Friction and Wear of Material*, John Wiley and Sons, Inc., Cambridge, Massachusetts (1964).

39) Ryan, T. W. III, Bond, T. J., and Schieman, R. D., "Understanding the Mechanism of Cylinder Bore and Ring Wear in Methanol Fueled SI Engines", *SAE Trans.* 861591 (1986).

40) Boehm, G., and Harrer, J., "Nickel Coated Pistons for Improved Durability in Knock Control Engines", *SAE Trans.* 900453 (1990).

41) Gerve, A., and Schatz, G., "Application of Cyclotrons in Technical and Analytical Studies", *Proc. 7th Int. Conf. on Cyclotrons and Their Applications,* Birkhauser, Bassel, 496 (1975).

42) Ettingger, K. V., Fremlin, J. H., and Askouri, N. A., "Measurement of Wear and Corrosion by Surface Irradiation with Charged Particle Beam", *Proc. 7th Int. Conf. on Cyclotron and Their Applications*, Birkhauser, Basel, 518 (1975).

43) Fritz, S. G., and Cataldi, G. R., "In Situ Piston Ring Wear Measurements in a Medium-Speed Diesel Engine", *STLE Lubrication Engineering*, Vol.46, No.6, 365 (1989).

44) Fritz, S. G., "Determining Wear in Internal Combustion Engines Using Radioactive Components", *SwRI Project* 03-1542 (1989).

45) Evans, R., "Radioisotope Method for Measuring Engine Wear : A Thin Layer Activation Method for the Measurement of Cam Follower Wear and Its Component with a Neutron Activation Method", *Wear*, Vol. 64, 311 (1980).

46) Blatchley, C. C., and Sioshansi, P., "Measuring Engine Wear by Surface Layer Activation : Extension to Nanometer Increments", *SAE Paper* 872155 (1987).

47) Schneider, E. W., and Blossfeld, D. H., "Real-Time Measurement of Camshaft Wear in an Automotive Engine - a Radiometric Method", *SAE Trans.* 902085 (1990).

48) Sioshansi, P., and Armini, A. J., "The Application of Ion Implantation for Large Scale Treatment of Ball Bearing Elements", Spire Corporation, presented at the Industry-Academia-Government Workshop (1984).

49) Schneider, E. W., and Blossfeld, D. H., "Method for Measurement of Piston Ring Rotation in an Operating Engine", *SAE Trans.* 900224 (1990).

50) Konstantinov, I.O., Leonov, A. I., and Mikheev, V. I., "Surface Activation for Wear Profile Studies of Piston Rings", *Wear*, Vol.141, 17 (1990).

51) Schneider, E. W., Blossfeld, D. H., and Balnaves, M. A., "Effect of Speed and Power Output on Piston Ring Wear in a Diesel Engine", *SAE Trans.* 880672 (1988).

52) Sheppard, S. R., and Suh, N. P., "The Effects of Ion Implantation on Friction and Wear of Metals", *Journal of Lubrication Technology,* Vol.104, 29 (1982).

53) Schock, H. J., Chung, Y., Rachel, T., Grummon, D. S., Schalek, R., Ronningen, R. M., McHarris, W. C., Hsieh, Y., and Gaydos, P., "Production and Implantation of Ions for Wear Studies and Monitoring of Machining Process", *MSUERL Report* 91-3 (1991).

54) Mallory, M. L., Ronningen, R. M., McHarris, W. C., Sherrill, B., Dardenne, Y. X., and Schock, H. J., "Tribology Studies: ^{7}Be Implantation in a Ceramic Sample by means of a Fragmented High-Energy ^{14}N Beam", *Nuclear Instruments and Method in Physics Research*, B40/41, 579 (1989).

55) McHarris, W. C., Mallory, M. L., Ronningen, R. M., Dardenne, Y. X., and Schock, H. J., "Gamma-Ray Spectroscopy of Implanted ^{7}Be and ^{22}Na for Tribology Studies", *MSUCL*-723 (1990).

56) Namazian, M., and Heywood, J. B., " Flow in Piston-Cylinder-Ring Crevices of a Spark-Ignition Engine : Effect on Hydrocarbon Emissions, Efficiency and Power", *SAE Trans.* 820088 (1982).

57) Kuo, T., Sellnau, M. C., Theobald, M. A., and Jones, J., "Calculation of Flow in the Piston-Cylinder-Ring Crevices of a Homogeneous-Charge Engine and Comparison with Experiment", *SAE Trans.* 890838 (1989).

58) Burnett, P. J., "Relationship Between Oil Consumption, Deposit Formation and Piston Ring Motion for Single-Cylinder Diesel Engines", SAE Paper 920089 (1992).

59) Rice, W. J., "Development of an Instrument for Real-Time Computation of Indicated Mean Effective Pressure", *NASA Technical Paper* 2238 (1984).

60) Furuhama, S., Hiruma, M., and Tsuzita, M., "Piston Ring Motion and its influence on Engine Tribology", *SAE Trans.* 790860 (1979).

61) Furuhama, S., and Hiruma, M., "Axial Movement of Piston Rings in the Groove", *ASLE Trans.*, Vol.15, No.4 (1972).

62) Brombolich, L. J., Personal Communication (1992).

63) Allen, D. G., Dudley, B. R., Middleton, B. R., and Parker D. A., "Prediction of Piston Ring-Cylinder Bore Oil Film Thickness in Two Particular Engines and Correlation with Experimental Evidence", *Piston Ring Scuffing*, London, Great Britain (1975).

64) Czichos, H., "Importance of Properties of Solids to Friction and Wear Behavior", NASA Conference Publication 2300, *Tribology in the 80's*, Vol. 1 (1984).

65) Blau, P. J., *Friction and Wear Transitions of Materials*, Noyes Publications, Park Ridge, New Jersey (1989).

66) Wallbridge, N. C., and Dowson, D., "Distribution of Wear Rate Data and a Statistical Approach to Sliding Wear Theory", *Wear*, Vol.119, 295 (1987).

67) Sarkar, A. D., *Friction and Wear*, Academic Press Inc. London LTD, London (1980).

68) Verbeek, H. J., "Tribological Systems and Wear Factors", *Wear*, Vol. 56, 81 (1979).

69) Brombolich, L. J., and McCormick, H. E., "Tribological Aspects of Cylinder Kit Systems in Adiabatic Engines", *SAE Trans.* 880018 (1988).

70) Dinaevsky, V. V., "Analysis of Distortions of Cylinders and Conformability of Piston Rings", *STLE Tribology Trans.*, Vol.33, No.1, 33 (1990).

71) Childs, T. H. C., and Sabbagh, F., "Boundary-Lubricated Wear of Cast Irons to Simulate Auto motive Piston Ring Wear Rates", *Wear*, Vol.134, 81 (1989).

72) Johnson, K. L., Greenwood, J. A., and Poon, S. Y., " A Simple Theory of Asperity Contact in Elastohydrodynamic Lubrication", *Wear*, Vol.19, 91 (1972).

73) Lee, Y. -Z., and Ludema, K. C., "The Shared-Load Wear Model in Lubricated Sliding Scuffing Criteria and Wear Coefficients", *Wear*, Vol.138, 13 (1990).

74) O'Callaghan, P. W., and Probert, S. D., "Prediction and Measurement of True Areas of Contact Between Solids", *Wear*, Vol.120, 29 (1987).

75) Sarkar, A. D., *Wear of Metals*, Pergamon Press, Oxford (1976).

76) Wu, C., and Zheng, C., "Effect of Waviness and Roughness on Lubricated Wear Related to Running-In", Wear, Vol.147, 323 (1991)

77) Barber, G. C., and Ludema, K. C., "The Break-In Stage of Cylinder-Ring Wear: A Correlation Between Fired Engines and A Laboratory Simulator", *Wear*, Vol. 118, 57 (1987).

78) Tabor, D., "Friction - The Present State of Our Understanding", *Journal of Lubrication Technology*, Vol.103, p169 (1981).

79) Suh, N. P., and Saka, N., *Fundamentals of Tribology*, The MIT Press, Cambridge, Massachusetts (1978)

80) Wang, Y., Chen, G., and Jiao, G., "Wear Prediction for Unlubricated Piston

Rings", *Wear*, Vol. 135, 227 (1990).

81) Somerton, C., Error Estimation Experiment, Heat Transfer Laboratory, Michigan State University (1992).

82) Murray, E. J., "A Survey of Scuffing in Spark Ignition Engines", Piston Ring Scuffing, London, Great Britain (1975).

83) Ronningen, R., Personal Communication (1991).

84) National Superconducting Cyclotron Laboratory, *Research Brief* - Center for Wear Research, January (1989).

85) Rachel, T., "An Evaluation of High Energy Ion Implantation for Wear Studies", Master's Thesis, Michigan State University (1991).

86) Enge, H., *Introduction to Nuclear Physics*, Addison-Wesley Publishing Company, Reading, Massachusetts (1966).

87) Mazzoldi, P., and Arnold, G. W., *Ion Beam Modification of Insulator*, Elsevier Science Publisher B. V., Amsterdam, Netherlands (1987).

88) Robinson, M. T., and Oen, O. S., "The Channeling of Energy Atoms in Crystal Lattices", *Applied Physics Letter*, Vol.2, 30 (1963).

89) Robinson, M. T., and Torrens, I. M., "Computer Simulation of Atomic-Displacement Cascades in Solids in the Binary-Collision Approximation", *Phy. Rev.*, B9, No.12, 5008 (1974).

90) Mayor, J. W., Erikson, L., and Davies, J. A., *Ion Implantation in Semiconductors*, Academic Press Inc., London (1970).

91) Wilson, W. D., Haggmark, L. G., and Biersack, J. P., "Calculation of nuclear stopping, ranges, and straggling in the low-energy region", *Phy. Rev., B*15, No.5, 2458 (1977).

92) Burkhardt, T., McHarris, W., Chung, Y., Lloyd, J., Rachel, T., Schock, H., Grummon, D., Sharek, R., Ronningen, R., and Mallory, M. L., "Developments in High Energy Ion Implantation for Wear Analysis", *MSU Status Report* MSUERL-90-5 (1990).